universität wien

MASTERARBEIT | MASTER'S THESIS

Titel | Title

Integrating molecular dynamics and micromagnetics for the investigation of nanoparticles in liquid carriers

verfasst von | submitted by

David Zehner BSc

angestrebter akademischer Grad | in partial fulfilment of the requirements for the degree of

Master of Science (MSc)

Wien | Vienna, 2024

Studienkennzahl lt. Studienblatt | Degree programme code as it appears on the student record sheet:	UA 066 876
Studienrichtung lt. Studienblatt | Degree programme as it appears on the student record sheet:	Masterstudium Physics
Betreut von | Supervisor:	Univ.-Prof. Dipl.-Ing. Dr.techn. Dieter Süss Privatdoz.

Abstract

This thesis presents a comprehensive investigation into the dynamic behavior of magnetic nanoparticles suspended in a viscous fluid, with a particular focus on their medical application in magnetic nanoparticle hyperthermia. The study integrates micromagnetic simulations with fluid dynamics, resulting in a detailed model that captures the interactions between magnetic moments, their embedding atomic crystal lattice, and the surrounding fluid environment. To facilitate future model extensions, the simulations are conducted by integrating the micromagnetic simulation framework magnum.np with the established soft matter software ESPResSo. A notable accomplishment of this research is the derivation of a self-consistent set of equations of motion for multi-domain particles in a liquid carrier, obtained through variational calculus. The study employs the Landau-Lifshitz-Gilbert equation and the Langevin equation to elucidate the linear and nonlinear dynamic responses of MNPs in varying magnetic field conditions. The research demonstrates that under certain conditions, the cases of zero and infinite anisotropy are equivalent. These extreme cases are thoroughly examined, demonstrating that the effective field model proposed by Martsenyuk, Raikher, and Shliomis offers high accuracy. Additionally, the study presents a closed-form solution for the zero-temperature case, adaptable to thermal conditions, which is able to explain the emergence of higher-order susceptibilities.

Kurzfassung

Diese Arbeit stellt eine umfassende Untersuchung des dynamischen Verhaltens von magnetischen Nanopartikeln (MNP) in einer viskosen Flüssigkeit vor, wobei der Schwerpunkt auf deren Anwendung in der magnetischen Nanopartikel-Hyperthermie liegt. Die Untersuchung integriert mikromagnetische Simulationen mit Strömungsdynamik und entwickelt ein detailliertes Modell, das die Wechselwirkungen zwischen magnetischen Momenten, dem atomaren Kristallgitter und der umgebenden Flüssigkeit beschreibt. Um zukünftige Modellerweiterungen zu ermöglichen, werden die Simulationen durch die Integration des mikromagnetischen Frameworks magnum.np mit der etablierten Soft-Matter-Software ESPResSo durchgeführt. Ein wichtiges Ergebnis dieser Forschung ist die Ableitung eines selbstkonsistenten Systems von Bewegungsgleichungen für Multidomänen-Partikel in einem flüssigen Trägermedium, das durch Variationsrechnung ermittelt wurde. Die Studie verwendet die Landau-Lifshitz-Gilbert-Gleichung sowie die Langevin-Gleichung, um die linearen und nichtlinearen dynamischen Reaktionen von MNPs unter verschiedenen Magnetfeldbedingungen zu untersuchen. Die Analyse zeigt, dass unter bestimmten Bedingungen die Fälle von verschwindender und unendlicher Anisotropie äquivalent sind. Diese Extremfälle werden gründlich analysiert und zeigen, dass das von Martsenyuk, Raikher und Shliomis vorgeschlagene effektive Feldmodell eine gute Approximation bietet. Darüber hinaus wird eine geschlossene Lösung für den athermischen Fall präsentiert, die an thermische Bedingungen anpassbar ist und das Auftreten von Suszeptibilitäten höherer Ordnung erklärt.

Acknowledgments

I would like to express my gratitude to all my colleagues, friends, and family who have provided me with wisdom, patience, and support along this journey.
I am especially grateful to my colleagues in the functional materials group. A big thank you to my office neighbors—Verena, Robert, Marcel, Michael, Philip, and Markus—for all our conversations about relevant and less relevant things. I am also thankful to Sabri Koraltan, whose support and inspiration have been with me since my bachelor's days, always reminding me of the exciting possibilities ahead. A special acknowledgment also goes to Santiago Helbig, without whose support this project would not have been possible.
I am grateful to Sofia Kantorivich and Deniz Mostarac for introducing me to the world of soft matter simulations and helping me understand its spirit. I also want to extend my sincere thanks to Dieter Süss and Claas Abert, who were always there to resolve the challenges I faced and encouraged me to explore new ideas.
I cannot forget to thank my family for always being there, picking up the phone, and standing by my side. Lastly, my deepest thanks go to my dear friends for their unwavering support. A special mention to Max for sharing countless lunches at Ali's Gemüsekebap, always keeping me well-fed and motivated.

Abbreviations, symbols, and physical constants

Symbol	Description	Unit
$\boldsymbol{H}$	Magnetic field	$\mathrm{A\,m^{-1}}$
$\boldsymbol{B}$	Magnetic flux density	T
$\boldsymbol{M}$	Magnetisation	$\mathrm{A\,m^{-1}}$
M_s	Saturation magnetisation	$\mathrm{A\,m^{-1}}$
$\boldsymbol{m}$	Normalised magnetisation	1
$\boldsymbol{\mu}$	Magnetic dipole moment	$\mathrm{Am^2}$
$\boldsymbol{L}$	Angular momentum	$\mathrm{kgm^2/s}$
$\boldsymbol{S}$	Angular moment associated with $\boldsymbol{\mu}$	$\mathrm{kgm^2/s}$
$\boldsymbol{T}$	Torque	$\mathrm{kgm^2/s^2}$
SLP	Specific Loss Rate	$\mathrm{W\,g^{-1}}$
χ	Susceptibility	

Tab. 1: List of frequently used symbols

Symbol	Description	Value
μ_0	Vacuum permeability	$4\pi \cdot 10^{-7}\,\mathrm{N/A^2}$
γ_e	Electron gyromagnetic ratio	$1.7609 \times 10^{11}\,\mathrm{T^{-1}\,s^{-1}}$
k_B	Boltzmann constants	$1.381 \times 10^{-23}\,\mathrm{J\,K^{-1}}$

Tab. 2: List of physical constants

Contents

1 Introduction **9**

2 Micromagnetics **11**
2.1 Magnetic interactions 12
2.1.1 Zeeman interaction 15
2.1.2 Exchange interaction 15
2.1.3 Anisotropy 16
2.1.4 Demagnetization 17

3 Colloids **21**

4 Coupled model **25**
4.1 Hamiltonian system 25
4.2 Dissipative system 28
4.3 Single-domain approximation 31
4.4 Rigid dipole approximation 33
4.5 Overdamped limit 34
4.6 Heat dissipation 35

5 Numerical implementation **37**
5.1 mmhd - A micromagnetic hydrodynamics solver 37
5.2 Discrete micromagnetics 38
5.3 Ensembles of Single-domain particles 40
5.4 Reduced units 41
5.5 Time integration 42

6 Equilibrium properties **45**
6.1 Energy minimization 46
6.2 Canonical partition function 49
6.3 Suspended single-domain particles 55
6.4 Immobilized single-domain particles 56

7 Dynamic response of single-domain particles **61**
7.1 Parameter reduction 61
7.2 Zero and infinite anisotropy 63
7.2.1 Linear regime 66
7.2.2 Deterministic regime 67
7.2.3 Quasi-equilibrium 67

7.2.4 Monodirectional fields 69
7.3 Hybrid Brownian and Néel relaxation 80

8 Conclusion **84**

Bibliography **89**

List of Figures **90**

1 Introduction

Magnetic nanoparticles promise new perspectives in medical applications, such as hyperthermia [1–3] for cancer therapy or magnetic particle imaging [4, 5]. In both applications, it is of significance to understand the behavior of these particles when suspended in a viscous carrier fluid, such as water or blood, and how they respond to external excitations by magnetic fields. To address this problem, it is necessary to integrate the two research areas of soft matter physics and the physics of magnetism.

Soft matter physics investigates the behavior of systems sensitive to thermal fluctuations. These systems may include polymers, liquid crystals, or small particles suspended in a carrier fluid. In the latter case, the entity is referred to as a *colloid*. Besides the random collisions between the colloidal particles and the molecules or atoms of the carrier fluid, they also interact with each other by Van-der-Waals interactions and other forces. In the case of magnetic particles, an important role is designated to dipolar interactions. The sum of these interactions heavily influences their mobility, for both translational and rotational movement.

The field of micromagnetics is a branch of physics that deals with the study of magnetic phenomena at small length scales. Its consideration is essential, as the response of a particle to a magnetic field is initially based on the quantum mechanical interaction between an atomic spin and the magnetic field. As the spins reside on atomic lattice sites, the dynamics of the spins and the motion of the particle's atoms are necessarily connected through various interactions.

This thesis focuses on the internal dynamics of individual magnetic nanoparticles, deliberately excluding interactions between different particles. The goal is to derive the equations of motion for all degrees of freedom within a single particle in a consistent manner. This task remains complex due to the various contributions that must be considered. The causal chain of events can be conceptualized as follows: First, the magnetic field induces motion in the atomic spins, which then affect the atoms in the crystal lattice. In rigid bodies, the motion of a single atom causes a collective movement of the entire particle, which is then also influenced by collisions with fluid molecules on the surface of the particle.

In general, all interactions are subject to a delay, with each operating on a different characteristic time scale. However, if a particular characteristic time scale is significantly smaller than the others, it can be approximated as instantaneous, thereby simplifying the analysis of the overall system.

The trajectories of the particle can be derived using Hamilton's theorem and the prin-

ciple of gyromagnetic precession, where spins precess around a magnetic field at a characteristic frequency determined by the gyromagnetic ratio of the electron. After introducing the relevant interactions in Chapters 2 and 3, the equations of motion for a Hamiltonian system will be derived in the first part of Chapter 4. Subsequently, the impact of dissipative forces and thermal fluctuations on these governing equations will be investigated.

Given the complexity of the system's dynamics, it is advantageous to also study its static equilibrium, which provides reliable approximations for near-equilibrium dynamics. This analysis is presented in Chapter 6 for the most general case as well as the common approximation of single-domain particles, in which all of the particle's spins are parallel to each other, resulting from strong exchange interactions.

Finally, Chapter 7 is dedicated to the description of the dynamical behavior of single-domain particles, where the equations of motion are transformed into a reduced form in terms of the minimum amount of parameters.

2 Micromagnetics

In ferromagnetic materials, quantum mechanical exchange interactions tend to align adjacent spins. This results in a characteristic length scale that is well above the lattice constant of the crystal structure, where the magnetic moments can be assumed to be parallel. This justifies the transition from discrete spins to a continuous vector field $\boldsymbol{M}(\boldsymbol{x})$ called *magnetization*. The magnitude of $\boldsymbol{M}$ is uniform throughout a magnetic particle and equals the spontaneous magnetization M_s. The magnetization can thus be written in terms of a unit vector field $\boldsymbol{m} = \boldsymbol{M}/M_\mathrm{s}$.

Let us denote the extent of the magnetic substance of a particle in a reference state by the manifold $\Omega_\mathrm{m} \subset \mathbb{R}^3$, setting the center of mass in the origin of our coordinate system. If the particle can move and rotate freely in space, the time-dependent position of a point $\widehat{\boldsymbol{x}}$ in the reference configuration is given by the Euclidian transformation T

$$T : \mathbb{R}^3 \times \mathbb{R} \to \mathbb{R}^3 \tag{2.1}$$

$$(\widehat{\boldsymbol{x}}, t) \mapsto \boldsymbol{R}(t)\widehat{\boldsymbol{x}} + \boldsymbol{d}(t), \tag{2.2}$$

where $\boldsymbol{R}(t)$ and $\boldsymbol{d}(t)$ are the time-dependent rotation matrix and displacement vector associated with the mechanical motion of the particle.

Given an arbitrary scalar, vector, or tensor field $A(\boldsymbol{x}, t)$ defined for all $\boldsymbol{x} \in \mathbb{R}^3$, we mainly are interested in its evaluation at the sites of the spins of the particle. Thus there exists a corresponding field

$$\tilde{A} : \Omega_\mathrm{m} \times \mathbb{R} \to \mathrm{Im}(A) \tag{2.3}$$

$$(\widehat{\boldsymbol{x}}, t) \mapsto A(T(\widehat{\boldsymbol{x}}, t), t), \tag{2.4}$$

where the domain of the coordinates can be restricted to Ω_m. Throughout this thesis, we shall not distinguish between A and $\tilde{A}$ and will use the notation $A(\widehat{\boldsymbol{x}}, t)$ when we intend to evaluate $A(T(\widehat{\boldsymbol{x}}, t), t)$.

For describing the system entirely in the particle frame where the magnetic domain always is identical to Ω_m, vector and tensor fields need to be rotated accordingly. For a vector field $\boldsymbol{A}$, the particle frame representation is given by $\widehat{\boldsymbol{A}} = \boldsymbol{R}^\top \boldsymbol{A}$ and for a tensor field $\boldsymbol{B}$ by $\widehat{\boldsymbol{B}} = \boldsymbol{R}^\top \boldsymbol{B}\boldsymbol{R}$. The notation $\widehat{\cdot}$ will be used throughout this thesis to distinguish between the laboratory and the particle frame.

As a final definition, let $\overline{A}$ denote the particle average of A, given by

$$\overline{A} = \frac{1}{V_\mathrm{m}} \int_{\Omega_\mathrm{m}} A(\widehat{\boldsymbol{x}})\, \mathrm{d}\widehat{\boldsymbol{x}} \tag{2.5}$$

where $V_\mathrm{m} = \int_{\Omega_\mathrm{m}} \mathrm{d}\widehat{\boldsymbol{x}}$ is the volume of the magnetic domain of the particle.

2.1 Magnetic interactions

The motivation for the micromagnetic model was to quantify the complex interplay of the interactions acting on and within ferromagnetic bodies. Whether the magnetization is uniform or in some vortex state depends on the strength of these interactions which is usually determined by material-specific properties. In this section, we aim to examine magnetic interactions that maintain the Hamiltonian structure of the system. Each of these interactions is associated with an energy functional that can depend on the magnetization and orientation of the particle. To subsequently model the mechanical motion of a magnetic particle, the functionals should be expressed using independent coordinates corresponding to the magnetization and orientation of the particle. It is not necessary to take into account the position of the particle since this thesis will not cover inhomogeneous fields or dipolar interactions between multiple mobile particles.
In order to compute the system's equations of motion, it is necessary to calculate functional derivatives with respect to infinitesimal changes in magnetization or physical rotation. For that purpose, we define the magnetic variation of $E[\boldsymbol{m}, \boldsymbol{R}, t]$ with respect to $\boldsymbol{m}$ as

$$\begin{aligned} \delta_{\boldsymbol{v}}^{\mathrm{mag}} E[\boldsymbol{m}, \boldsymbol{R}, t] &= \frac{\mathrm{d}}{\mathrm{d}\epsilon} E[\boldsymbol{m} + \epsilon \boldsymbol{v}, \boldsymbol{R}, t]\bigg|_{\epsilon=0} \\ &= \lim_{\epsilon \to 0} \frac{E[\boldsymbol{m} + \epsilon \boldsymbol{v}, \boldsymbol{R}, t] - E[\boldsymbol{m}, \boldsymbol{R}, t]}{\epsilon} \end{aligned} \tag{2.6}$$

for an arbitrary vector field $\boldsymbol{v}(\widehat{\boldsymbol{x}})$. However, we have to take into account that $\boldsymbol{m}$ must be normalized. This condition could be imposed by including Lagrange multipliers in the variation or by using arguments of classical mechanics [6, 7]. Here, the unit sphere condition should be demanded explicitly by constraining the vector field $\boldsymbol{v}$ to the adequate subset. To do so, consider the tensor field

$$\begin{aligned} \tilde{\boldsymbol{R}} : \Omega_\mathrm{m} &\to \mathrm{SO}(3) \\ \widehat{\boldsymbol{x}} &\mapsto \tilde{\boldsymbol{R}}(\widehat{\boldsymbol{x}}) \end{aligned} \tag{2.7}$$

which maps each point in the magnetic domain to a rotation matrix. Applying this field to the magnetization changes the orientation of each infinitesimal spin but preserves

the normalization constraint. Using Rodrigues' formula [8], $\tilde{\boldsymbol{R}}$ can be expressed as

$$\tilde{\boldsymbol{R}}(\widehat{\boldsymbol{x}}) = \cos(\phi(\widehat{\boldsymbol{x}}))\,\mathbf{1} + (1-\cos(\phi(\widehat{\boldsymbol{x}})))\,\widehat{\boldsymbol{n}}(\widehat{\boldsymbol{x}})\widehat{\boldsymbol{n}}^{\top}(\widehat{\boldsymbol{x}}) + \sin(\phi(\widehat{\boldsymbol{x}}))\,[\widehat{\boldsymbol{n}}(\widehat{\boldsymbol{x}})\times] \tag{2.8}$$

where each point $\widehat{\boldsymbol{x}}$ has an associated axis of rotation $\widehat{\boldsymbol{n}}(\widehat{\boldsymbol{x}})$ and angle $\phi(\widehat{\boldsymbol{x}})$. The quantity $[\widehat{\boldsymbol{n}}(\widehat{\boldsymbol{x}})\times]$ denotes the skew-symmetric cross-product matrix

$$[\widehat{\boldsymbol{n}}(\widehat{\boldsymbol{x}})\times] = \begin{pmatrix} 0 & -\widehat{n}_3(\widehat{\boldsymbol{x}}) & \widehat{n}_2(\widehat{\boldsymbol{x}}) \\ \widehat{n}_3(\widehat{\boldsymbol{x}}) & 0 & -\widehat{n}_1(\widehat{\boldsymbol{x}}) \\ -\widehat{n}_2(\widehat{\boldsymbol{x}}) & \widehat{n}_1(\widehat{\boldsymbol{x}}) & 0 \end{pmatrix}, \tag{2.9}$$

whose action on a vector field $\boldsymbol{a}$ is taking the cross product

$$[\widehat{\boldsymbol{n}}(\widehat{\boldsymbol{x}})\times]\boldsymbol{a}(\widehat{\boldsymbol{x}}) = \widehat{\boldsymbol{n}}(\widehat{\boldsymbol{x}}) \times \boldsymbol{a}(\widehat{\boldsymbol{x}}). \tag{2.10}$$

Since we want to consider the case of infinitesimal rotations, we multiply the field of angles ϕ by a scalar ϵ and neglect any higher order terms:

$$\begin{aligned} \tilde{\boldsymbol{R}}_{\epsilon}(\widehat{\boldsymbol{x}}) &= \cos(\epsilon\phi(\widehat{\boldsymbol{x}}))\,\mathbf{1} + (1-\cos(\epsilon\phi(\widehat{\boldsymbol{x}})))\,\widehat{\boldsymbol{n}}(\widehat{\boldsymbol{x}})\widehat{\boldsymbol{n}}^{\top}(\widehat{\boldsymbol{x}}) + \sin(\epsilon\phi(\widehat{\boldsymbol{x}}))\,[\widehat{\boldsymbol{n}}(\widehat{\boldsymbol{x}})\times] \\ &\approx \mathbf{1} + \epsilon\phi(\widehat{\boldsymbol{x}})\,[\widehat{\boldsymbol{n}}(\widehat{\boldsymbol{x}})\times] \quad \text{for} \quad \epsilon \ll 1 \\ &= \mathbf{1} + \epsilon[\boldsymbol{\phi}(\widehat{\boldsymbol{x}})\times]. \end{aligned} \tag{2.11}$$

By making use of the linearity of $[\cdot\times]$, the angle and the axis have been combined to the field of Euler vectors $\boldsymbol{\phi} = \phi\widehat{\boldsymbol{n}}$, whose norm corresponds to the rotation angle, and direction to the rotation axis. Thus, the variation of the energy on transforming the magnetization by the rotation $\tilde{\boldsymbol{R}}_{\boldsymbol{\phi},\epsilon}$ associated to an arbitrary vector field $\boldsymbol{\phi}$ is given by

$$\begin{aligned} &\frac{\mathrm{d}}{\mathrm{d}\epsilon} E[\tilde{\boldsymbol{R}}_{\boldsymbol{\phi},\epsilon}\boldsymbol{m}, \boldsymbol{R}, t]\bigg|_{\epsilon=0} \\ =&\frac{\mathrm{d}}{\mathrm{d}\epsilon} E[\boldsymbol{m} + \epsilon\boldsymbol{\phi}\times\boldsymbol{m}, \boldsymbol{R}, t]\bigg|_{\epsilon=0} \\ =&\delta^{\mathrm{mag}}_{\boldsymbol{\phi}\times\boldsymbol{m}} E[\boldsymbol{m}, \boldsymbol{R}, t]. \end{aligned} \tag{2.12}$$

In the special case where $\boldsymbol{\phi}$ is uniform, the transformation $\boldsymbol{m} \to \boldsymbol{m} + \epsilon\boldsymbol{\phi}\times\boldsymbol{m}$ corresponds to an infinitesimal rotation of $\boldsymbol{m}$ about the axis given by $\boldsymbol{\phi}/|\boldsymbol{\phi}|$. This step leads to the second transformation that can be applied to the particle: Rather than transforming the magnetization, we should look at the case of physically rotating the particle while keeping the magnetization fixed in space. To avoid confusion between vector fields and single vectors, the vector field $\boldsymbol{v}$ is replaced by a rotation axis $\widehat{\boldsymbol{a}} \in \mathbb{R}^3$. Applying the corresponding rotation to the physical orientation of the particle leads

to the variation

$$\begin{aligned} &\frac{\mathrm{d}}{\mathrm{d}\epsilon} E[\boldsymbol{m}, \tilde{\boldsymbol{R}}_{\widehat{\boldsymbol{a}},\epsilon}\boldsymbol{R}, t]\Big|_{\epsilon=0} \\ &= \frac{\mathrm{d}}{\mathrm{d}\epsilon} E[\boldsymbol{m}, \boldsymbol{R} + \epsilon[\widehat{\boldsymbol{a}}\times]\boldsymbol{R}, t]\Big|_{\epsilon=0} \\ &=: \delta^{\mathrm{mech}}_{[\widehat{\boldsymbol{a}}\times]\boldsymbol{R}} E[\boldsymbol{m}, \boldsymbol{R}, t]. \end{aligned} \tag{2.13}$$

The following subsections present the calculations for both the variations under magnetization and mechanical rotation for each energy contribution. Nevertheless, there is a distinctive attribute of the energy functional that will prove particularly advantageous in this regard. For all but one contribution, the energy is fully determined by the local magnetization, such that $E = E[\widehat{\boldsymbol{m}}] = E[\boldsymbol{R}^\top \boldsymbol{m}]$. It can be demonstrated that applying a rotation matrix $\boldsymbol{R}'$ to both $\boldsymbol{m}$ and $\boldsymbol{R}$ does not affect the energy. This transformation can be understood as a rotation of the entire system in the global perspective, while maintaining the configuration in the particle frame perspective. If the corresponding magnetic interaction is independent of contributions from outside the particle, or in other words, space is isotropic concerning this interaction, the energy will remain unaltered under such transformations. Given that

$$E[\boldsymbol{R}'\boldsymbol{R}, \boldsymbol{m}] = E[\boldsymbol{R}^\top \boldsymbol{R}'^\top \boldsymbol{m}] = E[\boldsymbol{R}, \boldsymbol{R}'^\top \boldsymbol{m}], \tag{2.14}$$

which also has to hold for infinitesimal rotations $\tilde{\boldsymbol{R}}_{\widehat{\boldsymbol{a}},\epsilon}$, the mechanical variation can be expressed as

$$\begin{aligned} \delta^{\mathrm{mech}}_{[\widehat{\boldsymbol{a}}\times]\boldsymbol{R}} E[\boldsymbol{m}, \boldsymbol{R}, t] &= \frac{\mathrm{d}}{\mathrm{d}\epsilon} E[\left(\boldsymbol{R}^\top - \epsilon \boldsymbol{R}^\top [\widehat{\boldsymbol{a}}\times]\right) \boldsymbol{m}, t]\Big|_{\epsilon=0} \\ &= \frac{\mathrm{d}}{\mathrm{d}\epsilon} E[\boldsymbol{R}^\top \left(\mathbf{1} - \epsilon[\widehat{\boldsymbol{a}}\times]\right) \boldsymbol{m}, t]\Big|_{\epsilon=0} \\ &= \frac{\mathrm{d}}{\mathrm{d}\epsilon} E[\boldsymbol{R}^\top \left(\boldsymbol{m} - \epsilon[\widehat{\boldsymbol{a}}\times]\boldsymbol{m}\right), t]\Big|_{\epsilon=0} \\ &\overset{(\epsilon'=-\epsilon)}{=} \frac{\mathrm{d}}{\mathrm{d}(-\epsilon')} E[\boldsymbol{R}^\top \left(\boldsymbol{m} + \epsilon'[\widehat{\boldsymbol{a}}\times]\boldsymbol{m}\right), t]\Big|_{-\epsilon'=0} \\ &= -\delta^{\mathrm{mag}}_{\widehat{\boldsymbol{a}}\times\boldsymbol{m}} E[\boldsymbol{m}, \boldsymbol{R}, t]. \end{aligned} \tag{2.15}$$

Thus, it is sufficient to calculate the magnetic variation $\delta^{\mathrm{mag}}_{\widehat{\boldsymbol{a}}\times\boldsymbol{m}} E[\boldsymbol{m}, \boldsymbol{R}, t]$ for a constant vector $\widehat{\boldsymbol{a}}$ and take the negative to obtain the mechanical variation $\delta^{\mathrm{mech}}_{[\widehat{\boldsymbol{a}}\times]\boldsymbol{R}} E[\boldsymbol{m}, \boldsymbol{R}, t]$.

2.1.1 Zeeman interaction

The Zeeman interaction describes the interaction of a magnetic moment in an external magnetic field $\boldsymbol{H}_{\text{ext}}$ and is given by

$$E_{\text{ext}}[\boldsymbol{m}, \boldsymbol{R}, t] \equiv E_{\text{ext}}[\boldsymbol{m}, t] = -\mu_0 M_{\text{s}} \int_{\Omega_{\text{m}}} \boldsymbol{m}(\widehat{\boldsymbol{x}}) \cdot \boldsymbol{H}_{\text{ext}}(t) \, \mathrm{d}\widehat{\boldsymbol{x}}. \tag{2.16}$$

In general, $\boldsymbol{H}_{\text{ext}}$ may be space dependent, but for this thesis, it is sufficient to look at homogeneous fields. The magnetic variation $\delta^{\text{mag}}_{\boldsymbol{\phi}\times\boldsymbol{m}} E_{\text{ext}}[\boldsymbol{m}, t]$ for an arbitrary vector field $\boldsymbol{\phi}$ is given by

$$\begin{aligned} \delta^{\text{mag}}_{\boldsymbol{\phi}\times\boldsymbol{m}} E_{\text{ext}}[\boldsymbol{m}, t] &= \frac{\mathrm{d}}{\mathrm{d}\epsilon} E_{\text{ext}}[\boldsymbol{m} + \epsilon\boldsymbol{\phi} \times \boldsymbol{m}, t]\Big|_{\epsilon=0} \\ &= -\mu_0 M_{\text{s}} \int_{\Omega_{\text{m}}} (\boldsymbol{m} \times \boldsymbol{H}_{\text{ext}}(t)) \cdot \boldsymbol{\phi} \, \mathrm{d}\widehat{\boldsymbol{x}}. \end{aligned} \tag{2.17}$$

As the Zeeman energy only depends on the angle between $\boldsymbol{m}$ and the external field, there will be no change in energy under mechanical rotation of the particle, thus leading to a vanishing variation $\delta^{\text{mech}}_{[\widehat{\boldsymbol{a}}\times]\boldsymbol{R}} E_{\text{ext}}[\boldsymbol{m}, t] = 0$.

2.1.2 Exchange interaction

The exchange field arises from the quantum mechanical interaction of adjacent spins, which in the Heisenberg formulation is defined as [6]

$$E^{\text{ex}}_{ij} = -J\boldsymbol{s}_i \cdot \boldsymbol{s}_j, \tag{2.18}$$

where the coupling constant J is the exchange integral of the two respective wave functions. For the continuum, the product over the next neighbors can be expressed by the gradient

$$E_{\text{ex}}[\boldsymbol{m}, \boldsymbol{R}] = A \int_{\Omega_{\text{m}}} (\widehat{\boldsymbol{\nabla}}\widehat{\boldsymbol{m}})^2 \, \mathrm{d}\widehat{\boldsymbol{x}} = A \int_{\Omega_{\text{m}}} (\widehat{\boldsymbol{\nabla}}\boldsymbol{m})^2 \, \mathrm{d}\widehat{\boldsymbol{x}} \equiv E_{\text{ex}}[\boldsymbol{m}], \tag{2.19}$$

where A is the exchange constant being inherent to the material of the particle and $(\widehat{\boldsymbol{\nabla}}\boldsymbol{m})^2$ is the Frobenius inner product

$$(\widehat{\boldsymbol{\nabla}}\boldsymbol{m})^2 = \sum_{i,j} \left(\frac{\partial m_i}{\partial \widehat{x}_j} \right)^2. \tag{2.20}$$

As this is invariant under rotation by $\boldsymbol{R}$, the exchange energy is independent of $\boldsymbol{R}$ and its mechanical variation vanishes. For the magnetic variation, one obtains

$$\delta^{\mathrm{mag}}_{\boldsymbol{\phi}\times\boldsymbol{m}} E_{\mathrm{ex}}[\boldsymbol{m}] = \frac{\mathrm{d}}{\mathrm{d}\epsilon} A \sum_{i,j} \int_{\Omega_{\mathrm{m}}} \left(\frac{\partial(\boldsymbol{m} + \epsilon\boldsymbol{\phi}\times\boldsymbol{m})_i}{\partial \widehat{x}_j} \right)^2 \mathrm{d}\widehat{\boldsymbol{x}} \Big|_{\epsilon=0} \tag{2.21}$$

$$= 2A \sum_{i,j,a,b} \left(\int_{\partial\Omega_{\mathrm{m}}} \varepsilon_{abi} \frac{\partial m_i}{\partial \boldsymbol{n}} \phi_a m_b \,\mathrm{d}\boldsymbol{s} - \int_{\Omega_{\mathrm{m}}} \varepsilon_{abi} \frac{\partial^2 m_i}{\partial \widehat{x}_j^2} \phi_a m_b \,\mathrm{d}\widehat{\boldsymbol{x}} \right) \tag{2.22}$$

$$= 2A \int_{\partial\Omega_{\mathrm{m}}} (\boldsymbol{m} \times \frac{\partial \boldsymbol{m}}{\partial \boldsymbol{n}}) \cdot \boldsymbol{\phi} \,\mathrm{d}\boldsymbol{s} - \mu_0 M_{\mathrm{s}} \int_{\Omega_{\mathrm{m}}} (\boldsymbol{m} \times \boldsymbol{H}_{\mathrm{ex}}) \cdot \boldsymbol{\phi} \,\mathrm{d}\widehat{\boldsymbol{x}} \tag{2.23}$$

where the exchange field is given by $\boldsymbol{H}_{\mathrm{ext}} = 2A\Delta\boldsymbol{m}/\mu_0 M_{\mathrm{s}}$.

2.1.3 Anisotropy

In certain materials, an anisotropic crystal structure gives rise to magnetic anisotropy, where the magnetization favors being aligned with one or more *easy* axes. For the purpose of this thesis, it is sufficient to consider the case of only one easy axis, denoted by the unit vector $\boldsymbol{n}$. As with many micromagnetic quantities, the expression for the anisotropy energy is based on phenomenological considerations and multiplied with an experimentally determined material factor. Because the easy axis is undirected, meaning that both orientations of the magnetization are equivalent, we require the energy to be symmetric under sign reversal of $\boldsymbol{m}$ and $\boldsymbol{n}$. Neglecting higher orders, the expression

$$E_{\mathrm{ani}} = -K_{\mathrm{u}} \int_{\Omega_{\mathrm{m}}} (\boldsymbol{m}(\widehat{\boldsymbol{x}}) \cdot \boldsymbol{n})^2 \,\mathrm{d}\widehat{\boldsymbol{x}} \tag{2.24}$$

is a suitable and commonly used form. Since the easy axis is an artifact of the atomic crystal structure, it will rotate along with the orientation of the particle in space. We can arrive at an expression in terms of the rotation matrix $\boldsymbol{R}$ by substituting $\boldsymbol{n} = \boldsymbol{R}\widehat{\boldsymbol{n}}$, where the easy axis in the particle frame $\widehat{\boldsymbol{n}}$ is constant:

$$\begin{aligned} E_{\mathrm{ani}}[\boldsymbol{m}, \boldsymbol{R}] &= -K_{\mathrm{u}} \int_{\Omega_{\mathrm{m}}} (\boldsymbol{m}(\widehat{\boldsymbol{x}}) \cdot \boldsymbol{n})^2 \,\mathrm{d}\widehat{\boldsymbol{x}} \\ &= -K_{\mathrm{u}} \int_{\Omega_{\mathrm{m}}} \left(\boldsymbol{m}^\top(\widehat{\boldsymbol{x}}) \boldsymbol{R}\widehat{\boldsymbol{n}} \right)^2 \mathrm{d}\widehat{\boldsymbol{x}} \\ &= -K_{\mathrm{u}} \int_{\Omega_{\mathrm{m}}} \left((\boldsymbol{R}^\top \boldsymbol{m}(\widehat{\boldsymbol{x}})) \cdot \widehat{\boldsymbol{n}} \right)^2 \mathrm{d}\widehat{\boldsymbol{x}}. \end{aligned} \tag{2.25}$$

This allows for the calculation of the magnetic variation

$$\begin{aligned}\delta^{\mathrm{mag}}_{\boldsymbol{\phi}\times\boldsymbol{m}} E_{\mathrm{ani}}[\boldsymbol{m},\boldsymbol{R}] &= \frac{\mathrm{d}}{\mathrm{d}\epsilon} E_{\mathrm{ani}}[\boldsymbol{m}+\epsilon\boldsymbol{\phi}\times\boldsymbol{m},\boldsymbol{R}]\Big|_{\epsilon=0} \\ &= -2K_{\mathrm{u}}\int_{\Omega_{\mathrm{m}}} \left(\boldsymbol{m}^{\top}\boldsymbol{R}\widehat{\boldsymbol{n}}\right)(\boldsymbol{m}\times\boldsymbol{R}\widehat{\boldsymbol{n}})\cdot\boldsymbol{\phi}\,\mathrm{d}\widehat{\boldsymbol{x}} \\ &= -\mu_0 M_{\mathrm{s}}\int_{\Omega_{\mathrm{m}}} (\boldsymbol{m}\times\boldsymbol{H}_{\mathrm{ani}})\cdot\boldsymbol{\phi}\,\mathrm{d}\widehat{\boldsymbol{x}},\end{aligned} \tag{2.26}$$

where the anisotropy field $\boldsymbol{H}_{\mathrm{ani}}$ is given by

$$\boldsymbol{H}_{\mathrm{ani}}(\widehat{\boldsymbol{x}}) = \frac{2K_{\mathrm{u}}}{\mu_0 M_{\mathrm{s}}}(\boldsymbol{m}(\widehat{\boldsymbol{x}})\cdot\boldsymbol{R}\widehat{\boldsymbol{n}})\boldsymbol{R}\widehat{\boldsymbol{n}} = \frac{2K_{\mathrm{u}}}{\mu_0 M_{\mathrm{s}}}(\boldsymbol{m}(\widehat{\boldsymbol{x}})\cdot\boldsymbol{n})\boldsymbol{n}. \tag{2.27}$$

Due to (2.15), the mechanical variation is given by

$$\delta^{\mathrm{mech}}_{[\widehat{\boldsymbol{a}}\times]\boldsymbol{R}} E_{\mathrm{ani}}[\boldsymbol{m},\boldsymbol{R}] = -\delta^{\mathrm{mag}}_{\widehat{\boldsymbol{a}}\times\boldsymbol{m}} E_{\mathrm{ani}}[\boldsymbol{m},\boldsymbol{R}]. \tag{2.28}$$

2.1.4 Demagnetization

The demagnetization energy can be defined as the work that is required to bring together each (oriented) elementary magnetic moment of a body from an infinite distance to its respective site in the lattice. This interaction is based on the dipole-dipole interaction between two magnetic moments. However, a macroscopic classical approach is much more convenient for deriving an expression for the total demagnetization (or magnetostatic) energy of a body. The general relationship between the magnetisation $\widehat{\boldsymbol{M}}$, the magnetic flux density $\widehat{\boldsymbol{B}}$ and the demagnetisation field $\widehat{\boldsymbol{H}}^{\mathrm{dem}}$, given in the particle frame, is

$$\widehat{\boldsymbol{B}} = \mu_0\left(\widehat{\boldsymbol{H}}^{\mathrm{dem}} + \widehat{\boldsymbol{M}}\right). \tag{2.29}$$

Considering the two Maxwell equations for magnetostatic fields

$$\widehat{\boldsymbol{\nabla}}\cdot\widehat{\boldsymbol{B}} = 0 \tag{2.30}$$

$$\widehat{\boldsymbol{\nabla}}\times\widehat{\boldsymbol{H}}^{\mathrm{dem}} = 0, \tag{2.31}$$

one can express the demagnetisation field as $\widehat{\boldsymbol{H}}^{\mathrm{dem}} = -\widehat{\boldsymbol{\nabla}}u$ since its curl vanishes. Combined with (2.29), this can be reduced to the single equation

$$\widehat{\boldsymbol{\nabla}}\cdot\left(-\widehat{\boldsymbol{\nabla}}u + \widehat{\boldsymbol{M}}\right) = 0, \tag{2.32}$$

which can be solved for u in the whole space as

$$u(\widehat{\boldsymbol{x}}) = -\frac{1}{4\pi}\int_{\mathbb{R}^3} \frac{\widehat{\boldsymbol{\nabla}}' \cdot \widehat{\boldsymbol{M}}(\widehat{\boldsymbol{x}}')}{|\widehat{\boldsymbol{x}} - \widehat{\boldsymbol{x}}'|}\mathrm{d}\widehat{\boldsymbol{x}}'. \tag{2.33}$$

As $\boldsymbol{M} = 0$ outside the body, there will be no contribution to the integral from the outside region. Thus, assuming that $\boldsymbol{M} = M_\mathrm{s}\boldsymbol{m}$ inside the body, a quasi-singular behavior occurs at the boundary surface where $\boldsymbol{M}$ jumps to zero. In the idealized limit where the jump is discontinuous, (2.33) can be split into two contributions

$$u(\widehat{\boldsymbol{x}}) = -\frac{M_\mathrm{s}}{4\pi}\int_{\Omega_m} \frac{\widehat{\boldsymbol{\nabla}}' \cdot \widehat{\boldsymbol{m}}(\widehat{\boldsymbol{x}}')}{|\widehat{\boldsymbol{x}} - \widehat{\boldsymbol{x}}'|}\mathrm{d}\widehat{\boldsymbol{x}}' + \frac{M_\mathrm{s}}{4\pi}\oint_{\partial\Omega_m} \frac{\widehat{\boldsymbol{n}} \cdot \widehat{\boldsymbol{m}}(\widehat{\boldsymbol{x}}')}{|\widehat{\boldsymbol{x}} - \widehat{\boldsymbol{x}}'|}\mathrm{d}\widehat{\boldsymbol{s}}' \tag{2.34}$$

where the second term has been obtained by Green's theorem. If applied again, the expression for u simplifies to

$$u(\widehat{\boldsymbol{x}}) = \frac{M_\mathrm{s}}{4\pi}\int_{\Omega_m} \left(\widehat{\boldsymbol{\nabla}}'\frac{1}{|\widehat{\boldsymbol{x}} - \widehat{\boldsymbol{x}}'|}\right) \cdot \widehat{\boldsymbol{m}}(\widehat{\boldsymbol{x}}')\mathrm{d}\widehat{\boldsymbol{x}}', \tag{2.35}$$

which gives for the demagnetization field in the laboratory frame

$$\boldsymbol{H}^\mathrm{dem}(\widehat{\boldsymbol{x}}) = -\boldsymbol{R}\widehat{\boldsymbol{\nabla}}u = M_\mathrm{s}\int_{\Omega_m} \boldsymbol{R}\widehat{\boldsymbol{N}}(\widehat{\boldsymbol{x}} - \widehat{\boldsymbol{x}}')\boldsymbol{R}^\top\boldsymbol{m}(\widehat{\boldsymbol{x}}')\mathrm{d}\widehat{\boldsymbol{x}}', \tag{2.36}$$

where the demagnetization tensor $\widehat{\boldsymbol{N}}$ is given by

$$\widehat{N}_{ij}(\widehat{\boldsymbol{x}} - \widehat{\boldsymbol{x}}') = -\frac{1}{4\pi}\widehat{\nabla}_i\widehat{\nabla}'_j\frac{1}{|\widehat{\boldsymbol{x}} - \widehat{\boldsymbol{x}}'|}. \tag{2.37}$$

Analogous to the Zeeman energy, the total energy of the demagnetization field is given by

$$E^\mathrm{dem} = -\frac{\mu_0 M_\mathrm{s}}{2}\iint_{\Omega_\mathrm{m}} \boldsymbol{m}(\widehat{\boldsymbol{x}}) \cdot \boldsymbol{H}^\mathrm{dem}(\widehat{\boldsymbol{x}})\,\mathrm{d}\widehat{\boldsymbol{x}}\,\mathrm{d}\widehat{\boldsymbol{x}}' \tag{2.38}$$

$$= -\frac{\mu_0 M_\mathrm{s}^2}{2}\iint_{\Omega_\mathrm{m}} \boldsymbol{m}^\top(\widehat{\boldsymbol{x}})\boldsymbol{R}\widehat{\boldsymbol{N}}(\widehat{\boldsymbol{x}} - \widehat{\boldsymbol{x}}')\boldsymbol{R}^\top\boldsymbol{m}(\widehat{\boldsymbol{x}}')\,\mathrm{d}\widehat{\boldsymbol{x}}\,\mathrm{d}\widehat{\boldsymbol{x}}'. \tag{2.39}$$

$$\tag{2.40}$$

The factor 1/2 accounts for the quadratic dependence of the energy on the magneti-

zation $\boldsymbol{m}$. This finally allows us to evaluate the variations

$$\begin{aligned}\delta^{\mathrm{mag}}_{\boldsymbol{\phi}\times\boldsymbol{m}} E_{\mathrm{dem}}[\boldsymbol{m},\boldsymbol{R}] &= \frac{\mathrm{d}}{\mathrm{d}\epsilon} E_{\mathrm{dem}}[\boldsymbol{m}+\epsilon\boldsymbol{\phi}\times\boldsymbol{m},\boldsymbol{R}]\Big|_{\epsilon=0} \\ &= -\mu_0 M_{\mathrm{s}} \int_{\Omega_{\mathrm{m}}} (\boldsymbol{m}\times\boldsymbol{H}_{\mathrm{dem}})\cdot\boldsymbol{\phi}\,\mathrm{d}\widehat{\boldsymbol{x}} \\ &= -\delta^{\mathrm{mech}}_{[\widehat{\boldsymbol{a}}\times]\boldsymbol{R}} E_{\mathrm{dem}}[\boldsymbol{m},\boldsymbol{R}].\end{aligned} \tag{2.41}$$

3 Colloids

In theory, one could model a suspended nanoparticle by taking into account all collisions with a large number of surrounding carrier particles. However, this would require an unfeasible computational effort since the size of typical nanoparticles used in hyperthermia is some orders of magnitudes larger than the size of a water molecule, thus the computational effort would exceed any feasible limit. As a coarse-graining approach, Langevin proposed to model these hydrodynamic forces with two parts [9]: The viscous drag can be expressed as a torque and a force proportional to the translational and angular velocity of the particle

$$\boldsymbol{F}_{\mathrm{visc}} = -\boldsymbol{\Gamma}_{\mathrm{t}}\,\boldsymbol{v} \tag{3.1}$$

$$\boldsymbol{T}_{\mathrm{visc}} = -\boldsymbol{\Gamma}_{\mathrm{r}}\,\boldsymbol{\omega}, \tag{3.2}$$

with the geometry-dependent friction tensors $\boldsymbol{\Gamma}_{\mathrm{t}}$ and $\boldsymbol{\Gamma}_{\mathrm{r}}$. For spherical particles, there exist exact expressions (*Stokes*' law) for the latter, the values for cubes can only be determined experimentally or from simulations [10, 11]. For thin disks, there can also be found corresponding expressions [12]. Since this thesis will not cover interactions between particles and will focus only on their rotational behavior, the translational drag will not be elucidated further.

For all three geometries, the rotational friction tensors turn out to be a multiple of the identity matrix $\boldsymbol{\Gamma}_{\mathrm{r}} = \gamma_{\mathrm{r}}\mathbf{1}$. The respective values are displayed in Tab. 3. It shows that cubes exhibit a rotational drag about 30 percent larger than spheres with the same volume.

In addition to the viscous drag, collisions between the particle and the fluid molecules are modeled by an additional, rapidly fluctuating stochastic torque $\boldsymbol{T}_{\mathrm{th}}$ averaging out

	$\gamma_{\mathrm{r}}/\eta R^3$	$\gamma_{\mathrm{r}}/\eta V$
Sphere	$8\pi \approx 25.13$	6
Cube	64.139	8.017
Disk	10.667	$3.395/a$

Tab. 3: Diagonal element of the rotational friction tensors for the different particle geometries. In the first column, the values have been non-dimensionalized by ηR^3, in the second column by ηV where η is the dynamic viscosity of the carrier fluid, R the radius or semiside of the particle, V its volume, and a the disk's height-to-radius ratio.

to zero. Due to the large number of collisions occurring on a timescale much shorter than those of interest, the random noise can be assumed to be uncorrelated in time. Furthermore, one can assume the vector components of the random noise to be independent as well. These conditions can be formally expressed as

$$\langle T_{\mathrm{th},i}(t)\rangle = 0. \tag{3.3}$$
$$\langle T_{\mathrm{th},i}(t) T_{\mathrm{th},j}(t')\rangle = 2D\,\delta_{ij}\delta(t-t') \tag{3.4}$$

where D is the diffusion coefficient related to the random process. The noise usually is assumed as Gaussian, which can be justified by the large number of collisions and the consideration of the mean-value theorem.

The equation of motion for an arbitrary external torque $\boldsymbol{T}$ is thus given by

$$\dot{\boldsymbol{L}} = \boldsymbol{T} - \boldsymbol{\Gamma}_{\mathrm{r}}\boldsymbol{\omega} + \boldsymbol{T}_{\mathrm{th}}, \tag{3.5}$$

where the angular momentum $\boldsymbol{L}$ is given as the product of the inertia tensor and the angular velocity $\boldsymbol{L} = \boldsymbol{\Theta}\boldsymbol{\omega}$. Because the inertia tensor is bound to the particle's axes, its representation in the laboratory frame is itself time-dependent. It is thus useful to express it in terms of the respective tensor in the particle frame as $\boldsymbol{\Theta} = \boldsymbol{R}\widehat{\boldsymbol{\Theta}}\boldsymbol{R}^{\top}$. The time derivative $\dot{\boldsymbol{L}}$ is then given by

$$\dot{\boldsymbol{L}} = \frac{\mathrm{d}}{\mathrm{d}t}\left(\boldsymbol{R}\widehat{\boldsymbol{\Theta}}\boldsymbol{R}^{\top}\boldsymbol{\omega}\right) \tag{3.6}$$
$$= \dot{\boldsymbol{R}}\widehat{\boldsymbol{\Theta}}\boldsymbol{R}^{\top}\boldsymbol{\omega} + \boldsymbol{R}\widehat{\boldsymbol{\Theta}}\dot{\boldsymbol{R}}^{\top}\boldsymbol{\omega} + \boldsymbol{R}\widehat{\boldsymbol{\Theta}}\boldsymbol{R}^{\top}\dot{\boldsymbol{\omega}}. \tag{3.7}$$

For the derivative of the rotation matrix, the well-known expression [13]

$$\dot{\boldsymbol{R}} = [\boldsymbol{\omega}\times]\,\boldsymbol{R} \tag{3.8}$$

can be used, which simplifies (3.5) to

$$\dot{\boldsymbol{L}} = \boldsymbol{\omega}\times\boldsymbol{R}\widehat{\boldsymbol{\Theta}}\boldsymbol{R}^{\top}\boldsymbol{\omega} + \boldsymbol{R}\widehat{\boldsymbol{\Theta}}\boldsymbol{R}^{\top}\dot{\boldsymbol{\omega}}. \tag{3.9}$$

Plugging the latter expression into (3.5) yields the Langevin equation for an arbitrary rigid body [14]

$$\boldsymbol{R}\widehat{\boldsymbol{\Theta}}\boldsymbol{R}^{\top}\dot{\boldsymbol{\omega}} = \boldsymbol{T} - \boldsymbol{\Gamma}_{\mathrm{r}}\boldsymbol{\omega} + \boldsymbol{T}_{\mathrm{th}} + \boldsymbol{R}\widehat{\boldsymbol{\Theta}}\boldsymbol{R}^{\top}\boldsymbol{\omega}\times\boldsymbol{\omega}. \tag{3.10}$$

For the discussion of the diffusion properties of the particle, let assume that both the inertia and friction tensors are multiples of the identity. In this case, the Langevin equation reduces to

$$\Theta\dot{\boldsymbol{\omega}} = \boldsymbol{T} - \gamma_{\mathrm{r}}\boldsymbol{\omega} + \boldsymbol{T}_{\mathrm{th}}. \tag{3.11}$$

Its solution can be formally expressed as

$$\boldsymbol{\omega}(t) = \boldsymbol{\omega}(0)e^{-t/\tau_\omega} + \frac{1}{\Theta}\int_0^t \mathrm{d}t'\, e^{-(t-t')/\tau_\omega}\left(\boldsymbol{T}(t') + \boldsymbol{T}_{\mathrm{th}}(t')\right), \tag{3.12}$$

where $\tau_\omega = \Theta/\gamma_\mathrm{r}$. Despite the thermal noise being discontinuous everywhere, its integration can be carried out in a stochastic sense. However, expressions of this nature are generally meaningless without specifying an interpretation rule [15], which defines the evaluation point for coordinate-dependent prefactors in the integrand. As argued in [16], only the *Stratonovich* interpretation yields the correct physical equilibrium, whereas the *Itô* interpretation leads to incorrect results. Nevertheless, this issue is not relevant for the equation (3.12) and throughout this thesis since the ambiguity is resolved either by the absence of coordinates in the integrand or by the presence of the unit sphere constraint. As shown in [17], the difference between the Itô and Stratonovich interpretations would only result in a change in magnitude, which is prohibited by the model, rendering the two schemes equivalent.

The solution of (3.12) also reveals that τ_ω is the first characteristic time scale of the system. The subscript ω emphasizes that it is the characteristic time scale of the relaxation of the angular velocity. It relates the friction in the system to the particle's moment of inertia resisting the dissipative force. However, in the absence of a time-dependent torque, the system relaxes to an inertia-independent equilibrium state: In the case where $\boldsymbol{T}$ is constant in time and no thermal fluctuations are included, the particle will accelerate until reaching the terminal velocity $\boldsymbol{\omega}_\mathrm{final} = \boldsymbol{T}/\gamma_\mathrm{r}$. In the converse situation of a free particle in a thermalized fluid, the equipartition theorem requires that each component of the rotational kinetic energy takes the equilibrium value $k_\mathrm{B}T/2$, which is satisfied by setting the diffusion coefficient to

$$D = \gamma_\mathrm{r} k_\mathrm{B} T. \tag{3.13}$$

In the presence of both contributions, the angular velocity relaxes to a combination of the two. For common nanoparticle sizes and material parameters, the relaxation time τ_ω is typically within the range $10^{-12}\,\mathrm{s}$ to $10^{-9}\,\mathrm{s}$. This is considerably shorter than the timescales of interest and the frequency of external fields in hyperthermia problems. Under certain conditions, it is appropriate to neglect inertial effects and to take the limit $\tau_\omega, \Theta \to 0$, which means that the angular velocity instantaneously relaxes to its terminal velocity. Taking the limit in (3.12) causes the first term to vanish and leads to a delta distribution in the integrand, resulting in the *overdamped* solution

$$\boldsymbol{\omega}_\mathrm{d}(t) = \frac{1}{\gamma_\mathrm{r}}\left(\boldsymbol{T}(t) + \boldsymbol{T}_{\mathrm{th}}(t)\right), \tag{3.14}$$

which could be equivalently achieved by setting $\Theta = 0$ in (3.12). This approximation is widely applied in colloidal science and the investigation of hyperthermia [1, 18, 19], however, should be treated with care due to the fast processes occurring in magnetic

systems.

Given the solutions for the angular velocity and equation (3.8), we want to perform the integration to obtain a solution for the evolution of the particle's orientation. It is convenient not to find a solution for the rotation coordinate $\boldsymbol{R}$ but for an arbitrary body-fixed axis described by a unit vector $\boldsymbol{n}$ which evolves according to

$$\dot{\boldsymbol{n}} = \boldsymbol{\omega} \times \boldsymbol{n}. \tag{3.15}$$

In the absence of torque, the particle exhibits diffusion due to thermal fluctuations. The temporal autocorrelation of an arbitrary axis is then given by [20]

$$\langle \boldsymbol{n}(0)\boldsymbol{n}(t) \rangle = \left\langle |\boldsymbol{n}|^2 \right\rangle \, e^{-t/\tau_\mathrm{B}}. \tag{3.16}$$

This incorporates the Brownian diffusion time

$$\tau_\mathrm{B} = \frac{\gamma_\mathrm{r}}{2k_\mathrm{B}T}, \tag{3.17}$$

which denotes the characteristic time scale of the thermal fluctuations.

4 Coupled model

4.1 Hamiltonian system

As a first step, we want to derive the equations of motion for a mechanical-magnetic coupled system without energy dissipation. Therefore, thermal fluctuations, magnetic damping, and fluid-particle interactions shall not be included. The most elegant way to find the system's dynamics would be by applying the variational principle to a generalized Lagrange density involving the independent coordinates. However, as magnetic moments fundamentally differ from mechanic angular momenta, this requires rather unintuitive considerations for correctly modeling the kinetic energy of massless magnetic moments [6]. Instead, we should link angular velocity and magnetization to their corresponding angular momenta on which torques act, given by the variations of the potential energy of the system.

Given the general equation for the rotation of a rigid body (3.10) whilst omitting the friction term and thermal fluctuations yields

$$\boldsymbol{R}\widehat{\boldsymbol{\Theta}}\boldsymbol{R}^{\top}\dot{\boldsymbol{\omega}} = \boldsymbol{T}_{\mathrm{mech}} + \boldsymbol{R}\widehat{\boldsymbol{\Theta}}\boldsymbol{R}^{\top}\boldsymbol{\omega}\times\boldsymbol{\omega}, \tag{4.1}$$

where the external torque $\boldsymbol{T}_{\mathrm{mech}}$ is implicitly given by [21]

$$\boldsymbol{T}_{\mathrm{mech}}\cdot\delta\boldsymbol{\phi} = -\delta^{\mathrm{mech}}_{[\delta\boldsymbol{\phi}\times]\boldsymbol{R}}E[\boldsymbol{m},\boldsymbol{R},t]. \tag{4.2}$$

Collecting all non-vanishing terms of the interactions discussed up to this point, the equation of motion evaluates to

$$\begin{aligned}\boldsymbol{R}\widehat{\boldsymbol{\Theta}}\boldsymbol{R}^{\top}\dot{\boldsymbol{\omega}} &= -\mu_0 M_{\mathrm{s}}\int_{\Omega_{\mathrm{m}}}\boldsymbol{m}\times(\boldsymbol{H}_{\mathrm{ani}}+\boldsymbol{H}_{\mathrm{dem}})\,\mathrm{d}\widehat{\boldsymbol{x}} + \boldsymbol{R}\widehat{\boldsymbol{\Theta}}\boldsymbol{R}^{\top}\boldsymbol{\omega}\times\boldsymbol{\omega}\\ &= -\mu_0 M_{\mathrm{s}}V_{\mathrm{m}}\left(\overline{\boldsymbol{m}\times\boldsymbol{H}_{\mathrm{ani}}}+\overline{\boldsymbol{m}\times\boldsymbol{H}_{\mathrm{dem}}}\right) + \boldsymbol{R}\widehat{\boldsymbol{\Theta}}\boldsymbol{R}^{\top}\boldsymbol{\omega}\times\boldsymbol{\omega}.\end{aligned} \tag{4.3}$$

This shows that the mechanical behavior of a non-dissipative system is entirely driven by anisotropy and demagnetization, which follows from the fact that these are the only energetic contributions that depend on the physical orientation of the particle. However, we should look for an intuitive explanation of how this exact form arises. To do so, first assume that the tensor of inertia is diagonal, as is the case for spheres and cubes. This leads to the angular momentum being proportional to the angular velocity of the particle. Second, recall that the angular velocity is orthogonal to the plane of rotation. Thus, (4.3) shows that the particle accelerates its rotation in the

"average" plane spanned by the vector fields $\boldsymbol{m}$ and $\boldsymbol{H}_{\text{ani}} + \boldsymbol{H}_{\text{dem}}$. The contribution of the anisotropy field is proportional to

$$\boldsymbol{T}_{\text{ani}} \sim \boldsymbol{n} \times \overline{(\boldsymbol{n} \cdot \boldsymbol{m})\boldsymbol{m}} \tag{4.4}$$

and thus accelerates the easy axis to the weighted average of the magnetization, thereby favoring the spins closer aligned to the easy axis. The contribution of the demagnetization field cannot be broken down by the same analogy but will accelerate the particle towards the orientation of minimum demagnetization energy. However, this analysis assumed that the magnetization does not evolve in time, which is of course the case.

It happens that magnetic processes are usually orders of magnitude faster than the mechanical dynamics of the system. To find the magnetic equation of motion it should be referenced to Gilbert's derivations [7]. It is shown that the angular momentum $\boldsymbol{S}_i$ associated with an electron spin evolves according to

$$\dot{\boldsymbol{S}}_i = \mu_0 \boldsymbol{\mu}_i \times \boldsymbol{H}_i, \tag{4.5}$$

where $\boldsymbol{\mu}_i$ is the associated magnetic moment and $\boldsymbol{H}_i$ the magnetic field acting on it. To express this equation solely in terms of the magnetic moment, the relation between the angular momentum and the magnetic moment

$$\boldsymbol{\mu}_i = -\gamma_{\text{e}} \boldsymbol{S}_i, \tag{4.6}$$

is inserted into (4.5), yielding

$$\dot{\boldsymbol{\mu}}_i = -\gamma_{\text{e}} \mu_0 \boldsymbol{\mu}_i \times \boldsymbol{H}_i. \tag{4.7}$$

Hereby $\gamma_{\text{e}} \approx 1.76 \times 10^{11} \text{s}^{-1}\,\text{T}^{-1}$ is the gyromagnetic ratio of the electron. This equation thus describes the dynamics of a magnetic moment $\boldsymbol{\mu}_i$ associated with a single electron. To transition to the continuum, one can replace it by the continuous magnetization $\boldsymbol{m}(\widehat{\boldsymbol{x}})$ described in the last chapter. This gives the equation of motion

$$\begin{aligned} \dot{\boldsymbol{m}} &= -\gamma_{\text{e}} \mu_0 \boldsymbol{m} \times \boldsymbol{H}_{\text{eff}} \\ &= -\gamma_{\text{e}} \mu_0 \boldsymbol{m} \times (\boldsymbol{H}_{\text{ext}} + \boldsymbol{H}_{\text{ex}} + \boldsymbol{H}_{\text{ani}} + \boldsymbol{H}_{\text{dem}}). \end{aligned} \tag{4.8}$$

This is consistent with the magnetic variational calculus. However, (2.23) still includes the boundary term

$$2A \int_{\partial \Omega_{\text{m}}} (\boldsymbol{m} \times \frac{\partial \boldsymbol{m}}{\partial \boldsymbol{n}}) \cdot \boldsymbol{\phi} \, \mathrm{d}\boldsymbol{s} \tag{4.9}$$

integrated over the particle's surface. The full variational calculus [6] shows that this term has to vanish at all times for arbitrary $\boldsymbol{\phi}$, which will be forced by the used nu-

merical implementation.

There is one differential equation missing for the orientation of the particle expressed by the rotation matrix $\boldsymbol{R}$. Denote that the cross-product matrix of the angular velocity is given by

$$[\boldsymbol{\omega}\times] = \dot{\boldsymbol{R}}\boldsymbol{R}^{\top}. \tag{4.10}$$

By multiplying with $\boldsymbol{R}$ from the right we obtain the evolution of $\boldsymbol{R}$

$$\dot{\boldsymbol{R}} = [\boldsymbol{\omega}\times]\boldsymbol{R}. \tag{4.11}$$

Therefore, the system of equations of motions consists of the three equations that need to be solved in parallel:

$$\begin{aligned}
\dot{\boldsymbol{m}} &= -\gamma_{\mathrm{e}}\mu_0 \boldsymbol{m} \times (\boldsymbol{H}_{\mathrm{ext}} + \boldsymbol{H}_{\mathrm{ex}} + \boldsymbol{H}_{\mathrm{ani}} + \boldsymbol{H}_{\mathrm{dem}}) \\
\dot{\boldsymbol{\omega}} &= \boldsymbol{R}\widehat{\boldsymbol{\Theta}}^{-1}\boldsymbol{R}^{\top}\left(-\mu_0 M_{\mathrm{s}} V_{\mathrm{m}}\left(\overline{\boldsymbol{m}\times\boldsymbol{H}_{\mathrm{ani}}} + \overline{\boldsymbol{m}\times\boldsymbol{H}_{\mathrm{dem}}}\right) + \boldsymbol{R}\widehat{\boldsymbol{\Theta}}\boldsymbol{R}^{\top}\boldsymbol{\omega}\times\boldsymbol{\omega}\right) \\
\dot{\boldsymbol{R}} &= [\boldsymbol{\omega}\times]\boldsymbol{R}.
\end{aligned} \tag{4.12}$$

4.2 Dissipative system

Gilbert damping

In physical systems, the magnetization is subject to other interactions with internal degrees of freedom. The effect of these processes is dissipative, whereby magnetic potential energy is transformed into microscopic thermal motion in the form of spin waves, lattice vibrations, or thermal excitation of conduction electrons. However, modelling these interactions is challenging, particularly in continuous approximation. Instead, Gilbert [7] proposed a phenomenological damping torque with a damping parameter α that can be determined experimentally. He shows that the damping leads to an additional magnetic field proportional to the rate of change of the magnetization. For rotating particles, this rate of change should be taken in the particle frame since the damping is caused by magnetization motion relative to the atomic lattice [22–24]. The Gilbert damping field $\boldsymbol{H}_\mathrm{G}$ expressed in the laboratory frame is thus given by

$$\begin{aligned}\boldsymbol{H}_\mathrm{G} = \boldsymbol{R}\widehat{\boldsymbol{H}}_\mathrm{G} &= -\frac{\alpha}{\gamma_\mathrm{e}\mu_0}\boldsymbol{R}\dot{\widehat{\boldsymbol{m}}} \\ &= -\frac{\alpha}{\gamma_\mathrm{e}\mu_0}\boldsymbol{R}\frac{\mathrm{d}}{\mathrm{d}t}(\boldsymbol{R}^\top\boldsymbol{m}) \\ &= -\frac{\alpha}{\gamma_\mathrm{e}\mu_0}(\dot{\boldsymbol{m}} + \boldsymbol{m}\times\boldsymbol{\omega}).\end{aligned} \tag{4.13}$$

The transformation into the laboratory frame unravels another contribution which can be connected to the *Barnett* effect [25] that describes how mechanical rotation induces a change in magnetization. The former derivation suggests that the Barnett effect is a consequence of the symmetry of relative motion: A rotating magnetization causes the same damping torque as a rotating particle with opposite angular velocity.

For simplification, the Gilbert damping field is split up into the damping field

$$\boldsymbol{H}_\mathrm{damp} = -\frac{\alpha}{\gamma_\mathrm{e}\mu_0}\dot{\boldsymbol{m}} \tag{4.14}$$

and the Barnett field

$$\boldsymbol{H}_\mathrm{Bar} = -\frac{\alpha}{\gamma_\mathrm{e}\mu_0}\boldsymbol{m}\times\boldsymbol{\omega}. \tag{4.15}$$

Including the Gilbert damping, the gyromagnetic equation becomes the Landau-Lifshitz-Gilbert (LLG) equation

$$\dot{\boldsymbol{m}} = -\gamma_\mathrm{e}\mu_0\boldsymbol{m}\times\boldsymbol{H}_\mathrm{eff} + \alpha\boldsymbol{m}\times\dot{\boldsymbol{m}} \tag{4.16}$$

in its implicit form, with the effective field given by

$$\boldsymbol{H}_{\text{eff}} = \boldsymbol{H}_{\text{ext}} + \boldsymbol{H}_{\text{ex}} + \boldsymbol{H}_{\text{ani}} + \boldsymbol{H}_{\text{dem}} + \boldsymbol{H}_{\text{Bar}}. \tag{4.17}$$

Isolating $\dot{\boldsymbol{m}}$ finally yields

$$\dot{\boldsymbol{m}} = -\frac{\gamma_{\text{e}}\mu_0}{1+\alpha^2}\boldsymbol{m} \times \boldsymbol{H}_{\text{eff}} - \frac{\alpha\gamma_{\text{e}}\mu_0}{1+\alpha^2}\boldsymbol{m} \times (\boldsymbol{m} \times \boldsymbol{H}_{\text{eff}}). \tag{4.18}$$

This is the more common form of the Landau-Lifshitz-Gilbert equation and consists of two terms: The precession term $\propto \boldsymbol{m} \times \boldsymbol{H}_{\text{eff}}$ is, up to the prefactor and the Barnett field, equivalent to the conservative system and thus describes the precession of the magnetization around the effective field. The second term is the so-called damping term and leads to a relaxation of $\boldsymbol{m}$ towards $\boldsymbol{H}_{\text{eff}}$. However, this picture breaks down for the Barnett field: Recalling that $\boldsymbol{H}_{\text{Bar}} \propto \boldsymbol{m} \times \boldsymbol{\omega}$ is always orthogonal to $\boldsymbol{m}$, it is impossible for the magnetization to align with $\boldsymbol{H}_{\text{Bar}}$. Evaluating the Barnett field-related terms of the LLG and making use of the vector identity

$$\boldsymbol{m} \times (\boldsymbol{m} \times (\boldsymbol{m} \times \boldsymbol{\omega})) = -\boldsymbol{m} \times \boldsymbol{\omega} \tag{4.19}$$

results in

$$\begin{aligned} \dot{\boldsymbol{m}}_{\text{Bar}} &= -\frac{\gamma_{\text{e}}\mu_0}{1+\alpha^2}\boldsymbol{m} \times \boldsymbol{H}_{\text{Bar}} - \frac{\alpha\gamma_{\text{e}}\mu_0}{1+\alpha^2}\boldsymbol{m} \times (\boldsymbol{m} \times \boldsymbol{H}_{\text{Bar}}). \\ &= -\frac{\alpha}{1+\alpha^2}\boldsymbol{m} \times (\boldsymbol{m} \times -\boldsymbol{\omega}) - \frac{\alpha^2}{1+\alpha^2}\boldsymbol{m} \times \boldsymbol{\omega}. \end{aligned} \tag{4.20}$$

This reveals that the dynamics corresponding to the Barnett field swaps the damping and precession nature of the two terms: The original precession term leads to a relaxation of the magnetization towards $-\boldsymbol{\omega}$, and the damping term produces a precession corresponding to a magnetic field parallel to $+\boldsymbol{\omega}$ with a different α-dependence than for the other terms in the LLG. This dependence can be best understood by taking the limit of infinite damping

$$\lim_{\alpha\to\infty} \dot{\boldsymbol{m}}_{\text{Bar}} = \boldsymbol{\omega} \times \boldsymbol{m}, \tag{4.21}$$

where the magnetization co-rotates with the lattice as no relative motion is possible due to damping. The quadratic α-dependence in the numerator ensures that it does not vanish in the limit.

For small damping, however, the quadratic term can be neglected. Including an alternative expression for the Barnett field $\boldsymbol{H}'_{\text{Bar}} = -\boldsymbol{\omega}/\gamma_{\text{e}}\mu_0$ in the original damping term of the LLG leads to an equivalent formulation up to $\mathcal{O}(\alpha^2)$ [23, 26].

Magnetic thermal fluctuations

By the fluctuation-dissipation theorem, for each dissipation mechanism, there exist corresponding thermal fluctuations. For the viscous damping, these are modeled by the Langevin equation. What is left is to add fluctuations associated with the Gilbert damping in the form of a stochastic magnetic field $\boldsymbol{H}_{\mathrm{th}}$. Usually, these fluctuations are described by a Gaussian random properties with the following properties [27]:

$$\langle H_{\mathrm{th},i}(\widehat{\boldsymbol{x}},t)\rangle = 0 \tag{4.22}$$

$$\langle H_{\mathrm{th},i}(\widehat{\boldsymbol{x}},t)H_{\mathrm{th},j}(\widehat{\boldsymbol{x}}',t')\rangle = 2D\delta_{ij}\delta^3(\widehat{\boldsymbol{x}}-\widehat{\boldsymbol{x}}')\delta(t-t') \tag{4.23}$$

The thermal field is assumed uncorrelated in space and time, moreover, all components are retrieved from independent Gaussian distributions. The constant D can be derived from the Fokker-Planck equation associated with the Landau-Lifshitz-Gilbert equation. It is noted that there exist multiple equivalent formulations that may or may not include the thermal field in the precession or damping term of the LLG. Here, it is chosen to add the thermal fluctuations to the effective field $\boldsymbol{H}_{\mathrm{eff}}$, and thus appear in both of the terms. To obtain the correct stationary Boltzmann distribution for static systems, it is shown that D takes the value

$$D = \frac{\alpha k_{\mathrm{B}} T}{\mu_0^2 \gamma_{\mathrm{e}} M_{\mathrm{s}}}, \tag{4.24}$$

which naturally yields the characteristic time scale [16]

$$\tau_0 = \frac{(1+\alpha^2) M_{\mathrm{s}} V_{\mathrm{m}}}{2\alpha\gamma_{\mathrm{e}} k_{\mathrm{B}} T}, \tag{4.25}$$

corresponding to the relaxation time of a free single-domain particle.

Up to this point, it has not been discussed how the Gilbert damping and thermal fluctuations are related to the mechanical motion of the particle. Given that the damping transforms magnetic potential energy into microscopic thermal motion, the change in magnetic angular momentum is compensated by an equal but opposite change in mechanical angular momentum. We therefore need to add the torque $\boldsymbol{T}_{\mathrm{G}}$ associated to the Gilbert damping and thermal fluctuations, given by the difference between the RHS of the Landau-Lifshitz-Gilbert and the gyromagnetic equation

$$\boldsymbol{T}_{\mathrm{G}} = -\frac{M_{\mathrm{s}} V_{\mathrm{m}}}{\gamma_{\mathrm{e}}} \left(\overline{\dot{\boldsymbol{m}}} - \overline{\dot{\boldsymbol{m}}|_{T=0}^{\alpha=0}} \right) \tag{4.26}$$

$$= -\frac{M_{\mathrm{s}} V_{\mathrm{m}}}{\gamma_{\mathrm{e}}} \overline{\dot{\boldsymbol{m}}} - \mu_0 M_{\mathrm{s}} V_{\mathrm{m}} \overline{\boldsymbol{m} \times (\boldsymbol{H}_{\mathrm{ext}} + \boldsymbol{H}_{\mathrm{ani}} + \boldsymbol{H}_{\mathrm{dem}})} \tag{4.27}$$

$$\tag{4.28}$$

to the mechanical equation of motion with the opposite sign.

Set of equations

Given the equations of motion of the non-dissipative system (4.12), the LLG (4.18) and the additional damping, stochastic, and compensation torques, it should be derived a self-consistent set of equations. In fact, what is left is to collect all torques and simplify the equation of motion for the angular velocity $\boldsymbol{\omega}$. Denoting the equation of the Hamiltonian system by $\dot{\boldsymbol{\omega}}_{\mathrm{Ham}}$, adding the dissipative torques yields

$$\dot{\boldsymbol{\omega}} = \dot{\boldsymbol{\omega}}_{\mathrm{Ham}} + \boldsymbol{R}\widehat{\boldsymbol{\Theta}}^{-1}\boldsymbol{R}^{\top}\left(-\gamma_{\mathrm{r}}\boldsymbol{\omega} + \boldsymbol{T}_{\mathrm{th}} - \boldsymbol{T}_{\mathrm{G}}\right). \tag{4.29}$$

This results in the self-consistent set of equations

$$\begin{aligned}
\dot{\boldsymbol{\omega}} &= \boldsymbol{R}\widehat{\boldsymbol{\Theta}}^{-1}\boldsymbol{R}^{\top}\left(\mu_0 M_{\mathrm{s}} V_{\mathrm{m}}\overline{\boldsymbol{m}} \times \boldsymbol{H}_{\mathrm{ext}} + \frac{M_{\mathrm{s}}V_{\mathrm{m}}}{\gamma_{\mathrm{e}}}\overline{\dot{\boldsymbol{m}}} - \gamma_{\mathrm{r}}\,\boldsymbol{\omega} + \boldsymbol{T}_{\mathrm{th}} + \boldsymbol{R}\widehat{\boldsymbol{\Theta}}\boldsymbol{R}^{\top}\boldsymbol{\omega}\times\boldsymbol{\omega}\right)\\
\dot{\boldsymbol{m}} &= -\frac{\gamma_{\mathrm{e}}\mu_0}{1+\alpha^2}\boldsymbol{m}\times\boldsymbol{H}_{\mathrm{eff}} - \frac{\alpha\gamma_{\mathrm{e}}\mu_0}{1+\alpha^2}\boldsymbol{m}\times(\boldsymbol{m}\times\boldsymbol{H}_{\mathrm{eff}})\\
\dot{\boldsymbol{R}} &= [\boldsymbol{\omega}\times]\boldsymbol{R},
\end{aligned} \tag{4.30}$$

where the effective field is given by

$$\boldsymbol{H}_{\mathrm{eff}} = \boldsymbol{H}_{\mathrm{ext}} + \boldsymbol{H}_{\mathrm{ex}} + \boldsymbol{H}_{\mathrm{ani}} + \boldsymbol{H}_{\mathrm{dem}} + \boldsymbol{H}_{\mathrm{Bar}} + \boldsymbol{H}_{\mathrm{th}}. \tag{4.31}$$

4.3 Single-domain approximation

For small particles, the aligning effect of the exchange field dominates the demagnetization field and the magnetization $\boldsymbol{m}$ can be assumed to be uniform throughout the particle, meaning that

$$\boldsymbol{m}(\widehat{\boldsymbol{x}}) \equiv \boldsymbol{m} = \overline{\boldsymbol{m}}. \tag{4.32}$$

Thus, one should take the particle average of the RHS of the LLG and obtains

$$\dot{\boldsymbol{m}} = \overline{\dot{\boldsymbol{m}}} = -\frac{\gamma_{\mathrm{e}}\mu_0}{1+\alpha^2}\boldsymbol{m}\times\overline{\boldsymbol{H}_{\mathrm{eff}}} - \frac{\alpha\gamma_{\mathrm{e}}\mu_0}{1+\alpha^2}\boldsymbol{m}\times(\boldsymbol{m}\times\overline{\boldsymbol{H}_{\mathrm{eff}}}). \tag{4.33}$$

This simplifies the expression for two of the contributions in the effective magnetic field: First, it is obvious that the exchange field drops out as all derivatives of $\boldsymbol{m}$ vanish. Second, one finds that the demagnetization field

$$\overline{\boldsymbol{H}_{\mathrm{dem}}} = \frac{M_{\mathrm{s}}}{V_{\mathrm{m}}}\iint_{\Omega_m}\boldsymbol{R}\widehat{\boldsymbol{N}}(\widehat{\boldsymbol{x}}-\widehat{\boldsymbol{x}}')\boldsymbol{R}^{\top}\boldsymbol{m}\,\mathrm{d}\widehat{\boldsymbol{x}}\mathrm{d}\widehat{\boldsymbol{x}}' =: -M_{\mathrm{s}}\,\boldsymbol{R}\widehat{\boldsymbol{\mathcal{N}}}\boldsymbol{R}^{\top}\boldsymbol{m} \tag{4.34}$$

reduces to a matrix-vector-product of the integrated demagnetization tensor $\widehat{\boldsymbol{\mathcal{N}}}$ and the magnetization. Due to symmetry, integrating the demagnetization tensor over a sphere leads to a matrix being a multiple of the identity [28, 29]. Thus, the demagnetization

field is parallel to the magnetization and gets absorbed by taking the vector product in the LLG. For disks, however, $\widehat{\boldsymbol{\mathcal{N}}}$ is a diagonal matrix of the form

$$\widehat{\boldsymbol{\mathcal{N}}} = N_h\, \widehat{\boldsymbol{e}}_h \widehat{\boldsymbol{e}}_h^{\top} + N_r \left(\mathbf{1} - \widehat{\boldsymbol{e}}_h \widehat{\boldsymbol{e}}_h^{\top}\right) \tag{4.35}$$

with the demagnetizing factors N_h and N_r corresponding to the disk axis $\boldsymbol{e}_h$ and the in-plane directions, respectively. These factors depend on the radius-to-height ratio of the disk and can be calculated using elliptic integrals and hypergeometric series [30]. Rearranging the terms in (4.35) and omitting contributions parallel to the magnetization, the average demagnetization field takes the form

$$\overline{\boldsymbol{H}_{\mathrm{dem}}} = M_{\mathrm{s}}(N_{\mathrm{r}} - N_{\mathrm{h}})(\boldsymbol{e}_h \cdot \boldsymbol{m})\boldsymbol{e}_h, \tag{4.36}$$

which, by comparison with (2.27), corresponds to an anisotropy field with the anisotropy constant

$$K_{\mathrm{dem}} = \frac{1}{2}\mu_0 M_{\mathrm{s}}^2 (N_{\mathrm{r}} - N_{\mathrm{h}}). \tag{4.37}$$

For long rods, the anisotropy constant is positive and corresponds to an uniaxial anisotropy along the disk's symmetry axis. For flat disks, however, $K_{\mathrm{dem}} < 0$, and thus, the effect is that the field tends to maximize the angle between the magnetization and the disk axis, hence the magnetization is forced to lie in the disk plane. If the easy axis of the disk related to the magnetocrystalline uniaxial anisotropy coincides with the disk axis, one can combine the anisotropy contributions by defining the effective anisotropy constant $K_{\mathrm{eff}} = K_{\mathrm{u}} + K_{\mathrm{dem}}$. Throughout this thesis, the demagnetization field will be omitted in the single-domain approximation, bearing in mind that the anisotropy constant is adapted accordingly.

It is also worth noting that the thermal field can be simplified when taking the particle average $\overline{\boldsymbol{H}_{\mathrm{th}}}$. Recalling that $\boldsymbol{H}_{\mathrm{th}}(\widehat{\boldsymbol{x}})$ is only defined to be a Gaussian, zero-mean random variable satisfying the variance relation (4.23), it is trivial to show that $\overline{\boldsymbol{H}_{\mathrm{th}}}$ is also Gaussian distributed with zero mean. Computing the expectation variance $\left\langle \overline{H_{\mathrm{th},i}}(t)\overline{H_{\mathrm{th},}j}(t')\right\rangle$ yields

$$\begin{aligned}
\left\langle \overline{H_{\mathrm{th},i}}(t)\overline{H_{\mathrm{th},j}}(t')\right\rangle &= \frac{1}{V_{\mathrm{m}}^2}\iint_{\Omega_{\mathrm{m}}} \left\langle H_{\mathrm{th},i}(\widehat{\boldsymbol{x}},t) H_{\mathrm{th},j}(\widehat{\boldsymbol{x}}',t')\right\rangle \,\mathrm{d}\widehat{\boldsymbol{x}}\,\mathrm{d}\widehat{\boldsymbol{x}}' \\
&= \frac{1}{V_{\mathrm{m}}^2}\iint_{\Omega_{\mathrm{m}}} 2D\delta_{ij}\delta^3(\widehat{\boldsymbol{x}} - \widehat{\boldsymbol{x}}')\delta(t-t')\,\mathrm{d}\widehat{\boldsymbol{x}}\,\mathrm{d}\widehat{\boldsymbol{x}}' \\
&= \frac{2D}{V_{\mathrm{m}}}\delta(t-t') = \frac{2\alpha k_{\mathrm{B}}T}{\mu_0^2\gamma_{\mathrm{e}}M_{\mathrm{s}}V_{\mathrm{m}}}\delta(t-t').
\end{aligned} \tag{4.38}$$

Therefore, the thermal fluctuations can be modeled by a single, Gaussian, zero-mean random vector satisfying (4.38).

For completeness, the set of equations for the single-domain approximation is given by

$$\dot{\boldsymbol{\omega}} = \boldsymbol{R}\widehat{\boldsymbol{\Theta}}^{-1}\boldsymbol{R}^{\top}\left(\mu_0 M_{\mathrm{s}} V_{\mathrm{m}} \overline{\boldsymbol{m}} \times \boldsymbol{H}_{\mathrm{ext}} + \frac{M_{\mathrm{s}} V_{\mathrm{m}}}{\gamma_{\mathrm{e}}} \dot{\overline{\boldsymbol{m}}} - \gamma_{\mathrm{r}}\,\boldsymbol{\omega} + \boldsymbol{T}_{\mathrm{th}} + \boldsymbol{R}\widehat{\boldsymbol{\Theta}}\boldsymbol{R}^{\top}\boldsymbol{\omega} \times \boldsymbol{\omega}\right) \tag{4.39}$$

$$\dot{\overline{\boldsymbol{m}}} = -\frac{\gamma_{\mathrm{e}}\mu_0}{1+\alpha^2}\overline{\boldsymbol{m}} \times \overline{\boldsymbol{H}_{\mathrm{eff}}} - \frac{\alpha\gamma_{\mathrm{e}}\mu_0}{1+\alpha^2}\overline{\boldsymbol{m}} \times (\overline{\boldsymbol{m}} \times \overline{\boldsymbol{H}_{\mathrm{eff}}}) \tag{4.40}$$

$$\dot{\boldsymbol{R}} = [\boldsymbol{\omega}\times]\boldsymbol{R}, \tag{4.41}$$

with $\boldsymbol{H}_{\mathrm{eff}}$ being the same effective field as for the full model, except that the exchange field and the demagnetization field for spheres and cubes can be omitted.

4.4 Rigid dipole approximation

Another approximation can be obtained when not only considering a uniform magnetization but also assuming that $\boldsymbol{m}$ is strictly bound to the anisotropy axis $\boldsymbol{n}$. This commonly used, so-called rigid dipole approximation [31] shows to be very applicable for small particles under the influence of weak external fields, where the exchange and anisotropy field dominate the other contributions and the anisotropy energy is large compared to the thermal energy. As magnetic relaxation happens at much shorter time scales than mechanical rotation, the magnetization will settle nearly instantaneously aligned with the anisotropy axis and thus, rotate along with the particle as

$$\dot{\overline{\boldsymbol{m}}} = \boldsymbol{\omega} \times \overline{\boldsymbol{m}}. \tag{4.42}$$

Substituting into (4.40) results in the rigid equations

$$\begin{aligned}
\dot{\boldsymbol{\omega}} &= \boldsymbol{R}\widehat{\boldsymbol{\Theta}}^{-1}\boldsymbol{R}^{\top}\left(\mu_0 M_{\mathrm{s}} V_{\mathrm{m}} \overline{\boldsymbol{m}} \times (\boldsymbol{H}_{\mathrm{ext}} - \frac{\boldsymbol{\omega}}{\gamma_{\mathrm{e}}\mu_0}) - \gamma_{\mathrm{r}}\,\boldsymbol{\omega} + \boldsymbol{T}_{\mathrm{th}} + \boldsymbol{R}\widehat{\boldsymbol{\Theta}}\boldsymbol{R}^{\top}\boldsymbol{\omega} \times \boldsymbol{\omega}\right) \\
\dot{\overline{\boldsymbol{m}}} &= \boldsymbol{\omega} \times \overline{\boldsymbol{m}} \\
\dot{\boldsymbol{R}} &= [\boldsymbol{\omega}\times]\boldsymbol{R}.
\end{aligned} \tag{4.43}$$

4.5 Overdamped limit

For either the complete model or any of the latter approximations, the equation of motion for the angular velocity can be further simplified for small particles. For these, inertia tends to be negligible [31, 32]. It is argued that the viscous damping happens so quickly that the particle is essentially always moving with its terminal velocity. Taking the general equation

$$\boldsymbol{R}\widehat{\boldsymbol{\Theta}}^{-1}\boldsymbol{R}^{\top}\dot{\boldsymbol{\omega}} = \boldsymbol{T}(t,\boldsymbol{m},\boldsymbol{R},\boldsymbol{\omega}) - \gamma_{\mathrm{r}}\,\boldsymbol{\omega} + \boldsymbol{R}\widehat{\boldsymbol{\Theta}}\boldsymbol{R}^{\top}\boldsymbol{\omega}\times\boldsymbol{\omega} \tag{4.44}$$

for an arbitrary torque $\boldsymbol{T}$ containing all thermal and magnetic contributions, and let inertia approach zero, on arrives at the equation

$$\boldsymbol{\omega} = \frac{\boldsymbol{T}(t,\boldsymbol{m},\boldsymbol{R},\boldsymbol{\omega})}{\gamma_{\mathrm{r}}}. \tag{4.45}$$

In all discussed sets of equations, τ contains a ω-dependence, caused by the Barnett effect or as a consequence of the rigid equation of motion. These terms are bound by

$$\frac{M_{\mathrm{s}}V_{\mathrm{m}}}{\gamma_{\mathrm{e}}}\,|\boldsymbol{\omega}|, \tag{4.46}$$

thus can be omitted in (4.45) if the friction parameter γ_{r} exceeds

$$\gamma_{\mathrm{r}} \gg \frac{M_{\mathrm{s}}V_{\mathrm{m}}}{\gamma_{\mathrm{e}}}\,, \tag{4.47}$$

which, for spheres without a surfactant layer is equivalent to

$$\eta \gg \frac{M_{\mathrm{s}}}{6\gamma_{\mathrm{e}}}\,. \tag{4.48}$$

Plugging in common material parameters, the viscosity of the carrier fluid usually exceeds the right-hand side by at least two orders of magnitude and therefore allows to neglect these contributions. (4.45) thus becomes

$$\boldsymbol{\omega} = \frac{1}{\gamma_{\mathrm{r}}}\left(\mu_0 M_{\mathrm{s}}V_{\mathrm{m}}\overline{\boldsymbol{m}}\times\boldsymbol{H}_{\mathrm{ext}} + \frac{M_{\mathrm{s}}V_{\mathrm{m}}}{\gamma_{\mathrm{e}}}\overline{\dot{\boldsymbol{m}}}|_{\boldsymbol{\omega}=0} + \boldsymbol{T}_{\mathrm{th}}\right). \tag{4.49}$$

4.6 Heat dissipation

For the application of hyperthermia, the most important quantity is the amount of energy dissipated by the external excitation of the dipole which is transferred to the carrier fluid. Taking the Hamiltonian

$$\mathcal{H} = \mathcal{T} + \mathcal{V} = \frac{1}{2}\boldsymbol{\omega}^\top \boldsymbol{R}\widehat{\boldsymbol{\Theta}}\boldsymbol{R}^\top\boldsymbol{\omega} + E_{\mathrm{mag}}[\boldsymbol{m}, \boldsymbol{R}, t], \tag{4.50}$$

the rate of change of energy is given by the total time derivative [32]

$$\frac{\mathrm{d}\mathcal{H}}{\mathrm{d}t} = \frac{\partial\mathcal{H}}{\partial t} + \frac{\partial\mathcal{H}}{\partial\boldsymbol{\omega}}\cdot\dot{\boldsymbol{\omega}} + \int_{\Omega_\mathrm{m}} \frac{\partial\mathcal{H}}{\partial\boldsymbol{m}}\cdot\dot{\boldsymbol{m}}\,\mathrm{d}\widehat{\boldsymbol{x}} - \boldsymbol{T}_{\mathrm{mech}}\cdot\boldsymbol{\omega}. \tag{4.51}$$

Since the only time-dependent term is the Zeeman energy, we identify it with the hysteresis power, i.e. the energy that is pumped into the system by the external field. The other terms correspond to the heat dissipated by viscous and Gilbert damping, which in fact do not need to be evaluated: Assuming periodic excitation, the motion of the particle will also be periodic after an initial relaxation into a steady state. While inertial effects can lead to periodic behavior at time scales longer than the excitation frequency or even to chaotic motion, averaging over an ensemble of independent particles results in a steady state corresponding to the excitation signal. Consequently, for large times t, the evolution of the average energy is also periodic:

$$\langle\mathcal{H}[\boldsymbol{m}(t), \boldsymbol{R}(t), t]\rangle = \langle\mathcal{H}[\boldsymbol{m}(t+\tau), \boldsymbol{R}(t+\tau), t+\tau]\rangle\,, \tag{4.52}$$

where τ is the period of the external field. From this follows that

$$\int_t^{t+\tau} \left\langle\frac{\mathrm{d}\mathcal{H}}{\mathrm{d}t}\right\rangle \mathrm{d}t = 0. \tag{4.53}$$

This indicates that, in the steady state, the net energy transfer between the particle and the environment over one oscillation period of the external field is zero. Therefore, the energy that is transferred to the carrier fluid within one oscillation period equals the net energy that the particle gains from the external excitation given by

$$\langle E_{\mathrm{hyst}}\rangle = \int_t^{t+\tau} \left\langle\frac{\partial\mathcal{H}}{\partial t}\right\rangle \mathrm{d}t = -\mu_0 M_\mathrm{s} V_\mathrm{m} \int_t^{t+\tau} \langle\overline{\boldsymbol{m}}\rangle\cdot\dot{\boldsymbol{H}}_{\mathrm{ext}}\,\mathrm{d}t, \tag{4.54}$$

from which can be obtained the specific loss power (SLP) defined as the rate of dissipated power normalized to the unit mass of the particle [33]

$$\mathrm{SLP} = -\frac{\mu_0 M_\mathrm{s} V_\mathrm{m}}{\rho V\tau} \int_t^{t+\tau} \langle\overline{\boldsymbol{m}}\rangle\cdot\dot{\boldsymbol{H}}_{\mathrm{ext}}\,\mathrm{d}t. \tag{4.55}$$

5 Numerical implementation

The lack of integration between micromagnetics and molecular dynamics is evident in the absence of comprehensive numerical frameworks capable of modeling both external and internal degrees of freedom. To address this and facilitate future extensions, it has been chosen to start with two established code libraries from each research area. These libraries offer a wide range of features that extend far beyond the scope of this thesis. The molecular dynamics part is carried out by *ESPResSo* [34], a C++-based library offering particle-particle interactions as well as hydrodynamic models and active matter, where most relevant to the scope of this thesis is its efficient integrator for the Langevin equation. For the micromagnetic part, it is made use of *magnum.np* [35], a PyTorch-based finite-difference simulation package with GPU acceleration. The merge of these libraries is done by a custom-written Python package.
The first section of this chapter is devoted to the custom-written code library, after which the transition to the micromagnetic model will be elaborated. Finally, the proposed time integration will be briefly described.

5.1 mmhd - A micromagnetic hydrodynamics solver

The development of a coupled solver library was motivated by the performance and readability demonstrated by magnum.np, which combines high computational efficiency with user-friendly simulation scripts. The goal is to extend these advantages to coupled problems, despite the constraints posed by ESPResSo's closed environment. ESPResSo is highly optimized for pre-initialized problems that do not require dynamic data access during the simulation run. However, when running simulations that demand real-time data exchange, accessing values from an ESPResSo instance can be slow due to its MPI (Message Passing Interface) capability for parallelization and its communication bridge with Python. The MPI integration has the additional consequence that updating a particle's state typically triggers a recalculation of all forces. This process can introduce performance bottlenecks and may lead to unexpected behavior and significant systematic errors in time integration.

The mmhd framework aims to provide a user-friendly platform for various simulation types, enabling the initialization of magnum.np and ESPResSo instances with the specified parameters while ensuring consistency in the time integrator and optimizing performance. It also automates the necessary conversions between different coordinate and unit systems, which will be discussed in detail in the following sections.

5.2 Discrete micromagnetics

In the finite difference scheme, continuous scalar or vector fields, such as the magnetization of a particle are coarse-grained over rectangular cells. A single value $\boldsymbol{m}_i$ associated with the midpoint $\boldsymbol{x}_i$ of each cell represents the value of the field throughout the cell, approximating the continuous function by a discontinuous step function. The particle frame coordinates $\widehat{\boldsymbol{x}}_i = (\hat{x}_i, \hat{y}_i, \hat{z}_i)^\top$ are arranged in a regular (equidistant) fashion, spanning a cuboidal region of size $L_x \times L_y \times L_z$ as

$$\begin{aligned} -L_x/2 < \hat{x}_i < L_x/2 \\ -L_y/2 < \hat{y}_i < L_y/2 \\ -L_z/2 < \hat{z}_i < L_x/2, \end{aligned} \tag{5.1}$$

where each of the cells has a volume $V = \Delta x \Delta y \Delta z$. Setting the origin to the center of mass, the coordinates in the lab frame can be thus written as $\boldsymbol{x}_i = \boldsymbol{R}\widehat{\boldsymbol{x}}_i$. To simulate a non-cuboidal shape, we embed it in the simulation box and set the magnetization to zero outside the magnetic domain Ω_m, ensuring that the sum of the cell volumes inside the magnetic domain approaches V_m.

Given the LLG in its continuous form, the corresponding discretized differential equation for each of the N cell magnetizations $\boldsymbol{m}_i$ can be derived as

$$\dot{\boldsymbol{m}}_i = \boldsymbol{F}_i(\boldsymbol{m}_1, \dots \boldsymbol{m}_N, \boldsymbol{R}\widehat{\boldsymbol{x}}_1, \dots \boldsymbol{R}\widehat{\boldsymbol{x}}_N), \tag{5.2}$$

where $\boldsymbol{F}_i$ is a function that can depend on each of the magnetization values and the positions of the corresponding cells. Particularly for micromagnetic-affine readers, it is emphasized that this list of differential equations is sufficient for the description of the problem, and why we constrain ourselves to impose the particles's structure in our computations has to be well thought out. The motivation behind this is the following: The molecular dynamics library needs to be provided with quantities in the laboratory frame, and we want to minimize the number of reference frame conversions during the hot loop of the time integration. In addition, the GPU parallelization of PyTorch should be efficiently used, which is achieved by expressing (parts of) the functions $\boldsymbol{F}_i$ in terms of elementary functions acting on an array storing all magnetization values. The first question is in which coordinate system to store the magnetization values.
The following analysis is split into two parts: First, we look at the case of working in the laboratory frame and investigate the form of $\boldsymbol{F}_i$ for each of the field contributions involved in this thesis.

The first group of fields comprised of the external and Barnett field as well as the thermal fluctuations only depend on the magnetization and the volume of the respective cell and thus are invariant under the change of the rotation coordinate $\boldsymbol{R}$ and take the same form for each cell $\boldsymbol{F}_i(\boldsymbol{m}_i) = \boldsymbol{F}(\boldsymbol{m}_i)$. The latter is true for the anisotropy field, which however depends on the particle's orientation since $\boldsymbol{n}$ is given by $\boldsymbol{R}\widehat{\boldsymbol{n}}$ with $\widehat{\boldsymbol{n}} = \text{const}$. Because no other magnetization values are involved, any quantity obtained

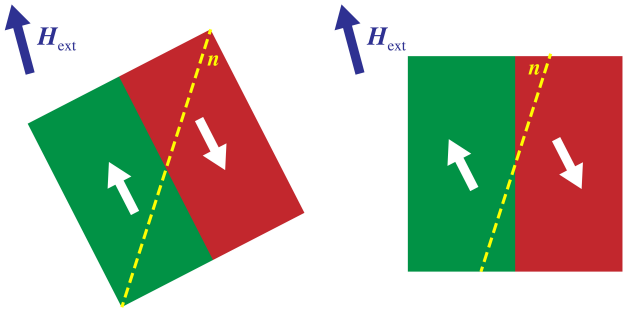

Fig. 1: **Laboratory frame micromagnetics.** Given the physical configuration of a particle with easy axis in the [111] direction (left), the numerical representation (right) in a cell system aligned with the standard axes yields equivalent averages, energies, and dynamics for external, anisotropy, and exchange interactions.

by averaging over all cells, such as the macrospin $\overline{\boldsymbol{m}}$ is independent of the structural arrangement of the cells.

In contrast, this is not true for the exchange field: Its torque is given by a function of the form

$$\boldsymbol{F}_i^{\text{ex}} = \boldsymbol{F}_i^{\text{ex}}(\boldsymbol{m}_i, \boldsymbol{m}_{n_1(i)}, \dots \boldsymbol{m}_{n_6(i)}), \tag{5.3}$$

where $n_1(i), \dots n_6(i)$ denote the indeces of the 6 neighboring cells of cell i, with exception of the boundary cells. At this point, it is obvious to be beneficial to store the magnetization values in a three-dimensional grid labeled by $\boldsymbol{m}_{i,j,k}$ such that $\boldsymbol{F}_{i,j,k}^{\text{ex}}$ can be expressed as $\boldsymbol{F}_{i,j,k}^{\text{ex}}(\boldsymbol{m}_i, \boldsymbol{m}_{i\pm1,j\pm1,k\pm1})$ and Python slicing operators can be used to access the magnetization values of the neighboring cells.

This derivation may seem redundant to readers familiar with micromagnetic simulations, yet introduced a model that is not equivalent to the commonly used one which stores quantities in the particle frame of reference. The difference is best explained visually (Fig. 1) for the example of a cubical particle in a domain-wall state. Of the contributions discussed up to this point, only the anisotropy depends on the particle orientation, which thus can be incorporated by updating the easy axis $\boldsymbol{n}$ during time integration. Working in the laboratory frame has the benefit of not requiring any coordinate system conversions of large arrays, thus facilitating more advanced simulation models such as the transfer of the whole magnetization state to the molecular dynamics solver for the simulation of magnetic interactions between micromagnetically described particles.

However, this enhancement is thwarted by the introduction of the demagnetization

field. In magnum.np, the demagnetization field is calculated via a demagnetization kernel that needs to be initialized at the first call of the field. This kernel is obtained by restructuring the Fourier transform of the demagnetization tensor $\widehat{\boldsymbol{N}}$, which necessarily needs to be evaluated in the particle frame, as the respective laboratory frame quantity is not constant under rotation. During integration, one could evaluate $\boldsymbol{N} = \boldsymbol{R}\widehat{\boldsymbol{N}}\boldsymbol{R}^\top$ or compute the particle frame magnetization $\widehat{\boldsymbol{m}} = \boldsymbol{R}^\top \boldsymbol{m}$ for all cells at each time step, which for the present model has not been implemented.

Instead, it has been chosen a particle frame description. Here, the evolution of the magnetization is given by

$$\dot{\widehat{\boldsymbol{m}}}_{i,j,k} = \widehat{\boldsymbol{F}}_{i,j,k}(\widehat{\boldsymbol{m}}_{0,0,0}, \ldots, \widehat{\boldsymbol{x}}_{0,0,0}, \ldots) + \widehat{\boldsymbol{m}}_{i,i,k} \times \boldsymbol{\omega}, \tag{5.4}$$

with the additional cross-product term of the magnetization and the angular velocity of the body. The functions $\widehat{\boldsymbol{F}}_{i,j,k}$ are related to their laboratory frame counterpart by

$$\widehat{\boldsymbol{F}}_{i,j,k}(\widehat{\boldsymbol{m}}_{0,0,0}, \ldots, \widehat{\boldsymbol{x}}_{0,0,0}, \ldots) = \boldsymbol{R}^\top \boldsymbol{F}_{i,j,k}(\boldsymbol{R}\widehat{\boldsymbol{m}}_{0,0,0}, \ldots, \boldsymbol{R}\widehat{\boldsymbol{x}}_{0,0,0}, \ldots). \tag{5.5}$$

We reexamine the contributions of each field. The thermal field remains rotation-independent, as multiplying it by $\boldsymbol{R}$ does not alter its statistical properties. For the external field, we note that to obtain $\widehat{\boldsymbol{F}}$ when given $\boldsymbol{H}_{\text{ext}}$ in the lab frame, this requires a rotation by $\boldsymbol{R}^\top$. In return, the dependencies for the anisotropy and demagnetization field are lifted, which is obvious as they do not involve interactions with the environment of the particle. Finally, the exchange energy is again rotation-independent.

The particle frame representation offers the advantage of not requiring coordinate system transformations of large arrays during time integration, given that the magnetization array is not transferred to the molecular dynamics solver. Only the external field needs to be transformed to the rotating coordinate system, and the average torques required in the mechanical equation of motion need to be transformed back to the laboratory frame. Additionally, no modifications have been made to magnum.np, allowing us to benefit from future updates and improvements.

5.3 Ensembles of Single-domain particles

The present micromagnetic solver allows for the simulation of a single particle discretized into an arbitrary amount of cells. Due to the ergodicity of the system, this approach should theoretically enable us to obtain time averages equivalent to those of a large ensemble. However, in practice, this is not computationally feasible. Therefore, this thesis also intensively studies the single-domain approximation, leveraging PyTorch's parallelization features not for multiple cells of one particle, but for a large ensemble of single-domain particles.

In this approach, the only field contributions come from the external, Barnett, and

thermal fields, as well as the anisotropy interaction. The discretization cells do not represent a continuous vector field $\boldsymbol{m}$, but rather values for individual dipoles. The cell volume is set to match the volume of the particle's magnetic domain, regardless of its exact shape.

Magnum.np also allows for the anisotropy to be set individually for each cell. For these simulations, it is necessary to transfer the entire magnetization array to ESPResSo, as each particle is treated separately with individual coordinates $\boldsymbol{m}_i, \boldsymbol{R}_i$ and $\boldsymbol{\omega}_i$. Given the prior discussion, working in the laboratory frame is superior for these simulations.

5.4 Reduced units

Because some features in ESPResSo are limited to working with single-precision floating point numbers, we need to rescale our material parameters in such a way that their range of magnitude becomes narrower, improving the numerical stability of the solver. For the present implementation, the rescaling system of Kaiser [36] has been adapted which is given by

$$[\text{energy}] = 10 k_\text{B} T_\text{room} = 4.05 \times 10^{-20}\,\text{J} \tag{5.6}$$

$$[\text{length}] = R \tag{5.7}$$

$$[\text{mass}] = 1000\,\text{kg/m}^3 \times [\text{length}]^3 \tag{5.8}$$

$$[\text{time}] = [\text{length}] \times [\text{mass}]^{\frac{1}{2}} \times [\text{energy}]^{-\frac{1}{2}} \tag{5.9}$$

$$[\text{electric current}] = M_\text{s} V_\text{m} \times [\text{length}]^{-2}, \tag{5.10}$$

where R is the radius of the particle. Ideally, both magnum.np and ESPResSo are provided with the simulation parameters in the reduced unit system, but it has been decided to maintain SI units in the micromagnetic solver because the Runge-Kutta integrator and possibly other elements of magnum.np are optimized for typical magnetic parameters in SI units. Hence, the values to be transfered between the two software packages are converted at each time step, using a custom-build unit conversion class.

5.5 Time integration

Using two isolated software packages written in different programming languages prevents us from solving the coupled equations of motion in a self-consistent fashion. However, sufficient accuracy can be achieved by solving the LLG equation with the micromagnetic solver and the Langevin equation with the molecular dynamics solver separately, allowing them to communicate at small time intervals. In magnum.np, time integration is done using the Runge–Kutta–Fehlberg 4(5) (RKF45) method with an adaptive time step. ESPResSo, on the other hand, uses an adapted rotational version of the Velocity-Verlet algorithm [37, 38], expressing the particle's orientation by quaternions $\boldsymbol{q}$ and having a fixed time step.

As discussed, for the micromagnetic problem, the solver is storing the magnetization in the particle frame of reference, therefore the LLG with the additional term $\widehat{\boldsymbol{m}} \times \boldsymbol{\omega}$ should be integrated. However, the term is omitted instead, and the rotation of the magnetization in the particle frame is done after the mechanical integration to avoid an incorrect drift of the laboratory frame magnetization. This would be caused by the evident mismatch of the Runge-Kutta and velocity-Verlet integrator.

Consider, for example, the situation of a spherical particle subject to only the exchange energy at zero temperature, rotating with an initial angular velocity. If the magnetization initially is in a relaxed state, it holds that $\dot{\boldsymbol{m}} = 0$ until eternity, therefore $\dot{\widehat{\boldsymbol{m}}} = \widehat{\boldsymbol{m}} \times \boldsymbol{\omega}$. Integrating the mechanical equations $\Theta\dot{\boldsymbol{\omega}} = -\gamma_{\mathrm{r}}\boldsymbol{\omega}$ and $\dot{\boldsymbol{R}} = [\boldsymbol{\omega}\times]\boldsymbol{R}$ yields a trajectory $\boldsymbol{R}(t)$. Given that $\boldsymbol{m}(t) = \boldsymbol{R}(t)\widehat{\boldsymbol{m}}(t)$, it is certain that the obtained trajectory $\boldsymbol{m}(t)$ stays not constant in time since $\widehat{\boldsymbol{m}}$ and $\boldsymbol{R}$ are obtained by different integration methods. Because we are most interested in the accurate description of $\boldsymbol{m}(t)$, we force it to be, at least in the absence of coupling interactions, to equal the solution of the micromagnetic integrator. This issue does not affect the simulation of single-domain particles since the micromagnetic integrator already gives $\boldsymbol{m}(t)$ in the lab frame.

The entire integration algorithm is as follows:

Propagation of the magnetization

$$\boldsymbol{m}_{t+\Delta t} = \boldsymbol{R}(\boldsymbol{q}_t)\widehat{\mathcal{L}}_{\mathrm{RKF45}}[\widehat{\boldsymbol{\omega}}_t, \boldsymbol{q}_t]_{t+\Delta t,t}(\widehat{\boldsymbol{m}}_t) \quad \text{(micromagnetic)}$$

$$\boldsymbol{m}_{t+\Delta t} = \mathcal{L}_{\mathrm{RKF45}}[\boldsymbol{\omega}_t, \boldsymbol{q}_t]_{t+\Delta t,t}(\boldsymbol{m}_t) \quad \text{(single-domain)}$$

Propagation of the angular velocity for a half-step

$$\widehat{\boldsymbol{\omega}}_{t+\Delta t/2} = \boldsymbol{\omega}_t + \frac{\Delta t}{2}\widehat{\boldsymbol{\Theta}}^{-1}\left(\boldsymbol{R}^{\top}(\boldsymbol{q}_t)\boldsymbol{T}(\overline{\boldsymbol{m}}_t, \boldsymbol{\omega}_{t-\Delta t/2}, \boldsymbol{q}_t, t) + \widehat{\boldsymbol{\Theta}}\widehat{\boldsymbol{\omega}}_t \times \widehat{\boldsymbol{\omega}}_t\right)$$

Propagation of the quaternion

$$\boldsymbol{q}_{t+\Delta t} = (1-\lambda)\boldsymbol{q}_t + \Delta t\, \dot{\boldsymbol{q}}_t + \frac{\Delta t^2}{2}\ddot{\boldsymbol{q}}_t$$

Propagation of the angular velocity for the second half-step

$$\widehat{\boldsymbol{\omega}}^{(0)}_{t+\Delta t} = \widehat{\boldsymbol{\omega}}_{t+\Delta t/2} + \frac{\Delta t}{2}\widehat{\boldsymbol{\Theta}}^{-1}\boldsymbol{R}^{\top}(\boldsymbol{q}_{t+\Delta t})\boldsymbol{T}(\overline{\boldsymbol{m}}_{t+\Delta t}, \boldsymbol{\omega}_{t+\Delta t/2}, \boldsymbol{q}_{t+\Delta t}, t+\Delta t)$$

Rotation of the particle frame magnetization (only micromagnetic)

$$\widehat{\boldsymbol{m}}_{t+\Delta t} = \boldsymbol{R}^{\top}(\boldsymbol{q}_{t+\Delta t})\boldsymbol{m}_{t+\Delta t}$$

The colors indicate whether an equation or quantity is evaluated in ESPResSo (turquoise), magnum.np (purple) or the custom-written code (black).
The operator $\mathcal{L}_{\mathrm{RKF45}}[\boldsymbol{\omega}_t, \boldsymbol{q}_t]_{t+\Delta t,t}(\boldsymbol{m}_t)$ denotes that the magnetization at time t is integrated with the RKF45 method until the time $t+\Delta t$, where the quaternion and angular velocity are taken as parameters and held constant at time t. For the sake of this overview, $\boldsymbol{R}(\boldsymbol{q}_t)$ describes the rotation matrix associated with $\boldsymbol{q}_t$, whereas in the code the transformation is directly applied via a quaternion-vector multiplication, which will not be elaborated further.

One of the benefits of working in a reduced system of units is that the reduced time step for the Velocity-Verlet integrator is supposed to be independent of the SI material parameters. However, the proposed scales are based on a hydrodynamic simulation that differs from the present system. Concerning the numerical stability, there exists an upper limit for the time step caused by the frictional term in the explicit integration of the angular velocity given by

$$\widehat{\boldsymbol{\omega}}^{(0)}_{t+\Delta t} = \widehat{\boldsymbol{\omega}}_{t+\Delta t/2} - \frac{\Delta t}{2}\gamma_{\mathrm{r}}\widehat{\boldsymbol{\Theta}}^{-1}\widehat{\boldsymbol{\omega}}_{t+\Delta t/2} = \left(\mathbf{1} - \frac{\Delta t}{2}\gamma_{\mathrm{r}}\widehat{\boldsymbol{\Theta}}^{-1}\right)\widehat{\boldsymbol{\omega}}_{t+\Delta t/2}, \tag{5.11}$$

which requires

$$\Delta t < \frac{2\widehat{\Theta}_{ii}}{\gamma_{\mathrm{r}}} \quad \text{for} \quad i = 1,2,3 \tag{5.12}$$

to ensure that the angular velocity does not increase due to friction, preventing divergence. For isotropic particles, this condition simplifies to $\Delta t < 2\tau_\omega$. Although the time step must be significantly smaller than this upper bound to accurately model inertial effects, for processes with longer time scales, the time step can approach this limit, resulting in near-overdamped trajectories.

6 Equilibrium properties

Static problems are helpful in understanding the properties of a fluctuating system, as there often can be derived exact expressions for equilibrium quantities. Hereby, we do not care about time evolution, but only the average of a quantitiy over a large timespan or a sample of multiple, identical, non-interacting particles. If we impose the external field to be constant, one obtains the time-independent Hamiltonian

$$\mathcal{H} = \mathcal{T} + \mathcal{V} = \frac{1}{2}\widehat{\boldsymbol{L}}^{\top}\widehat{\boldsymbol{\Theta}}^{-1}\widehat{\boldsymbol{L}} + E_{\mathrm{mag}}[\boldsymbol{m}, \boldsymbol{R}] \tag{6.1}$$

where the magnetic potential E_{mag} is given by

$$E_{\mathrm{mag}}[\boldsymbol{m}, \boldsymbol{R}] = E_{\mathrm{ext}}[\boldsymbol{m}] + E_{\mathrm{ex}}[\boldsymbol{m}] + E_{\mathrm{ani}}[\boldsymbol{m}, \boldsymbol{R}] + E_{\mathrm{dem}}[\boldsymbol{m}, \boldsymbol{R}]. \tag{6.2}$$

However, it is much more practical to express the potential in terms of the magnetization $\widehat{\boldsymbol{m}}$ in the particle frame because removes the rotational dependency of the anisotropy and demagnetization term and only introduces a trivial dependence in the external field term. Thus, the potential can be equivalently expressed as

$$E_{\mathrm{mag}}[\widehat{\boldsymbol{m}}, \boldsymbol{R}] = E_{\mathrm{ext}}[\widehat{\boldsymbol{m}}, \boldsymbol{R}] + E_{\mathrm{ex}}[\widehat{\boldsymbol{m}}] + E_{\mathrm{ani}}[\widehat{\boldsymbol{m}}] + E_{\mathrm{dem}}[\widehat{\boldsymbol{m}}]. \tag{6.3}$$

To study the parameter dependence, it is helpful to normalize the potential by the magnetostatic energy

$$E_{\mathrm{m}} = \frac{\mu_0 M_{\mathrm{s}}^2 V_{\mathrm{m}}}{2} \tag{6.4}$$

which, expressed in terms of particle frame quantities, yields

$$\mathcal{E} = \frac{E_{\mathrm{mag}}}{K_{\mathrm{m}}} = -\frac{2H_{\mathrm{ext}}}{M_{\mathrm{s}}}\overline{\widehat{\boldsymbol{m}}} \cdot \boldsymbol{R}^{\top}\boldsymbol{h} - \frac{H_{\mathrm{K}}}{M_{\mathrm{s}}}\overline{(\widehat{\boldsymbol{m}} \cdot \widehat{\boldsymbol{n}})^2} + l_{\mathrm{ex}}^2\overline{(\boldsymbol{\nabla}\widehat{\boldsymbol{m}})^2} - \overline{\widehat{\boldsymbol{m}} \cdot \left(\widehat{\boldsymbol{N}} * \widehat{\boldsymbol{m}}\right)}, \tag{6.5}$$

where the external field is given by $\boldsymbol{H}_{\mathrm{ext}} = H_{\mathrm{ext}}\boldsymbol{h}$ and

$$l_{\mathrm{ex}} = \sqrt{\frac{AV_{\mathrm{m}}}{E_{\mathrm{m}}}} \tag{6.6}$$

denotes the so-called exchange length. The strength of the anisotropy interaction is given by the coercivity $H_{\mathrm{K}} = 2K_{\mathrm{u}}/\mu_0 M_{\mathrm{s}}$.

It is beneficial to extract the volume dependence of the averages in the energy function and integrate it into the parameters. To do so, we fix a state for $\boldsymbol{m}$, for example, a distinct vortex state, and expand the particle equally in all directions, thereby expanding the magnetization configuration as well. This can be formally written as

$$\widehat{\boldsymbol{x}} \mapsto \lambda \widehat{\boldsymbol{x}} \tag{6.7}$$

$$\boldsymbol{m}(\widehat{\boldsymbol{x}}) \mapsto \boldsymbol{m}(\lambda \widehat{\boldsymbol{x}}). \tag{6.8}$$

It can be shown that the external field, demagnetization, and anisotropy terms remain invariant under this transformation. However, the exchange term scales with $1/\lambda^2$, which means the reduced potential is not invariant if the exchange length l_{ex} is kept constant. To circumvent this, we define the "diameter" of the particle d as a characteristic length scale that is specific to the shape of the particle. For spheres and disks, d should correspond to their actual diameter, while for cubes, it should correspond to their side length. Incorporating this characteristic length into the expression for the potential yields:

$$\mathcal{E} = -\frac{2H_{\mathrm{ext}}}{M_{\mathrm{s}}}\overline{\widehat{\boldsymbol{m}}} \cdot \boldsymbol{R}^{\top}\boldsymbol{h} - \frac{H_{\mathrm{K}}}{M_{\mathrm{s}}}\overline{(\widehat{\boldsymbol{m}} \cdot \widehat{\boldsymbol{n}})^2} + \left(\frac{l_{\mathrm{ex}}}{d}\right)^2 \overline{d^2(\boldsymbol{\nabla}\widehat{\boldsymbol{m}})^2} - \overline{\widehat{\boldsymbol{m}} \cdot (\widehat{\boldsymbol{N}} * \widehat{\boldsymbol{m}})}. \tag{6.9}$$

Thus, for all particle shapes, $\mathcal{E}$ is invariant under these scaling transformations when keeping l_{ex}/d constant.

6.1 Energy minimization

First, we want to look at the ground state configuration for a given set of shape and material parameters. For a mobile system, in which the particle can rotate, the ground state configuration $(\widehat{\boldsymbol{m}}_0, \boldsymbol{R}_0)$ is formally defined by minimizing the energy functional

$$\mathcal{E}_0 = \mathcal{E}[\widehat{\boldsymbol{m}}_0, \boldsymbol{R}_0] = \min_{\substack{\widehat{\boldsymbol{m}} \in \mathcal{F}(\Omega_{\mathrm{m}}) \\ \boldsymbol{R} \in \mathrm{SO}(3)}} \mathcal{E}[\widehat{\boldsymbol{m}}, \boldsymbol{R}], \tag{6.10}$$

where $\mathcal{F}(\Omega_{\mathrm{m}})$ is the set of all vector fields defined in the magnetic domain Ω_{m} which satisfy the unit sphere and boundary constraint

$$|\boldsymbol{m}(\widehat{\boldsymbol{x}})| = 1 \quad \forall \widehat{\boldsymbol{x}} \in \Omega_{\mathrm{m}} \tag{6.11}$$

$$\boldsymbol{m}(\widehat{\boldsymbol{x}}) \times \frac{\partial \boldsymbol{m}}{\partial \boldsymbol{n}}(\widehat{\boldsymbol{x}}) = 0 \quad \forall \widehat{\boldsymbol{x}} \in \partial\Omega_{\mathrm{m}}. \tag{6.12}$$

A required, but not sufficient criterion for the ground state configuration is that both the magnetic and mechanical variation vanish for arbitrary displacements. These are

given by

$$\boldsymbol{m}(\widehat{\boldsymbol{x}}) \times \boldsymbol{H}_{\text{eff}}(\widehat{\boldsymbol{x}}) = 0 \quad \forall \widehat{\boldsymbol{x}} \in \Omega_{\text{m}} \tag{6.13}$$

$$\overline{\boldsymbol{m} \times \boldsymbol{H}_{\text{dem}}} + \overline{\boldsymbol{m} \times \boldsymbol{H}_{\text{ani}}} + \overline{\boldsymbol{m} \times \boldsymbol{H}_{\text{ex}}} = 0, \tag{6.14}$$

which, after substituting the first condition into the second is equivalent to

$$\boldsymbol{m}(\widehat{\boldsymbol{x}}) \times \boldsymbol{H}_{\text{eff}}(\widehat{\boldsymbol{x}}) = 0 \quad \forall \widehat{\boldsymbol{x}} \in \Omega_{\text{m}} \tag{6.15}$$

$$\overline{\boldsymbol{m}} \times \boldsymbol{H}_{\text{ext}} = 0. \tag{6.16}$$

We could thus use any numerical minimizer to look for extreme points that satisfy both conditions, but instead, we can apply a useful trick: It can be seen in the energy functional (6.9) that the external field poses the only contribution that causes anisotropy in the laboratory frame perspective. So instead of trying to satisfy (6.16) by varying $\boldsymbol{m}$, we can impose it by adapting the external field term to always be parallel to $\overline{\boldsymbol{m}}$ by setting

$$\boldsymbol{H}_{\text{ext}} = H_{\text{ext}} \frac{\overline{\boldsymbol{m}}}{|\overline{\boldsymbol{m}}|}. \tag{6.17}$$

Hence, (6.16) vanishes and moreover, we removed the rotational degree of freedom from the energy functional which takes now the form

$$\mathcal{E} = -\frac{2H_{\text{ext}}}{M_{\text{s}}} |\overline{\widehat{\boldsymbol{m}}}| - \frac{H_{\text{K}}}{M_{\text{s}}} \overline{(\widehat{\boldsymbol{m}} \cdot \widehat{\boldsymbol{n}})^2} + \left(\frac{l_{\text{ex}}}{d}\right)^2 \overline{d^2 (\boldsymbol{\nabla} \widehat{\boldsymbol{m}})^2} - \overline{\widehat{\boldsymbol{m}} \cdot \left(\widehat{\boldsymbol{N}} * \widehat{\boldsymbol{m}}\right)}. \tag{6.18}$$

With this functional, we can perform energy minimization with the magnetization as the only degree of freedom to obtain the ground state of a mobile particle. In addition, we obtained the order parameter $|\overline{\boldsymbol{m}}|$ that represents both the magnitude of the macrospin of the particle as well as its projection onto the external field. As the external field increases, its value should approach $|\overline{\boldsymbol{m}}| = 1$, for zero field its value is governed by the other contributions. It seems we changed the effect of the external field from an anisotropic bias to an isotropic aligning interaction akin to the exchange interaction but with infinite range and equally weighting all other spins of the particle.

In the absence of an external magnetic field, the phase space of magnetic spheres exhibits two distinct configurations, as illustrated in Fig. 2. When the magnetic anisotropy is small or the diameter of the sphere is large, the magnetization tends to form a vortex state. In this state, the vortex axis, and consequently the macrospin, is perpendicular to the anisotropy axis (Fig. 3). As the particle radius decreases, the vortex configuration becomes unstable, leading to a transition where a uniform magnetization becomes the energetically favorable configuration. For anisotropies smaller than $H_{\text{K}} < M_{\text{s}}/2$, this transition is relatively smooth. The spins initially tangent to the vortex gradually realign to point along the vortex axis. However, for higher

anisotropy values, this transition occurs abruptly at a specific threshold.

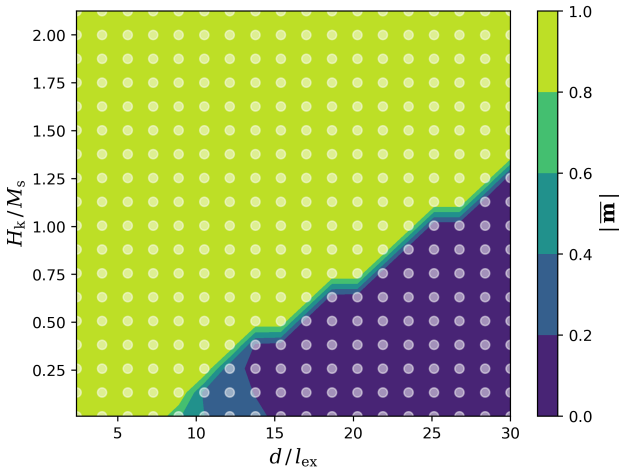

Fig. 2: **Zero-field phase space for spherical particles.**

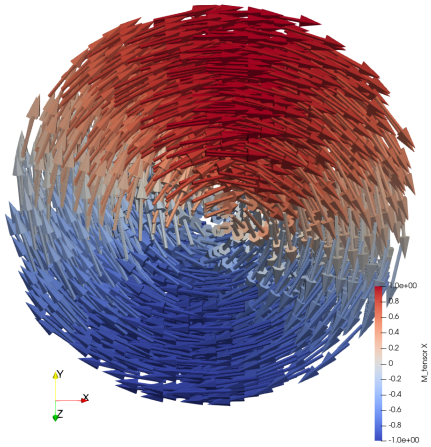

Fig. 3: **Zero-field ground state of a magnetite sphere with $R = 90\,\mathrm{nm}$.** The sphere inhibits a vortex configuration, with the vortex core direction normal to the anisotropy axis (x-axis). The used material parameters correspond to $d = 15.6\,l_{ex}$ and $H_K = M_s/10$.

6.2 Canonical partition function

Assuming that the carrier fluid is a large enough heat bath with constant temperature $T = 1/k_\mathrm{B}\beta$, we can formally define the partition function Z as

$$Z = \mathcal{N} \int_{\mathcal{F}(\Omega_\mathrm{m})} \int_{\mathrm{SO}(3)} \int_{\mathbb{R}^3} \mathcal{D}\widehat{\boldsymbol{m}}\, \mathrm{d}\boldsymbol{R}\, \mathrm{d}\widehat{\boldsymbol{L}}\, e^{-\beta \mathcal{H}[\widehat{\boldsymbol{L}}, \widehat{\boldsymbol{m}}, \boldsymbol{R}]}, \tag{6.19}$$

where $\mathcal{N}$ is an unknown normalization factor. The expression $\int_{\mathcal{F}(\Omega_\mathrm{m})} \mathcal{D}\widehat{\boldsymbol{m}}$ is to be understood as an integral over all vector fields in $\mathcal{F}(\Omega_\mathrm{m})$. Its analytical evaluation should not be pursued further as it may even be ill-defined. However, we will come back to it in the single-domain approximation where it reduces to an ordinary surface integral. For the general case, however, one can still perform the integrations over the momentum and rotation coordinate. To shorten notation, the Zeeman term is isolated by defining

$$\mathcal{V}[\widehat{\boldsymbol{m}}, \boldsymbol{R}] = \mathcal{V}_0[\widehat{\boldsymbol{m}}] - \mu_0 V_\mathrm{m} M_\mathrm{s} H_\mathrm{ext} \overline{\widehat{\boldsymbol{m}}} \cdot \boldsymbol{R}^\top \boldsymbol{h}. \tag{6.20}$$

Rearranging and factoring the partition function yields

$$Z = \mathcal{N} \underbrace{\int_{\mathbb{R}^3} \mathrm{d}\widehat{\boldsymbol{L}}\, e^{-\beta \widehat{\boldsymbol{L}}^\top \widehat{\boldsymbol{\Theta}}^{-1} \widehat{\boldsymbol{L}}/2}}_{Z_\mathrm{kin}(\beta)} \cdot \int_{\mathcal{F}(\Omega_\mathrm{m})} \mathcal{D}\widehat{\boldsymbol{m}}\, e^{-\beta \mathcal{V}_0[\widehat{\boldsymbol{m}}]} \int_{\mathrm{SO}(3)} \mathrm{d}\boldsymbol{R}\, e^{\xi\, \overline{\widehat{\boldsymbol{m}}} \cdot \boldsymbol{R}^\top \boldsymbol{h}}, \tag{6.21}$$

where ξ is the commonly used Langevin parameter

$$\xi = \frac{\mu_0 M_\mathrm{s} V_\mathrm{m} H_\mathrm{ext}}{k_\mathrm{B} T}. \tag{6.22}$$

One can perform the integration over all rotation matrices by considering that in the given expression, its only effect is to rotate the field axis $\boldsymbol{h}$ over the unit sphere. Absorbing any constants in the normalization factor $\mathcal{N}$, this yields

$$\int_{\mathrm{SO}(3)} \mathrm{d}\boldsymbol{R}\, e^{\xi\, \overline{\widehat{\boldsymbol{m}}} \cdot \boldsymbol{R}^\top \boldsymbol{h}} \propto \frac{\sinh(\xi |\overline{\widehat{\boldsymbol{m}}}|)}{\xi |\overline{\widehat{\boldsymbol{m}}}|} \tag{6.23}$$

and thus the partition function becomes

$$Z = \mathcal{N} Z_\mathrm{kin}(\beta) \int_{\mathcal{F}(\Omega_\mathrm{m})} \mathcal{D}\widehat{\boldsymbol{m}}\, \frac{\sinh(\xi |\overline{\widehat{\boldsymbol{m}}}|)}{\xi |\overline{\widehat{\boldsymbol{m}}}|}\, e^{-\beta \mathcal{V}_0[\widehat{\boldsymbol{m}}]}. \tag{6.24}$$

Stuck with the remaining integral, the question arises of what we gained at this point. By successfully integrating over the rotational coordinate, we obtained the probability distribution of the particle's rotation for a given external field and magnetization

configuration without evaluating the other magnetic interactions. This should be made use of in the numerical simulations: Due to the architecture of the present numerical implementation as well as the longer relaxation times of the mechanical processes, transforming the hybrid system into a purely micromagnetic one drastically improves simulation performance. This transformation only affects the Zeeman term, as it is the only contribution that depends on the orientation of the particle. To arrive at the correct term, the partition function should be expressed without the rotational integration as

$$Z = \mathcal{N} Z_{\mathrm{kin}}(\beta) \int_{\mathcal{F}(\Omega_{\mathrm{m}})} \mathcal{D}\widehat{\boldsymbol{m}}\; e^{-\beta \mathcal{V}_0[\widehat{\boldsymbol{m}}] - \beta F_{\mathrm{ext}}} \tag{6.25}$$

with the free Zeeman energy F_{ext}. Comparing with (6.24) yields

$$F_{\mathrm{ext}} = -\frac{1}{\beta} \log \left(\frac{\sinh(\xi |\overline{\widehat{\boldsymbol{m}}}|)}{\xi |\overline{\widehat{\boldsymbol{m}}}|} \right). \tag{6.26}$$

The term "free energy" should be treated with care in this context since the given expression still contains $\widehat{\boldsymbol{m}}$ as one of the coordinates. Rather, F_{ext} should be referred to as the free energy with respect to $\boldsymbol{R}$ which contains the information about the equilibrium behavior of $\boldsymbol{R}$ for a given magnetization configuration, external field magnitude, and temperature. This function should thus lead to a modified expression for the external field that does not depend on the instantaneous orientation of the particle anymore.

To prove this to be consistent, this expression will be derived using two different approaches: The first one follows Brown's argument [39] where he states that for isothermal processes, it is the Helmholtz function that plays the role of the energy function, from which the "forces" can be derived with respect to the "coordinates". Hence, we again apply the variational calculus with which we derived the field expression in the first place, this time for F_{ext} instead of E_{ext}. Applying the chain rule yields

$$\begin{aligned}
\delta^{\mathrm{mag}}_{\boldsymbol{\phi}\times\boldsymbol{m}} F_{\mathrm{ext}}[|\overline{\boldsymbol{m}}|] &= \frac{\mathrm{d}}{\mathrm{d}\epsilon} F_{\mathrm{ext}}[|\overline{\boldsymbol{m} + \epsilon\boldsymbol{\phi} \times \boldsymbol{m}}|]\Big|_{\epsilon=0} && (6.27)\\
&= \frac{\partial F_{\mathrm{ext}}}{\partial |\overline{\boldsymbol{m}}|} \frac{\partial |\overline{\boldsymbol{m}}|}{\partial |\overline{\boldsymbol{m}}|^2} \frac{\mathrm{d}}{\mathrm{d}\epsilon} |\overline{\boldsymbol{m} + \epsilon\boldsymbol{\phi} \times \boldsymbol{m}}|^2 \Big|_{\epsilon=0} && (6.28)\\
&= -\mu_0 M_{\mathrm{s}} H_{\mathrm{ext}} \frac{L(\xi|\overline{\boldsymbol{m}}|)}{|\overline{\boldsymbol{m}}|} \int_{\Omega_{\mathrm{m}}} (\boldsymbol{m}(\widehat{\boldsymbol{x}}) \times \overline{\boldsymbol{m}}) \cdot \boldsymbol{\phi}(\widehat{\boldsymbol{x}})\, \mathrm{d}\widehat{\boldsymbol{x}}, && (6.29)
\end{aligned}$$

where L is the Langevin function given by

$$L(x) = \coth x - \frac{1}{x}. \tag{6.30}$$

Thus, the averaged external field is

$$\boldsymbol{H}'_{\text{ext}} = H_{\text{ext}}\, L(\xi|\overline{\boldsymbol{m}}|)\, \frac{\overline{\boldsymbol{m}}}{|\overline{\boldsymbol{m}}|}. \tag{6.31}$$

The second approach is to take the average of the external field over all orientations of the particle with the proper weights of the Boltzmann distribution. This results in

$$\widehat{\boldsymbol{H}}'_{\text{ext}} = H_{\text{ext}} \left\langle \widehat{\boldsymbol{h}} \right\rangle_{\boldsymbol{R}} = H_{\text{ext}} \frac{\int_{\text{SO(3)}} \mathrm{d}\boldsymbol{R}\, \widehat{\boldsymbol{h}}\, e^{\xi \overline{\widehat{\boldsymbol{m}}} \cdot \boldsymbol{R}^\top \boldsymbol{h}}}{\int_{\text{SO(3)}} \mathrm{d}\boldsymbol{R}\, e^{\xi \overline{\widehat{\boldsymbol{m}}} \cdot \boldsymbol{R}^\top \boldsymbol{h}}} \tag{6.32}$$

$$= H_{\text{ext}}\, L(\xi|\overline{\widehat{\boldsymbol{m}}}|) \frac{\overline{\widehat{\boldsymbol{m}}}}{|\overline{\widehat{\boldsymbol{m}}}|}, \tag{6.33}$$

which is the same expression as (6.31), given in the particle frame. This result is somehow intuitive: Since the macrospin is the only quantity by which the particle interacts with the external fields, all contributions that are not paralell cancel out in a fluctuating system. However, $\overline{\boldsymbol{m}}$ is not always parallel to the external field either, for that reason the magnitude is reduced by the Langevin function, which takes values between zero and one. In the limit of strong fields or low temperatures, $L(\xi|\overline{\boldsymbol{m}}|)$ approaches one and is therefore consistent with the derivations for the ground state discussed in the last section.

It could not be found any publications applying this mean-field approach, but there has been made use of the counterpart: In [40], interacting magnetic nanoparticles are studied, where they are assumed to be in a rigid, single domain state bound to the anisotropy axis. There, the thermal fluctuations of the particles with respect to an external field they exhibit have been averaged not by altering the field, but the dipoles themselves. The resulting expression for the mean macrospin closely corresponds to the average external field expression proposed above.

It is worth noting that this modification does not introduce a systematic error because it results in an identical partition function that accurately describes a static system. However, this method is ineffective for addressing dynamic problems. Integrating out the mechanical part assumes that mechanical processes occur on a much faster timescale than magnetic processes, allowing for the assumption of instantaneous relaxation. In reality, this assumption does not hold for physical parameters.

At this point, we define the magnetic order parameter

$$m_{\parallel} := \langle \overline{\boldsymbol{m}} \cdot \boldsymbol{h} \rangle \tag{6.34}$$

as the projection of the macrospin onto the external field. For the averaged external field, this results in

$$m_{\parallel} = \langle |\overline{\boldsymbol{m}}| \coth(\xi |\overline{\boldsymbol{m}}|) \rangle - \frac{1}{\xi}. \tag{6.35}$$

This is the general expression for the Langevin value for macrospins of variable magnitude. For single domain particles with $|\overline{\boldsymbol{m}}| = 1$, this corresponds to the standard result $L(\xi)$. For arbitrary configurations, however, we are still left with a non-trivial average, depending on all energy contributions of the system.

We now again take into account the rotational degree of freedom and want to deduct all the parameters relevant for the static description of the system. The spatial part of the partition function is determined by the Boltzmann factor $-\beta\mathcal{V}$ which can be brought into the form

$$-\beta\mathcal{V} = \xi\, \overline{\widehat{\boldsymbol{m}}} \cdot \boldsymbol{R}^{\top} \boldsymbol{h} + \sigma \overline{(\widehat{\boldsymbol{m}} \cdot \widehat{\boldsymbol{n}})^2} + \lambda \left(- \left(\frac{l_{\mathrm{ex}}}{d} \right)^2 \overline{d^2 (\boldsymbol{\nabla} \widehat{\boldsymbol{m}})^2} + \overline{\widehat{\boldsymbol{m}} \cdot \left(\widehat{\boldsymbol{N}} * \widehat{\boldsymbol{m}} \right)} \right) \tag{6.36}$$

with the parameters given by

$$\xi = \frac{\mu_0 M_{\mathrm{s}} V_{\mathrm{m}} H_{\mathrm{ext}}}{k_{\mathrm{B}} T}, \quad \sigma = \frac{K_{\mathrm{u}} V_{\mathrm{m}}}{k_{\mathrm{B}} T}, \quad \lambda = \frac{\mu_0 M_{\mathrm{s}}^2 V_{\mathrm{m}}}{2 k_{\mathrm{B}} T}, \quad \frac{l_{\mathrm{ex}}}{d} = \sqrt{\frac{2A}{\mu_0 M_{\mathrm{s}}^2 d^2}}. \tag{6.37}$$

The micromagnetic system is thus characterized by four parameters: ξ represents the quotient of the Zeeman energy and the thermal energy of the particle, quantifying the thermal stability of the projection of the macrospin onto the external field. The anisotropy parameter σ describes the thermal stability of the alignment of each atomic spin along the easy axis since the orientation and magnitude of the macrospin are not solely determined by the average of the individual spin orientations.

For the remaining contributions, it was decided to quantify the relative strength of the exchange energy compared to the demagnetization energy by l_{ex}/d. Furthermore, the thermal stability of their equilibrium should be specified by the magnetostatic energy ratio λ, a parameter that also plays an important role when considering interactions between multiple dipoles suspended in a fluid.

Fig. 4 shows the equilibrium configurations for a magnetite sphere of radius $R = 90\,\mathrm{nm}$, whose material parameters are provided by Tab. 4. By applying the external field in the averaged form (6.31), we could obtain these hystereses with magnum.np only,

M_s	Saturation magnetization	$400\,\mathrm{kA\,m^{-1}}$
K_u	Uniaxial anisotropy constant	$10\,\mathrm{kJm^{-3}}$
A	Exchange constant	$1.33 \times 10^{-11}\,\mathrm{Jm^{-1}}$
α	Gilbert damping parameter	0.08
ρ	Density	$5170\,\mathrm{kgm^{-3}}$

Tab. 4: Selected material parameters of magnetite.

and removed the otherwise necessary choice of the angle between the easy axis and the external field.

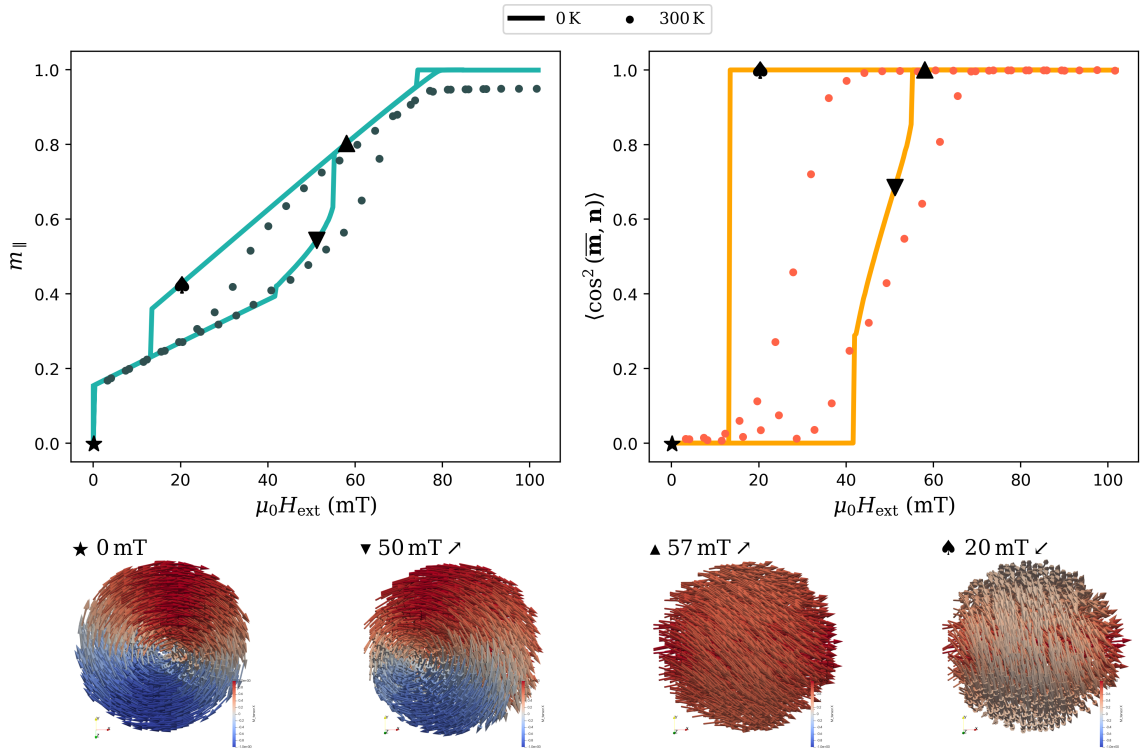

Fig. 4: **Hysteresis of suspended 90 nm magnetite spheres.** The left curve shows the equilibrium values for $m_\parallel$, while the right curve shows the angle between the macrospin and the easy axis at equilibrium. At zero field, the sphere is magnetized in a vortex configuration with its axis orthogonal to the easy axis. At $\approx 40\,\text{mT}$, the vortex starts to rotate until it collapses into another vortex structure with its core parallel to the easy axis. The system shows similar behavior at room temperature, but is able to occupy intermediate states, leading to less pronounced transitions. The bottom figures show the characteristic configurations at zero temperature, where the color indicates the projection of a given spin onto the easy axis (x-axis).

6.3 Suspended single-domain particles

For single-domain particles with rotational degrees of freedom, the partition function can be evaluated explicitly and is given by

$$Z = \mathcal{N} Z_{\mathrm{kin}}(\beta) \cdot \int_{\mathcal{F}_{\mathrm{uni}}(\Omega_{\mathrm{m}})} \int_{\mathrm{SO}(3)} \mathcal{D}\widehat{\boldsymbol{m}}\, \mathrm{d}\boldsymbol{R}\ e^{\xi\, \widehat{\boldsymbol{m}} \cdot \boldsymbol{R}^{\top} \boldsymbol{h} + \sigma (\widehat{\boldsymbol{m}} \cdot \widehat{\boldsymbol{n}})^2}, \tag{6.38}$$

where $\mathcal{F}_{\mathrm{uni}}$ denotes the space of all uniform magnetization configurations. We already evaluated the integral over $\boldsymbol{R}$ for the general case, where we can substitute $|\widehat{\boldsymbol{m}}| = 1$:

$$Z = \mathcal{N} Z_{\mathrm{kin}}(\beta)\, \frac{\sinh(\xi)}{\xi} \int_{\mathcal{F}_{\mathrm{uni}}(\Omega_{\mathrm{m}})} \mathcal{D}\widehat{\boldsymbol{m}}\ e^{\sigma (\widehat{\boldsymbol{m}} \cdot \widehat{\boldsymbol{n}})^2}. \tag{6.39}$$

We are left with the integral over all magnetization configurations, which for a single macrospin is just the integral over the 2-sphere. Changing to spherical coordinates and without loss of generality, setting $\widehat{\boldsymbol{n}} = \boldsymbol{e}_z$, the integral evaluates to

$$\int_0^{\pi} \mathrm{d}\theta\, \sin\theta\, e^{\sigma \cos^2\theta} = \sqrt{\frac{\pi}{\sigma}}\, \mathrm{erfi}(\sqrt{\sigma}), \tag{6.40}$$

where erfi denotes the imaginary error function. Absorbing all constant factors into $\mathcal{N}$ then gives for the partition function

$$Z = \mathcal{N} Z_{\mathrm{kin}}(\beta)\ \frac{\sinh(\xi)}{\xi}\ \frac{\mathrm{erfi}(\sqrt{\sigma})}{\sqrt{\sigma}}. \tag{6.41}$$

This allows us to evaluate the expectation value of all moments of $\boldsymbol{m} \cdot \boldsymbol{h}$ and $(\boldsymbol{m} \cdot \boldsymbol{n})^2$ by differentiation of Z

$$\langle (\boldsymbol{m} \cdot \boldsymbol{h})^n \rangle = \frac{1}{Z} \frac{\partial^n Z}{\partial \xi^n} \tag{6.42}$$

$$\left\langle (\boldsymbol{m} \cdot \boldsymbol{n})^{2n} \right\rangle = \frac{1}{Z} \frac{\partial^n Z}{\partial \sigma^n}. \tag{6.43}$$

$$\tag{6.44}$$

Because the partition function separates in ξ and σ, the moments depend only on the respective parameter. The first two moments of $\boldsymbol{m} \cdot \boldsymbol{h}$ as well as $\langle (\boldsymbol{m} \cdot \boldsymbol{n})^2 \rangle$ are illustrated in Fig. 5. From the expectation of the order parameter given by $m_{\parallel} = L(\xi)$, one can also calculate the static initial susceptibility

$$\chi_0 = \frac{\partial (M_{\mathrm{s}} m_{\parallel})}{\partial H_{\mathrm{ext}}} = \frac{\mu_0 M_{\mathrm{s}}^2 V_{\mathrm{m}}}{k_{\mathrm{B}} T} L'(\xi)|_{\xi=0} = \frac{\mu_0 M_{\mathrm{s}}^2 V_{\mathrm{m}}}{3 k_{\mathrm{B}} T}. \tag{6.45}$$

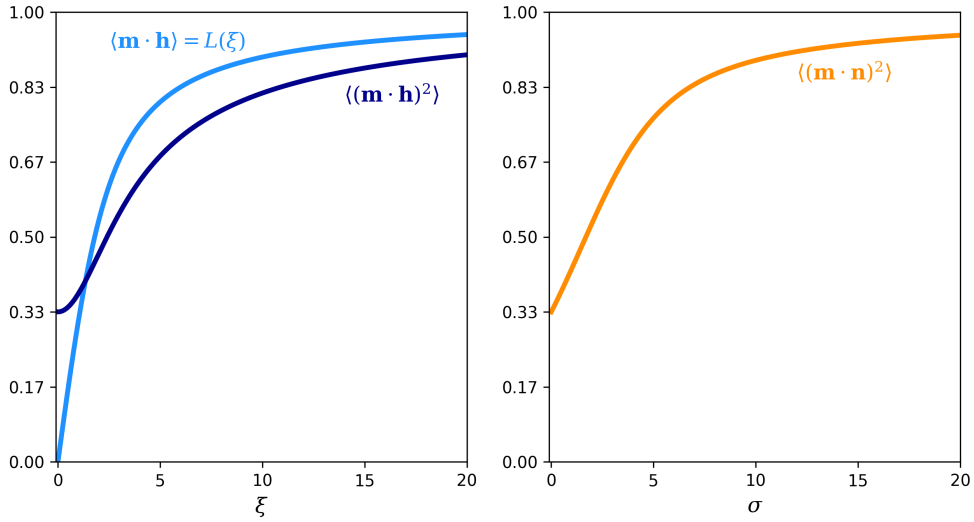

Fig. 5: Equilbrium values for single-domain particles.

6.4 Immobilized single-domain particles

Investigating a system where the orientation of the easy axis of a particle is fixed in space is crucial for understanding the magnetic properties of both immobilized and mobile systems, as it gives greater insights into the magnetic properties of the system. By performing the integration over $\boldsymbol{R}$ in the latter derivation, we effectively lost all the information about the interplay between the anisotropy and the Zeeman interaction because we assumed that the easy axis instantaneously aligns with the field by mechanical rotation.

In the context of statistical canonical description, the concept of time is absent. Therefore, all relaxation processes are treated as being equally fast, which does not reflect reality, where magnetic relaxations occur at rates that typically are orders of magnitudes faster than the mechanical processes. It can thus be concluded that the solid matrix of immobilized easy axes offers greater insight into the short-time behavior of the hybrid system. In the case of zero temperature, a static description is provided by the Stoner-Wolfarth model [41, 42]. The model predicts equilibrium configurations and hysteresis behavior without consideration of thermal fluctuations. This model can be extended to incorporate temperature effects, as described by Chuev [43] by allowing the magnetization to overcome energy barriers with a probability that depends on temperature. However, this is beyond the scope of this thesis.

Instead, we will focus on deriving the partition function for a system with immobilized easy axes within the canonical ensemble framework. Unlike the athermal Stoner-Wohlfarth model, the canonical ensemble posits that states with equal energy are visited with equal probability, implying that sufficient time has passed for every en-

ergy barrier to be overcome. Whether this is appropriate depends on the values of σ and ξ as well as the time scale of interest.

The partition function of the immobilized system is given by

$$Z = \mathcal{N} Z_{\mathrm{kin}}(\beta) \int_{\mathcal{F}(\Omega_{\mathrm{m}})} \mathcal{D}\widehat{\boldsymbol{m}}\ e^{\xi\, \widehat{\boldsymbol{m}} \cdot \boldsymbol{R}^{\top} \boldsymbol{h} + \sigma (\widehat{\boldsymbol{m}} \cdot \widehat{\boldsymbol{n}})^2}. \tag{6.46}$$

Again, it should be used spherical coordinates, parametrizing the dipole by

$$\widehat{\boldsymbol{m}} = (\sin\theta\cos\phi, \sin\theta\sin\phi, \cos\theta)^{\top} \tag{6.47}$$

and setting the easy axis to be the z-axis, which is valid for the general case, as $\widehat{\boldsymbol{n}}$ is neither one of the coordinates nor is its orientation important because we integrate over all $\widehat{\boldsymbol{m}}$. What is of relevance is the relation between $\widehat{\boldsymbol{n}}$ and $\widehat{\boldsymbol{h}} = \boldsymbol{R}^{\top}\boldsymbol{h}$, and by parametrizing one of them, one is left with an additional degree of freedom. From symmetry arguments, it is only the angle between the easy axis and the field that matters. Hence, let $\widehat{\boldsymbol{h}}$ lie in the xz-plane parametrized by

$$\widehat{\boldsymbol{h}} = (\sin\alpha, 0, \cos\alpha)^{\top}. \tag{6.48}$$

Transforming to spherical coordinates and substituting the parametrizations lead to the integral to be solved, which is denoted by

$$Q(\alpha) = \frac{1}{4\pi} \int_0^{\pi} \int_0^{2\pi} \mathrm{d}\theta\, \mathrm{d}\phi\ \sin\theta\, e^{\xi(\sin\alpha\sin\theta\cos\phi + \cos\alpha\cos\theta) + \sigma\cos^2\theta}, \tag{6.49}$$

and evaluates to

$$Q(\alpha) = \int_0^1 \mathrm{d}x\, e^{\sigma x^2}\ \cosh(x\,\xi\cos\alpha)\, I_0(\xi\sin\alpha\sqrt{1-x^2}). \tag{6.50}$$

Here, I_0 denotes the modified Bessel function of the first kind of order zero. The given expression is in its most compact form and cannot be integrated further. Nevertheless, we can integrate it numerically for given values of ξ, σ, and α. To obtain the expectation value of the field projection $m_{\parallel}$ for an ensemble of immobilized particles with randomly distributed easy axes, we first compute the expectation under an external field with angle α and then integrate over all all field directions

$$m_{\parallel} = \frac{1}{2} \int_0^{\pi} \mathrm{d}\alpha\ \sin\alpha\, \frac{1}{Q\,(\alpha)} \frac{\partial}{\partial\xi} Q(\alpha). \tag{6.51}$$

In Fig. (6), the resulting magnetization curve is compared with the zero-temperature hysteresis curve of an immobilized ensemble obtained from simulations.

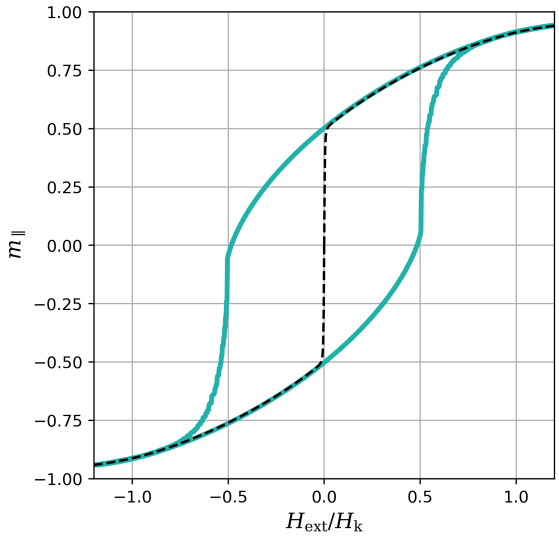

Fig. 6: **Magnetization curve of an immobilized system at zero temperature.** The solid curve has been obtained by simulating an ensemble of 10^6 particles with uniformly distributed easy axes. The solution provided by the statistical analysis at a value of $\sigma = 200$ (dashed line) accurately models the energy minimization in the region where the majority of spins are in the hemisphere with positive field projection but assumes that they are able to overcome the energy barrier as soon as the field direction flips.

By assuming $\xi \ll 1$ and neglecting higher powers, it is in fact possible to evaluate $Q(\alpha)$. This is also useful for oscillating fields, where the initial response occurs under a small field magnitude. Given the expectation value for the dipole component parallel to a field that encloses an angle α with $\widehat{\boldsymbol{n}}$

$$m_\parallel(\alpha) = Q\left(\alpha\right)\frac{\partial}{\partial\xi}Q(\alpha), \tag{6.52}$$

omitting terms of higher order in ξ yields

$$m_\parallel(\alpha) = \frac{\xi}{4}\frac{\int_0^1 \mathrm{d}x\, e^{\sigma x^2}\left(x^2\left(1+3\cos(2\alpha)\right)+1-\cos(2\alpha)\right)}{\int_0^1 \mathrm{d}x\, e^{\sigma x^2}}. \tag{6.53}$$

By applying Feynman's integration trick and defining

$$R(\sigma) = \int_0^1 \mathrm{d}x\, e^{\sigma x^2} = \frac{2}{\sqrt{\pi}}\frac{\mathrm{erfi}(\sqrt{\sigma})}{\sqrt{\sigma}}, \tag{6.54}$$

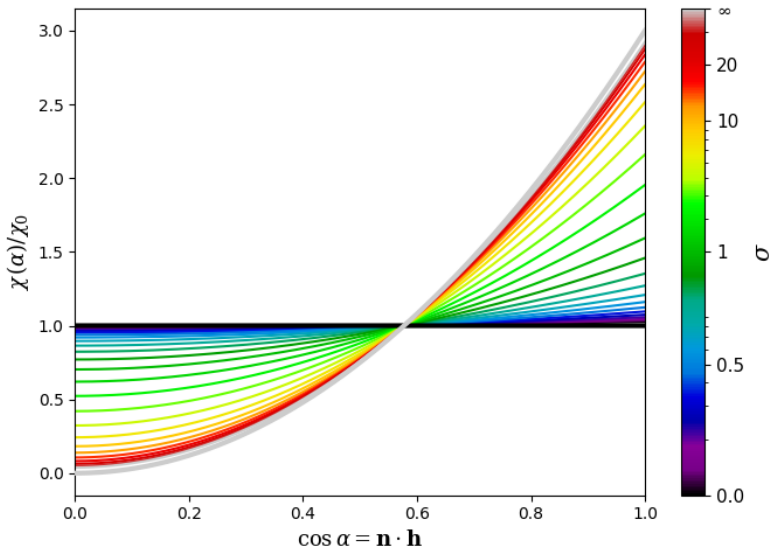

Fig. 7: **Angle-dependent susceptibility for external fields of small magnitude.**

one obtains

$$m_{\parallel}(\alpha) = \frac{\xi}{4}\left(1 + \frac{R'(\sigma)}{R(\sigma)}\right) + \frac{\xi\cos 2\alpha}{4}\left(\frac{3R'(\sigma)}{R(\sigma)} - 1\right). \tag{6.55}$$

Performing the integration (6.51) yields $m_{\parallel} = \xi/3$, hence the magnetization of an ensemble with randomly oriented easy axes is independent of anisotropy for small fields. By (6.45), the angle-dependent initial susceptibility can be computed as follows:

$$\chi(\alpha) = \frac{\partial(M_s m_{\parallel}(\alpha))}{\partial H_{\text{ext}}} = \frac{3\chi_0}{4}\left(1 + \frac{R'(\sigma)}{R(\sigma)} + \cos 2\alpha\left(\frac{3R'(\sigma)}{R(\sigma)} - 1\right)\right) \tag{6.56}$$

Fig. (7) illustrates the nontrivial influence of the anisotropy on the angle-dependent susceptibility. It is of particular significance to consider the values at the extreme points, denoted by

$$\chi_{\parallel} = \chi(\alpha = 0) = 3\chi_0\frac{R'(\sigma)}{R(\sigma)} \tag{6.57}$$

$$\chi_{\perp} = \chi(\alpha = \pi/2) = \frac{3\chi_0}{2}\left(1 - \frac{R'(\sigma)}{R(\sigma)}\right), \tag{6.58}$$

corresponding to fields parallel and orthogonal to the easy axis. As shown in [44], differentiating between parallel and transverse relaxation modes and identifying their characteristic time scale provides a robust dynamical model for the hybrid system.

7 Dynamic response of single-domain particles

7.1 Parameter reduction

In contrast to systems in equilibrium, describing their dynamical behavior still poses an active field of research, where a variety of approaches are used for finding general solutions to the underlying equations of motion. In this chapter, it will be looked at single-domain particles. Even for the most simplified model of a spherical, rigid, single-domain particle in the overdamped limit exhibiting a static magnetic field, the inclusion of thermal fluctuations precludes the existence of a dynamical solution for the average magnetization. This is due to the emergence of an infinite hierarchy of equations, where the equation for $\mathrm{d}\langle m_i\rangle/\mathrm{d}t$ contains the second order moments $\mathrm{d}\langle m_i m_j\rangle/\mathrm{d}t$ whose derivative involves, the moments of the third order, and so on. Hence, it should be found the best possible reduction of the given set of equations to obtain general results for all material parameters and particle sizes. Taking the LLG

$$\dot{\boldsymbol{m}} = -\boldsymbol{m}\times\left[\left(\frac{\mathbf{1}}{\alpha}+[\boldsymbol{m}\times]\right)\frac{\alpha\gamma_\mathrm{e}\mu_0}{1+\alpha^2}\boldsymbol{H}_\mathrm{eff}\right], \tag{7.1}$$

where the effective field is given by

$$\boldsymbol{H}_\mathrm{eff} = \boldsymbol{H}_\mathrm{ext} + \frac{2K_\mathrm{u}}{\mu_0 M_\mathrm{s}}(\boldsymbol{m}\cdot\boldsymbol{n})\boldsymbol{n} - \frac{\alpha}{\gamma_\mathrm{e}\mu_0}\boldsymbol{m}\times\boldsymbol{\omega} + \boldsymbol{H}_\mathrm{th}, \tag{7.2}$$

it should be found an appropriate parametrization for the time dimension. A good choice is to parametrize the time in terms of the Néel time

$$\tau_0 = \frac{(1+\alpha^2)M_\mathrm{s}V_\mathrm{m}}{2\alpha\gamma_\mathrm{e}k_\mathrm{B}T} \tag{7.3}$$

as the characteristic time scale of the thermal noise. We thus define the reduced time and frequency as

$$t^0 = \frac{t}{\tau_0} \quad \text{and} \quad \boldsymbol{\omega}^0 = \boldsymbol{\omega}\,\tau_0. \tag{7.4}$$

Expressing the LLG in terms of these reduced quantities yields

$$\frac{\mathrm{d}\boldsymbol{m}}{\mathrm{d}t^0} = \tau_0 \dot{\boldsymbol{m}} = -\boldsymbol{m} \times \left[\left(\frac{\mathbf{1}}{\alpha} + [\boldsymbol{m}\times] \right) \boldsymbol{H}_{\mathrm{eff}}^0 \right], \tag{7.5}$$

where the reduced effective field $\boldsymbol{H}_{\mathrm{eff}}^0$ given by

$$\boldsymbol{H}_{\mathrm{eff}}^0 = \frac{\mu_0 M_\mathrm{s} V_\mathrm{m}}{2k_\mathrm{B}T} \boldsymbol{H}_{\mathrm{eff}} = \frac{\boldsymbol{\xi}(t^0)}{2} + \sigma(\boldsymbol{m}\cdot\boldsymbol{n})\boldsymbol{n} - \frac{\alpha^2}{1+\alpha^2}\boldsymbol{m}\times\boldsymbol{\omega}^0 + \frac{\mu_0 M_\mathrm{s} V_\mathrm{m}}{2k_\mathrm{B}T}\boldsymbol{H}_\mathrm{th}. \tag{7.6}$$

Despite the non-trivial prefactor of the thermal field, it is clear that the characteristic time scale of the thermal fluctuations still equals τ_0 as the structure of the LLG has not been changed by this scaling transformation. In fact, τ_0 is the only parameter that characterizes the underlying random process, besides the qualitative assumptions of it being Gaussian and having a vanishing mean value. This also can be seen in the Fokker-Planck equation associated with the LLG [16], where the term corresponding to the thermal fluctuations only depends on the time scale τ_0.

There are two reasons why this is not immediately obvious in the LLG: First, the thermal fluctuations are expressed in terms of a magnetic field for it to be included in the effective field to preserve the compactness of the equation. Second, in the present model, the thermal field is included in both the precession and damping terms, which are multiplied by different prefactors. This leads to the form of the diffusion coefficient D discussed. In summary, the diffusion coefficient D depends on the exact structure of the equation of motion whereas the Néel time τ_0 is inherent to the underlying system. As a consequence, the random process is independent of any parameters when scaling the time by τ_0.

The performed transformation yields a convenient parametrization of the system: The external field is described by the function $\boldsymbol{\xi}(t^0)$ which reduces to an amplitude vector/frequency pair when investigating sinusoidal fields. The anisotropy is quantified by the parameter σ, and the strengths of magnetic precession and the Barnett field are quantified by the Gilbert damping constant α. This is sufficient to describe the dynamics of the system in units of the Néel time, and by providing a value for the latter, the solution can be scaled accordingly.

A similar reparametrization should also be applied to the equation for the angular velocity given by (4.39), where expressing the time in terms of the Brownian relaxation time τ_B is the appropriate choice. For simplicity, it is again assumed that the inertia and friction tensors are multiples of the identity. Then, the equation can be simplified to

$$\frac{\mathrm{d}\boldsymbol{\omega}^\mathrm{B}}{\mathrm{d}t^\mathrm{B}} = \tau_\mathrm{B}^2 \dot{\boldsymbol{\omega}} = \frac{\tau_\mathrm{B}}{\tau_\omega}\left(\boldsymbol{m} \times \frac{\boldsymbol{\xi}(t^\mathrm{B})}{2} + \frac{\alpha}{1+\alpha^2}\frac{\mathrm{d}\boldsymbol{m}}{\mathrm{d}t^0} - \boldsymbol{\omega}^\mathrm{B} + \frac{\tau_\mathrm{B}}{\gamma_\mathrm{r}}\boldsymbol{T}_\mathrm{th} \right). \tag{7.7}$$

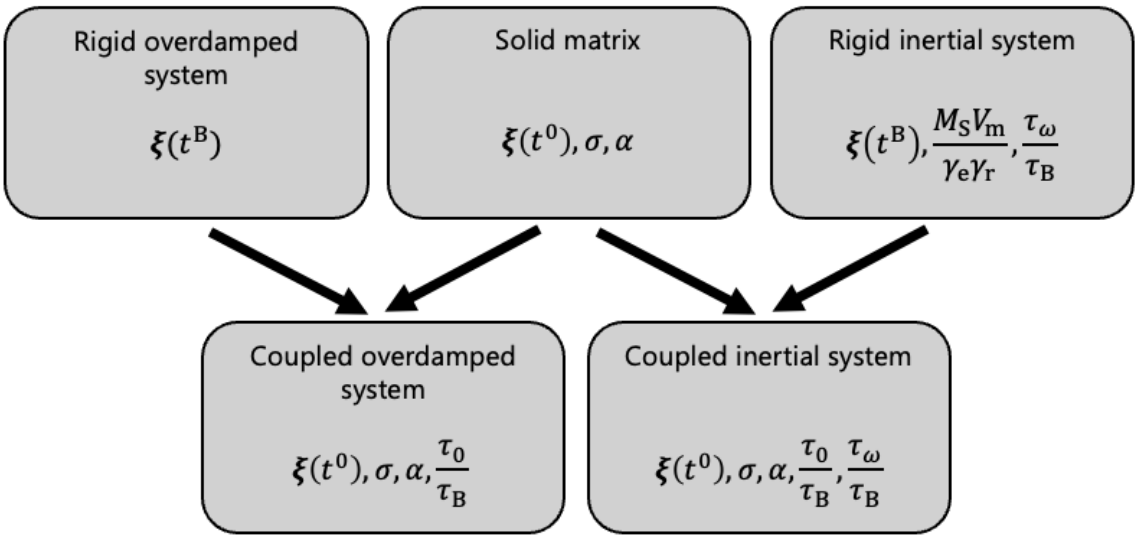

Fig. 8: Parameters to be specified for the models discussed.

For the overdamped limit, the LHS can be set to zero, and solving for $\boldsymbol{\omega}^{\mathrm{B}}$ yields

$$\boldsymbol{\omega}^{\mathrm{B}} = \boldsymbol{m} \times \frac{\boldsymbol{\xi}(t^{\mathrm{B}})}{2} + \frac{\alpha}{1+\alpha^2} \frac{\mathrm{d}\boldsymbol{m}}{\mathrm{d}t^0} + \frac{\tau_{\mathrm{B}}}{\gamma_{\mathrm{r}}} \boldsymbol{T}_{\mathrm{th}}. \tag{7.8}$$

It is noted that the prefactor of $\mathrm{d}\boldsymbol{m}/\mathrm{d}t^{\mathrm{B}}$ does in fact not depend on the Gilbert damping factor α as the Néel time contains the reciprocal value of $\alpha/(1+\alpha^2)$. However, this representation has been chosen to parametrize the equation by the minimal number of independent parameters.

We have thus parametrized the magnetic as well as the mechanical equations of motion by the respective characteristic time scale of the thermal fluctuations. For the solution of the coupled problem, it is then sufficient to provide the conversion between these time scales given by τ_0/τ_{B}. Fig. 8 provides an overview of the free parameters for the models discussed.

7.2 Zero and infinite anisotropy

In this section, the present model should be further reduced to the cases where the anisotropy can be omitted or assumed infinitely large, i.e. the particle behaves according to the rigid dipole model. It is shown that these two cases are in fact equivalent under certain conditions, apart from the characteristic time scales involved.

First, consider the equations of a rigid, isotropic, overdamped dipole in the reduced

unit system, given by

$$\frac{\mathrm{d}\boldsymbol{m}}{\mathrm{d}t^{\mathrm{B}}} = \boldsymbol{\omega}^{\mathrm{B}} \times \boldsymbol{m} \tag{7.9}$$

$$\boldsymbol{\omega}^{\mathrm{B}} = \boldsymbol{m} \times \frac{\boldsymbol{\xi}(t^{\mathrm{B}})}{2} + \frac{\alpha}{1+\alpha^2}\frac{\mathrm{d}\boldsymbol{m}}{\mathrm{d}t^0} + \frac{\tau_{\mathrm{B}}}{\gamma_{\mathrm{r}}}\boldsymbol{T}_{\mathrm{th}}. \tag{7.10}$$

Substituting the first equation into the second results in

$$\boldsymbol{\omega}^{\mathrm{B}} = \boldsymbol{m} \times \frac{\boldsymbol{\xi}(t^{\mathrm{B}})}{2} + \frac{M_{\mathrm{s}}V_{\mathrm{m}}}{\gamma_{\mathrm{e}}\gamma_{\mathrm{r}}}\boldsymbol{\omega}^{\mathrm{B}} \times \boldsymbol{m} + \frac{\tau_{\mathrm{B}}}{\gamma_{\mathrm{r}}}\boldsymbol{T}_{\mathrm{th}}, \tag{7.11}$$

where it is recalled that the second term must be omitted given that $M_{\mathrm{s}}V_{\mathrm{m}}/\gamma_{\mathrm{e}}\gamma_{\mathrm{r}} \ll 1$, which is indeed the case for typical material parameters. Finally, the explicit expression for $\boldsymbol{\omega}^{\mathrm{B}}$ can be inserted back into the (7.9) yielding an ordinary differential equation for the dipole

$$\frac{\mathrm{d}\boldsymbol{m}}{\mathrm{d}t^{\mathrm{B}}} = -\boldsymbol{m} \times \left(\boldsymbol{m} \times \frac{\boldsymbol{\xi}(t^{\mathrm{B}})}{2}\right) - \frac{\tau_{\mathrm{B}}}{\gamma_{\mathrm{r}}}\boldsymbol{m} \times \boldsymbol{T}_{\mathrm{th}}. \tag{7.12}$$

For the contrary case of zero anisotropy, take the LLG (7.5) with the effective field given by

$$\boldsymbol{H}^0_{\mathrm{eff}} = \frac{\mu_0 M_{\mathrm{s}} V_{\mathrm{m}}}{2k_{\mathrm{B}}T}\boldsymbol{H}_{\mathrm{eff}} = \frac{\boldsymbol{\xi}(t^0)}{2} - \frac{\alpha^2}{1+\alpha^2}\boldsymbol{m} \times \boldsymbol{\omega}^0 + \frac{\mu_0 M_{\mathrm{s}} V_{\mathrm{m}}}{2k_{\mathrm{B}}T}\boldsymbol{H}_{\mathrm{th}}. \tag{7.13}$$

Regarding the Barnett term, the overdamped equation for $\boldsymbol{\omega}^0$

$$\boldsymbol{\omega}^0 = \frac{\tau_0}{\tau_{\mathrm{B}}}\left(\boldsymbol{m} \times \frac{\boldsymbol{\xi}(t^{\mathrm{B}})}{2} + \frac{\alpha}{1+\alpha^2}\frac{\mathrm{d}\boldsymbol{m}}{\mathrm{d}t^0} + \frac{\tau_{\mathrm{B}}}{\gamma_{\mathrm{r}}}\boldsymbol{T}_{\mathrm{th}}\right). \tag{7.14}$$

shows that we can neglect the Barnett effect if

$$\frac{\alpha M_{\mathrm{s}} V_{\mathrm{m}}}{\gamma_{\mathrm{e}}\gamma_{\mathrm{r}}} \ll 1, \tag{7.15}$$

which is the equivalent condition as before apart from the additional prefactor α. Plugging in the effective field into (7.5) yields

$$\frac{\mathrm{d}\boldsymbol{m}}{\mathrm{d}t^0} = -\boldsymbol{m} \times \frac{\boldsymbol{\xi}(t^0)}{2\alpha} - \boldsymbol{m} \times \left(\boldsymbol{m} \times \frac{\boldsymbol{\xi}(t^0)}{2}\right) + \boldsymbol{f}_{\mathrm{th}}. \tag{7.16}$$

For compactness, the contribution of the thermal fluctuations has been included in the function $\boldsymbol{f}_{\mathrm{th}}$. When comparing (7.12) and (7.16), one observes that both equations

contain the damping term $\boldsymbol{m} \times (\boldsymbol{m} \times \boldsymbol{\xi}/2)$. However, the LLG equation includes an additional precession term that is inversely proportional to the Gilbert damping factor. Following previous arguments, the stochastic behavior of the two processes is also equivalent since both equations incorporate a multiplicative noise with a characteristic time scale equal to 1 in their respective unit system. We therefore can investigate the extreme cases of zero and infinite anisotropy with the generalized version of (7.16)

$$\dot{\boldsymbol{m}} = -\boldsymbol{m} \times \frac{\boldsymbol{\xi}(t')}{2\alpha} - \boldsymbol{m} \times \left(\boldsymbol{m} \times \frac{\boldsymbol{\xi}(t')}{2} \right) + \boldsymbol{f}_{\mathrm{th}}, \tag{7.17}$$

where $\dot{\boldsymbol{m}} = \mathrm{d}\boldsymbol{m}/\mathrm{d}t'$ and the reduced time t' is given by $t' = \tau_0$ or $t' = \tau_{\mathrm{B}}$ for the cases of zero and infinite anisotropy respectively. Regarding the precession term, it suffices to take the limit $\alpha \to \infty$ to obtain the rigid dipole solution.

The generalized equation can be numerically integrated to obtain the solution for a single particle. However, we should rather look at a large ensemble of non-interacting particles. In [16], it is shown how the underlying Fokker-Planck equation leads to the evolution of the ensemble average $\langle \boldsymbol{m} \rangle$

$$\langle \dot{\boldsymbol{m}} \rangle = - \langle \boldsymbol{m} \rangle \times \frac{\boldsymbol{\xi}(t')}{2\alpha} - \left\langle \boldsymbol{m} \times \left(\boldsymbol{m} \times \frac{\boldsymbol{\xi}(t')}{2} \right) \right\rangle - \langle \boldsymbol{m} \rangle \,, \tag{7.18}$$

which can be simplified to

$$\langle \dot{\boldsymbol{m}} \rangle = - \langle \boldsymbol{m} \rangle \times \frac{\boldsymbol{\xi}(t')}{2\alpha} + \left(\mathbf{1} - \left\langle \boldsymbol{m}\boldsymbol{m}^{\top} \right\rangle \right) \frac{\boldsymbol{\xi}(t')}{2} - \langle \boldsymbol{m} \rangle \,. \tag{7.19}$$

The reader might ask why this amount of emphasis is put on such a simple case, why essentially every interaction but the external field is not taken into consideration. A more detailed examination of the latter equation reveals that it involves two ensemble averages: the mean of all dipole vectors and the average of the outer product of the dipoles with themselves. The relationship between these averages is typically unknown if the system is not in a static equilibrium state. Deriving the differential equation of the second moment would result in a hierarchy of equations containing the ensemble average of the third moment, and so on. This infinite hierarchy cannot be resolved. There exist methods to close this hierarchy after a finite amount of steps n by approximating the n-th moment by those of lower orders [45]. However, this approach will not be pursued further.
Instead, the objective of this chapter is to characterize disparate regimes for which approximate analytical solutions can be identified, or the system can be reduced to a single-variable differential equation. The regimes that will be discussed are

- The **linear** regime: Starting from a zero-field equilibrium, the second moment $\left\langle \boldsymbol{m}\boldsymbol{m}^{\top} \right\rangle$ for a weak field $|\boldsymbol{\xi}(t')| \ll 1$ can be approximated by the linear term in the Taylor series of the corresponding equilibrium value given by $\left\langle \boldsymbol{m}\boldsymbol{m}^{\top} \right\rangle = \mathbf{1}/3$.

- The **deterministic** regime: If the external field is large throughout $|\boldsymbol{\xi}(t')| \gg 1$ and the situation of interest is dominated by the driving torque, the diffusion term $-\langle \boldsymbol{m} \rangle$ in (7.19) can be omitted and the equation can be solved for a single particle and then be integrated over a distribution of initial configurations.
- The **quasi-eqilibrium**: There are no assumptions made about the external field, but the probability distribution of configurations is assumed to take the same form as in a static equilibrium $\rho(\boldsymbol{m}, t) \propto \exp\left(\boldsymbol{\xi}_\mathrm{e}(t) \cdot \boldsymbol{m}\right)$ for an *effective* field $\boldsymbol{\xi}_\mathrm{e}$, which yields an equation $\left\langle \boldsymbol{m}\boldsymbol{m}^\top \right\rangle = \boldsymbol{F}(\langle \boldsymbol{m} \rangle)$ that can be substituted into (7.19).

7.2.1 Linear regime

The probability density $\rho(\boldsymbol{m}, t)$ for a single-domain particle under an external field is given by

$$\rho(\boldsymbol{m}, t) = \frac{e^{\boldsymbol{\xi}\cdot\boldsymbol{m}}}{Z} \quad \text{where} \quad Z = \frac{4\pi \sinh|\boldsymbol{\xi}|}{|\boldsymbol{\xi}|}. \tag{7.20}$$

The expectation value $\left\langle \boldsymbol{m}\boldsymbol{m}^\top \right\rangle$ can thus be evaluated by

$$\left\langle \boldsymbol{m}\boldsymbol{m}^\top \right\rangle_{ij} = \frac{1}{Z}\int_{|\boldsymbol{m}|=1} m_i m_j e^{\boldsymbol{\xi}\cdot\boldsymbol{m}}\,\mathrm{d}\boldsymbol{m} = \frac{1}{Z}\frac{\mathrm{d}^2 Z}{\mathrm{d}\xi_i \xi_j}, \tag{7.21}$$

which yields

$$\left\langle \boldsymbol{m}\boldsymbol{m}^\top \right\rangle = \frac{\boldsymbol{\xi}\boldsymbol{\xi}^\top}{\xi^2}\left(1 - \frac{3L(\xi)}{\xi}\right) + \frac{L(\xi)}{\xi}\,\mathbf{1}, \tag{7.22}$$

where $\xi = |\boldsymbol{\xi}|$ is the magnitude of the external field. Taking the limit where $\xi \ll 1$, the Langevin function up to linear order is given by $L(\xi) \approx \xi/3$, which causes the first term to vanish, and the second moment thus evaluates to

$$\left\langle \boldsymbol{m}\boldsymbol{m}^\top \right\rangle = \frac{\mathbf{1}}{3}. \tag{7.23}$$

Hence, a weak field does not alter the equilibrium value of $\left\langle \boldsymbol{m}\boldsymbol{m}^\top \right\rangle$ up to linear order. Substituting this into (7.19) results in the equation of motion in the linear regime

$$\langle \dot{\boldsymbol{m}} \rangle = -\langle \boldsymbol{m} \rangle \times \frac{\boldsymbol{\xi}(t')}{2\alpha} + \frac{\boldsymbol{\xi}(t')}{3} - \langle \boldsymbol{m} \rangle. \tag{7.24}$$

Since this equation only contains the mean dipole as a variable, it can be integrated with an ordinary ODE solver. It is even possible to find an analytic solution, which will be shown for selected special cases.

7.2.2 Deterministic regime

It is obvious that when a particle exhibits a torque from a large external field $|\boldsymbol{\xi}(t')| \gg 1$, thermal fluctuations do not change the trajectory of the dipole, and thus the diffusion term in (7.19) can be omitted

$$\langle \dot{\boldsymbol{m}} \rangle = - \langle \boldsymbol{m} \rangle \times \frac{\boldsymbol{\xi}(t')}{2\alpha} + \left(\mathbf{1} - \left\langle \boldsymbol{m}\boldsymbol{m}^{\top} \right\rangle \right) \frac{\boldsymbol{\xi}(t')}{2}. \tag{7.25}$$

This means that the problem becomes deterministic and can be solved for an individual dipole according to the LLG or the rigid dipole equation

$$\dot{\boldsymbol{m}} = -\boldsymbol{m} \times \frac{\boldsymbol{\xi}(t')}{2\alpha} + \frac{\boldsymbol{\xi}(t')}{2} - \left(\boldsymbol{m} \cdot \frac{\boldsymbol{\xi}(t')}{2} \right) \boldsymbol{m} \quad \text{with} \quad |\boldsymbol{m}| = 1, \tag{7.26}$$

after which an ensemble average can be obtained by integration of the solutions $\boldsymbol{m}(t, \boldsymbol{m}_0)$ over the corresponding initial configuration of the ensemble

$$\langle \boldsymbol{m}(t) \rangle = \int_{|\boldsymbol{m}_0|=1} \boldsymbol{m}(t, \boldsymbol{m}_0)\, \rho(\boldsymbol{m}_0)\, \mathrm{d}\boldsymbol{m}_0. \tag{7.27}$$

For the general case, this method requires more computational effort than the linear approximation as (7.26) has to be solved for each particle individually, but it occurs that special cases such as a fixed-axis field provide an analytical solution.

It is emphasized that the application of this approximation has strict limitations: Besides the requirement that $|\boldsymbol{\xi}(t')| \gg 1$ at all times, it is not possible to obtain correct trajectories when the dipoles tend to closely align with the field and are to be deflected again under a sharp angle. This is due to the fact that mainly the thermal fluctuations determine when a particle deflects from its aligned state.

7.2.3 Quasi-equilibrium

A very powerful tool to obtain trajectories on the whole field spectrum is the effective field method first proposed by Martsenyuk, Raikher, and Shliomis [46–48]. As previously stated, this approximation is predicated on the assumption that, at any given point in time, the distribution of dipoles adheres to a Boltzmann distribution

$$\rho(\boldsymbol{m}, t) = \frac{e^{\boldsymbol{\xi}_{\mathrm{e}} \cdot \boldsymbol{m}}}{Z} \quad \text{whith} \quad Z = \frac{4\pi \sinh |\boldsymbol{\xi}_{\mathrm{e}}|}{|\boldsymbol{\xi}_{\mathrm{e}}|}, \tag{7.28}$$

where the effective field $\boldsymbol{\xi}_{\mathrm{e}}$ is defined such that it generates the instantaneous average dipole [31]

$$\langle \boldsymbol{m}(t) \rangle = L(|\boldsymbol{\xi}_{\mathrm{e}}(t)|) \frac{\boldsymbol{\xi}_{\mathrm{e}}(t)}{|\boldsymbol{\xi}_{\mathrm{e}}(t)|}. \tag{7.29}$$

Inversing this relation yields

$$\boldsymbol{\xi}_{\mathrm{e}}(t) = L^{-1}(m(t))\frac{\langle \boldsymbol{m}(t)\rangle}{m(t)} \quad \text{where} \quad m(t) = |\langle \boldsymbol{m}(t)\rangle|, \tag{7.30}$$

where L^{-1} denotes the inverse of the Langevin function that can be well approximated by rational functions of desired complexity. For the following computations it has been used the approximation by Jedynak [49]

$$L^{-1}(x) = \frac{x(3 - 1.00651x^2 - 0.962251x^4 + 1.47353x^6 - 0.48953x^8)}{(1-x)(1+1.01524x)} \tag{7.31}$$

with a maximum relative error of 0.076%.

With the effective field being defined in terms of the first moment, one can calculate the second moment $\left\langle \boldsymbol{m}\boldsymbol{m}^{\top}\right\rangle$ given by (7.22)

$$\left\langle \boldsymbol{m}\boldsymbol{m}^{\top}\right\rangle = \frac{\langle \boldsymbol{m}\rangle \langle \boldsymbol{m}\rangle^{\top}}{m^2}\left(1 - \frac{3m}{L^{-1}(m)}\right) + \frac{m}{L^{-1}(m)}\,\mathbf{1}, \tag{7.32}$$

which can be substituted into the equation of motion (7.19)

$$\dot{\langle \boldsymbol{m}\rangle} = -\langle \boldsymbol{m}\rangle \times \frac{\boldsymbol{\xi}(t')}{2\alpha} + \left(1 - \frac{m}{L^{-1}(m)}\right)\frac{\boldsymbol{\xi}(t')}{2} + \left(\frac{3m}{L^{-1}(m)} - 1\right)\frac{\langle \boldsymbol{m}\rangle \cdot \boldsymbol{\xi}(t')}{2m^2}\langle \boldsymbol{m}\rangle - \langle \boldsymbol{m}\rangle\,. \tag{7.33}$$

Again, this equation only contains $\langle \boldsymbol{m}\rangle$ and its magnitude m as variables and thus can be integrated with an ODE solver. It will be shown that despite the gross simplification of the hierarchy model, trajectories obtained with the effective field equation are almost identical to those obtained from molecular dynamic or micromagnetic simulations of a large ensemble.

7.2.4 Monodirectional fields

The most relevant scenario is one in which the external field does not change its direction and can be written in the form

$$\boldsymbol{\xi}(t') = \xi(t')\,\boldsymbol{h}, \tag{7.34}$$

where $\xi(t')$ is the magnitude and $\boldsymbol{h}$ the normalized axis of the external field. Given the zero-field equilibrium state as the initial configuration, the only dipole component of interest is its projection onto the external field denoted by

$$m_{\parallel} = \langle \boldsymbol{m} \rangle \cdot \boldsymbol{h}, \tag{7.35}$$

since all other components vanish due to symmetry. Clearly, the gyromagnetic precession does not play a role, as the cross-product term vanishes when multiplying (7.19) with $\boldsymbol{h}$, yielding

$$\dot{m}_{\parallel} = \frac{\xi(t')}{2}\left(1 - \left\langle (\boldsymbol{m}\cdot\boldsymbol{h})^2 \right\rangle\right) - m_{\parallel}. \tag{7.36}$$

As the α-dependent precession is orthogonal to $\boldsymbol{h}$ and thus vanishes, the zero and infinite anisotropy scenarios are equivalent in this case.

We will approach this problem with each of the discussed approximations, starting with the linear regime. Here, the second moment $\langle (\boldsymbol{m}\cdot\boldsymbol{h})^2 \rangle = 1/3$ and the equation simplifies to

$$\dot{m}_{\parallel} = \frac{\xi(t')}{3} - m_{\parallel}. \tag{7.37}$$

It can be analytically solved, yielding

$$m_{\parallel}(t') = \frac{1}{3}\int_0^{t'} e^{-(t'-s)}\,\xi(s)\,\mathrm{d}s. \tag{7.38}$$

The general solution is therefore a convolution of the external field with the retarded Green's function $G(t) = \exp(-t)\Theta(t)$, where Θ denotes the Heaviside step function that ensures that causality is preserved, meaning fields in the future do not influence the dipole at earlier times. The given solution satisfies $m_{\parallel}(0) = 0$. If instead, one wants to obtain the steady-state trajectory under a periodic field, the lower integration bound can be set to negative infinity, meaning that the oscillation started infinitely far in the past and the particle relaxed to its periodic state. By the convolution theorem, a convolution in real space can be expressed as a multiplication in the Fourier space.

This can easily be derived by taking the Fourier transform of (7.37), which resolves to

$$m_{\parallel}^{*}(\omega') = \frac{1}{1+i\omega'}\frac{\xi^{*}(\omega')}{3}. \tag{7.39}$$

The Greens' function is directly proportional to the dynamic susceptibility $\chi(\omega')$ defined by

$$M_{\mathrm{s}} m_{\parallel}^{*}(\omega') = \chi(\omega') H_{\mathrm{ext}}^{*}(\omega'), \tag{7.40}$$

yielding the Debye-type susceptibility for a single particle

$$\chi(\omega') = \frac{1}{1+i\omega'}\frac{\mu_0 M_{\mathrm{s}}^2 V_{\mathrm{m}}}{3k_{\mathrm{B}}T}. \tag{7.41}$$

To obtain the susceptibility of an ensemble, the latter expression has to be multiplied by the volume fraction of the suspension of particles [50]. The frequency dependence of the latter expression can be expressed as

$$\frac{1}{1+i\omega'} = \frac{e^{-i\tan^{-1}(\omega')}}{\sqrt{1+\omega'^2}}, \tag{7.42}$$

from which the response of the dipole to the external field is obvious: Besides the reduction of the amplitude by a factor of $\sqrt{1+\omega'^2}$, the oscillation of the dipole gets shifted by $\Delta\phi = \tan^{-1}(\omega')$ to the left, retarding its response with increasing field frequency, and saturating at 90° for large frequencies.

We should now look at a general solution for periodic external fields. Given a signal with period $2\pi/\Omega'$, we can write it as a Fourier series

$$\xi(t') = \xi_0 + \sum_{n=1}^{\infty} a_n \cos(n\Omega' t') + b_n \sin(n\Omega' t'), \tag{7.43}$$

where $\max_{t'}|\xi(t')| \ll 1$ must be satisfied for the linear approximation to be valid.

Performing the integration

$$m_{\parallel}(t') = \frac{1}{3}\int_{-\infty}^{t'} e^{-(t'-s)}\,\xi(s)\,\mathrm{d}s \tag{7.44}$$

yields

$$m_{\parallel}(t') = \frac{\xi_0}{3} + \frac{1}{3}\sum_{n=1}^{\infty}\frac{(a_n - b_n n\Omega')\cos(n\Omega' t') + (b_n + a_n n\Omega')\sin(n\Omega' t')}{1+(n\Omega')^2}. \tag{7.45}$$

To determine the specific loss rate, we first compute the integral over one oscillation of the product of $m_\parallel$ and the field gradient

$$\int_0^{2\pi/\Omega'} m_\parallel(t')\dot{\xi}(t')\,dt' = -\frac{\pi\Omega'}{3}\sum_{n=1}^{\infty}\frac{n^2}{1+(n\Omega')^2}\left(a_n^2+b_n^2\right). \tag{7.46}$$

From this, the SLP (4.55) can be determined for zero and infinite anisotropy respectively

$$\mathrm{SLP}_{\sigma=0} = \frac{\mu_0 M_\mathrm{s} V_m}{\rho V}\frac{\alpha\gamma_\mathrm{e}\mu_0}{1+\alpha^2}\sum_{n=1}^{\infty}\frac{(n\Omega\tau_0)^2}{1+(n\Omega\tau_0)^2}\frac{H_n^2+{H'_n}^2}{3} \tag{7.47}$$

$$\mathrm{SLP}_{\sigma=\infty} = \frac{\mu_0 M_\mathrm{s} V_\mathrm{m}}{\rho V}\frac{\mu_0 M_\mathrm{s} V_\mathrm{m}}{\gamma_\mathrm{r}}\sum_{n=1}^{\infty}\frac{(n\Omega\tau_\mathrm{B})^2}{1+(n\Omega\tau_\mathrm{B})^2}\frac{H_n^2+{H'_n}^2}{3}. \tag{7.48}$$

H_n and H'_n denote the field amplitudes associated with the even and odd oscillations of frequency $n\Omega$. Given a field of the form $H_\mathrm{ext}(t) = H_0 \sin\Omega t$, the sum reduces to

$$\frac{(\Omega\tau)^2}{1+(\Omega\tau)^2}\frac{H_0^2}{3}. \tag{7.49}$$

For small frequencies, the function $(\Omega\tau)^2/(1+(\Omega\tau)^2)$ scales quadratic in $\Omega\tau$ which is due to the linear scaling of both the phase shift and the number of oscillations per unit of time. For large frequencies, the function saturates at 1 and the power losses become frequency-independent. Moreover, the losses become size-independent if the quotient of the magnetic core volume V_m and the total volume V including a potential shell layer is constant, and for the rigid case, if the friction tensor is proportional to V. This is summarized in Tab. 5 for spherical particles and for both cases of zero and infinite anisotropy. Fig. 9 illustrates how simulations confirm these results, although the signal-to-noise ratio in ESPResSo is low due to the smaller size of the simulated ensemble.

It is noteworthy that the range of the linear model can be slightly enhanced by substituting one occurrence of $\xi/3$ by the Langevin function $L(\xi)$ in the given expressions for the dipole trajectory and specific loss. This has been proposed by Rosenzweig [50], who suggests multiplying the susceptibility by an additional factor of $3L(\xi)/\xi$, which is equivalent.

	$\sigma = 0$	$\sigma = \infty$
$\Omega\tau \ll 1$	$\left(\frac{\mu_0 M_\mathrm{s} V H_0}{k_\mathrm{B} T}\right)^2 \frac{1+\alpha^2}{\alpha} \frac{M_s \Omega^2}{12\rho\gamma_\mathrm{e}}$	$\left(\frac{\mu_0 M_\mathrm{s} V H_0}{k_\mathrm{B} T}\right)^2 \frac{\eta\Omega^2}{2\rho}$
$\Omega\tau \gg 1$	$\frac{\mu_0 M_\mathrm{s} H_0^2}{3\rho} \frac{\alpha\gamma_\mathrm{e}\mu_0}{1+\alpha^2}$	$\frac{(\mu_0 M_\mathrm{s} H_0)^2}{18\eta\rho}$

Tab. 5: **Assymptotic expressions for the SLP of spherical particles in the linear regime.**

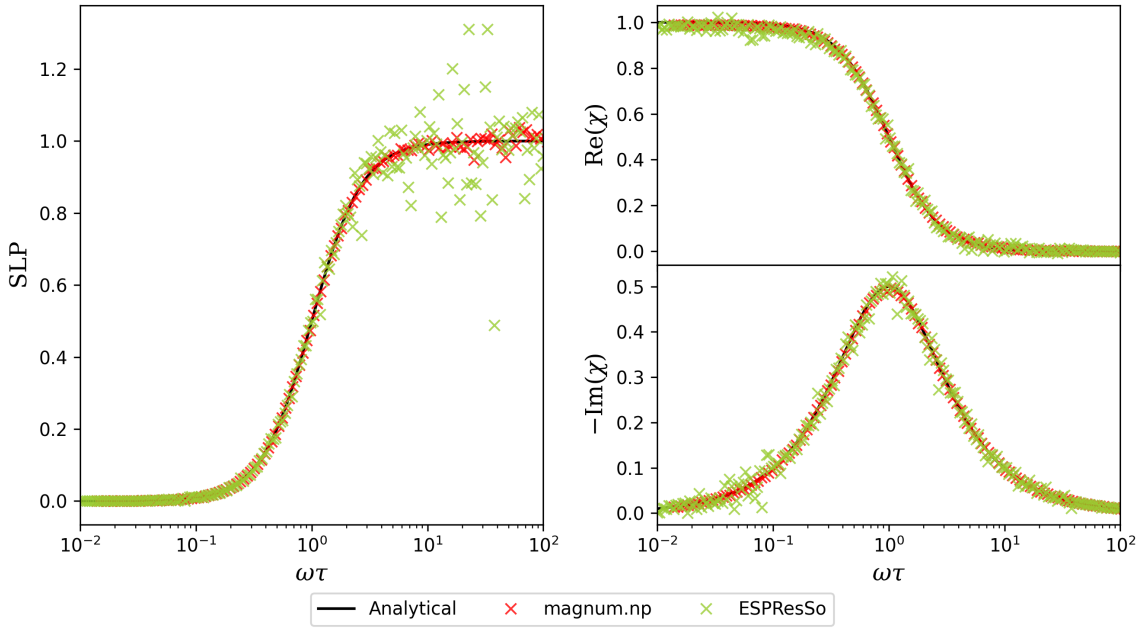

Fig. 9: **SLP and susceptibilty in the linear regime**. The simulations have been performed at a field amplitude $\xi = 1/2$. The ensemble simulated with magnum.np consists of 10^6 particles whereas in ESPResSo, the number of particles is 10^3 and 10^4 for low and high frequencies respectively.

We continue with the deterministic regime. Omitting the diffusion term, the equation of motion for the field projection of an individual dipole denoted by m_{ind} is

$$\dot{m}_{\mathrm{ind}} = \frac{\xi(t')}{2}\left(1 - m_{\mathrm{ind}}^2\right) \tag{7.50}$$

and gives the solution

$$m_{\mathrm{ind}}(t', m_0) = \frac{(m_0+1)e^{2\mathfrak{H}(t')} + (m_0-1)}{(m_0+1)e^{2\mathfrak{H}(t')} - (m_0-1)}, \tag{7.51}$$

where m_0 is the initial value at $t' = 0$ and $\mathfrak{H}(t')$ is the integral of the external field

$$\mathfrak{H}(t') = \int_0^{t'} \frac{\xi(s)}{2}\,\mathrm{d}s. \tag{7.52}$$

To obtain the average value of an ensemble of particles, let us assume it to be infinitely large so that the summation over all particles can be replaced by the integration

$$m_{\parallel}(t') = \int_{-1}^{1} m_{\mathrm{ind}}(t', m_0)\,\rho(m_0)\,\mathrm{d}m_0 \tag{7.53}$$

over a distribution of intial states $\rho(m_0)$. For a uniform distribution $\rho(m_0) = 1/2$, the solution is given in the compact form

$$m_{\parallel}(t') = \coth\mathfrak{H}(t') - \mathfrak{H}(t')\,\mathrm{csch}^2\mathfrak{H}(t'). \tag{7.54}$$

Similar to the Langevin function, the response function

$$R(x) = \coth x - x\,\mathrm{csch}^2 x \tag{7.55}$$

vanishes at $x = 0$ and reaches the plateaus of ± 1 at postive and negative infinity respectively. However, the functions are not to be confused as the Langevin function takes the field ξ as an argument, whereas R takes the time integral of the latter.

It is noted that despite the occurrence of ξ in the given expression, the temperature dependence is relieved by integrating the external field, as converting back to the non-reduced time induces the factor $1/\tau$, recovering the original form of the LLG or Langevin equation. The absence of the diffusion term introduces a significant systematic error for spins that are nearly parallel or antiparallel to the field, where thermal fluctuations have a substantial impact on the trajectory. Nevertheless, two observations can be made: First, these critical regions diminish with increasing field amplitude. Second, alternating fields with high frequencies prevent the dipole from aligning with the field, as the response is necessarily retarded. We should expect that the response

of the dipole to a high-frequency field $\xi(t') = \xi_0 \sin \Omega' t'$ is given by $m_\parallel(t') = R(\mathfrak{H}(t'))$, where $\mathfrak{H}$ evaluates to

$$\mathfrak{H}(t') = \frac{\xi_0}{2\Omega'} \left(1 - \cos(\Omega' t')\right). \tag{7.56}$$

This cannot be the true solution because $\mathfrak{H}$ and therefore $m_\parallel$ only take positive values, which can only represent a metastable state. Although diffusion may be negligible for the trajectory of a single oscillation, it causes the system to relax into a steady state that must be independent of the initial configuration in the distant past. As it is revealed, omitting the constant contribution in $\mathfrak{H}(t')$, such as

$$\mathfrak{H}(t') = -\frac{\xi_0}{2\Omega'} \cos(\Omega' t') \tag{7.57}$$

yields a good approximation when $\Omega'/\xi_0 \gg 1$. This expression for $\mathfrak{H}(t')$ does not violate the equation of motion and could have been obtained by fixing a uniform distribution of dipoles at time $t = \pi/2\Omega$ instead of $t = 0$.

The response of the dipole thus inhibits a phase lag of 90°, which is consistent with the high-frequency behavior observed in the linear regime. Indeed, when the magnitude of $\mathfrak{H}(t')$ is small, the response function can be approximated linearly as $R(x) \approx 2x/3$, which reproduces the trajectory observed for small fields and high frequencies in the linear regime. Although the error increases rapidly in the nonlinear region, this model succeeds in explaining the generation of higher-order responses, whose origin lies in the Taylor series expansion of R and the Fourier decomposition of powers of $\cos(\Omega' t')$ terms. Still, it does not enable phase lags other than 90 degrees, which are observed when increasing the field magnitude or decreasing the field frequency.

Let us allow this possibility, as well as a correction of the prefactor of $\mathfrak{H}$ by introducing the fit function

$$\mathfrak{H}_{\text{fit}}(t') = C \frac{\xi_0}{2\Omega'} \sin(\Omega' t' - \Delta\phi), \tag{7.58}$$

where C and $\Delta\Phi$ are to be fitted against the trajectories obtained by simulations. Indeed, as seen in Fig. 10, it can be found parameters for $\mathfrak{H}_{\text{fit}}$ that model the trajectories in the region $\Omega'/\xi_0 < 1$.

This leaves us with the dependence of the fitting parameters C and $\Delta\phi$ on the quotient Ω'/ξ (Fig. 11), where it has to be further examined whether this can be generalized for different field magnitudes ξ_0.

For $\Omega'/\xi \gg 1$, the specific loss power can be obtained numerically by

$$\mathrm{SLP}_{\sigma=0} = \frac{\mu_0 M_\mathrm{s} V_\mathrm{m} H_0}{\rho V} \frac{2\Omega}{\pi} \int_0^1 R\left(\frac{\alpha\mu_0\gamma_\mathrm{e} H_0}{(1+\alpha^2)\Omega}\, x\right) \frac{x}{\sqrt{1-x^2}}\,\mathrm{d}x \tag{7.59}$$

$$\mathrm{SLP}_{\sigma=\infty} = \frac{\mu_0 M_\mathrm{s} V_\mathrm{m} H_0}{\rho V} \frac{2\Omega}{\pi} \int_0^1 R\left(\frac{\mu_0 M_\mathrm{s} V_\mathrm{m} H_0}{\gamma_\mathrm{r}\Omega}\, x\right) \frac{x}{\sqrt{1-x^2}}\,\mathrm{d}x. \tag{7.60}$$

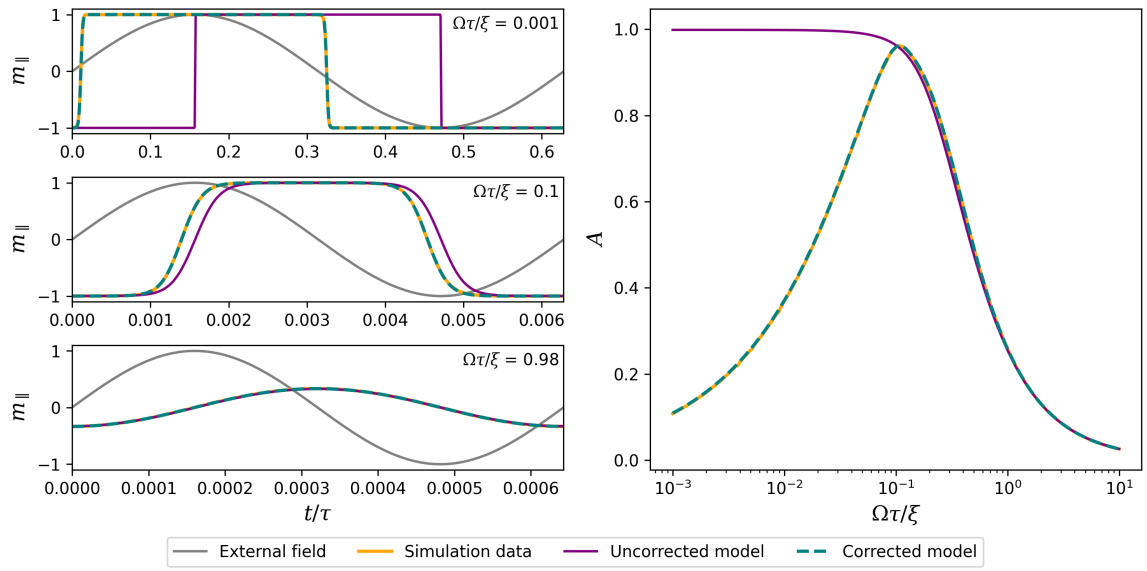

Fig. 10: **The (corrected) deterministic model.** Three exemplary trajectories on the left demonstrate how the fitted trajectories align with those obtained from numerical simulations. The third trajectory falls within the linear range and also aligns closely with the predictions of the uncorrected model. On the right, the peak of the normalized hysteresis area A indicates the point where increasing frequencies lead to a reduction in oscillation magnitude while decreasing frequencies result in a phase shift toward the external field. While varying the frequency $\Omega\tau$, the field magnitude has been fixed to $\xi_0 = 10^4$.

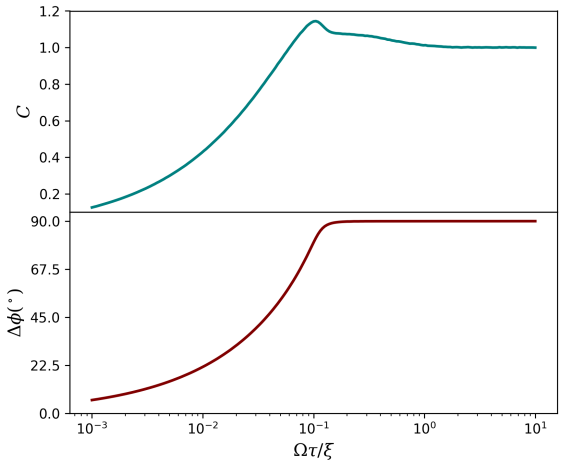

Fig. 11: **Fitted phase shift and prefactor for $\mathfrak{H}_{\text{fit}}$.** The fits have been obtained at a field magnitude of $\xi_0 = 10^4$. While the phase shift shows a regular behavior and saturates at 90 degrees around $\Omega\tau/\xi_0 \approx 0.1$, the irregularities in the curve of the prefactor C suggest that the fitting approach might not be generalizable at values close to the transition point.

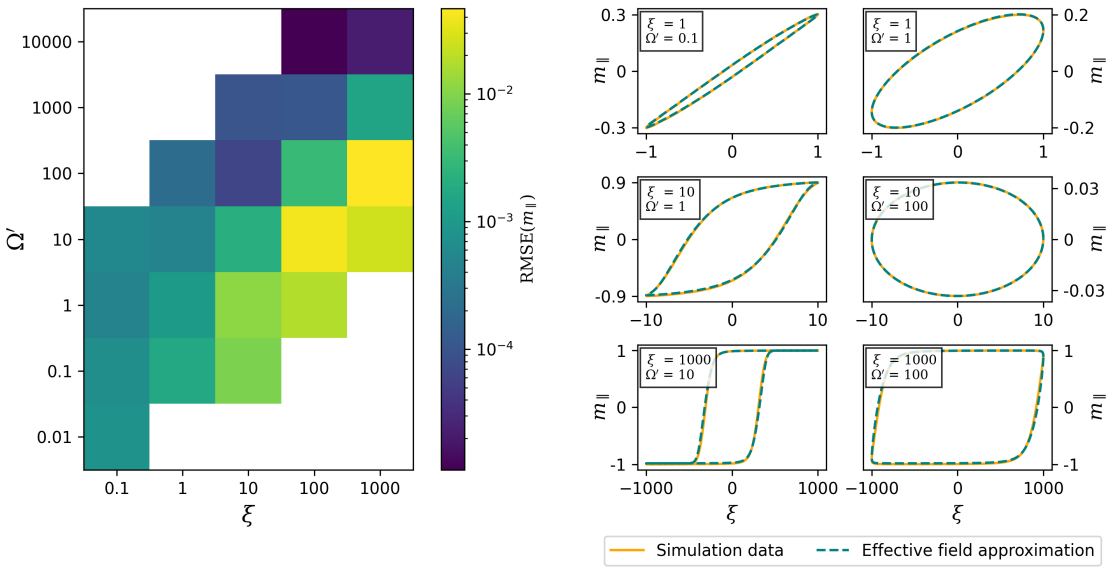

Fig. 12: **Comparison of the effective Field method and simulated trajectories.** For an ensemble of 10^6 particles, the root mean squared error $\mathrm{RMSE} = \sqrt{\langle (m^{\mathrm{sim}} - m^{\mathrm{eff}})^2 \rangle}$ has been computed to quantify the discrepancy between simulations and trajectories obtained using the effective field model for one steady-state oscillation. The left figure illustrates the RMSE values across different ξ and Ω'. The maximum observed error is 0.046 at $(\xi, \Omega') = (1000, 100)$. The right figure showcases various hysteresis loop types for different ξ and Ω', highlighting the model's performance across these parameter spaces.

Finally, let us conclude with the quasi-equilibrium model. Projecting (7.33) onto the fields axis yields

$$\dot{m}_\parallel = \left(1 - \frac{m}{L^{-1}(m)}\right)\frac{\xi(t')}{2} + \left(\frac{3m}{L^{-1}(m)} - 1\right)\frac{m_\parallel^2}{m^2}\frac{\xi(t')}{2} - m_\parallel. \tag{7.61}$$

Due to the symmetry of the plane orthogonal to the external field, all normal components of $\langle \boldsymbol{m} \rangle$ vanish and thus $m = m_\parallel$ if the system initially is in an equilibrium state. Given that, the equation simplifies to [47]

$$\dot{m}_\parallel = -m_\parallel \left(1 - \frac{\xi(t')}{L^{-1}(m_\parallel)}\right). \tag{7.62}$$

Although the nonlinearity of the (inverse) Langevin function prevents analytical solutions, this equation can be integrated using an ODE solver and is numerically stable. Fig. 12 demonstrates that this approximation performs well, with a maximum error of $\Delta m_\parallel \approx 0.05$ particularly occurring at high fields and low frequencies. If this deviation

is accepted, the effective field method allows for the rapid calculation of trajectories for any magnitude and frequency, as illustrated in Fig. 13. It is revealed that the overlap of phase shift and amplitude reduction leaves a narrow stripe where a large (normalized) hysteresis area A is possible. The normalization refers to spanning the hysteresis by $(\sin(\Omega t)/2, m_{\parallel}(t)/2)$, thus a maximum value of $A = 1$ can be obtained, corresponding to an infinitely sharp hysteresis with a 90° phase shift.

These heat maps demonstrate the transition from the linear to the nonlinear range. In the linear region, all four plotted quantities are solely dependent on frequency. However, a noticeable bend occurs in the range $1 < \xi < 10$. Beyond this range, the plots show an inclination that corresponds closely to a linear relationship. This behavior is consistent with the deterministic model, where the parameter ξ/Ω' serves as the characteristic parameter of the trajectory. It is also demonstrated that linearly approximating (7.62) leads to a field-dependent relaxation time [46]

$$\tau(\xi) = \tau\xi\frac{L'(\xi)}{L(\xi)}, \tag{7.63}$$

whose assymptote $\tau(\xi) \approx \tau/\xi$ for $\xi \to \infty$ gives the equivalent statement. However, comparing it to the curve of maximum hysteresis area in Fig. 13 shows a significant discrepancy between the two curves.

As can be seen, two important properties of the trajectory relevant for the hystereses area, which are the phase shift $\Delta\phi$ and the maximal amplitude, do not adhere to the same scaling law for high fields and frequencies. This is evidenced by the divergence in the incline of the two plots, which broadens the peaks with increasing magnitude and frequency. Moreover, the peak of the maximum hystereses area, in contrast to the linear range, is asymmetric when viewed on a logarithmic scale (also compare with Fig. 10). With the analytic deterministic model, we were able to characterize the right part of this peak due to a reduction in magnitude; however, we were unable to explain the varying phase shift that determines the left part.

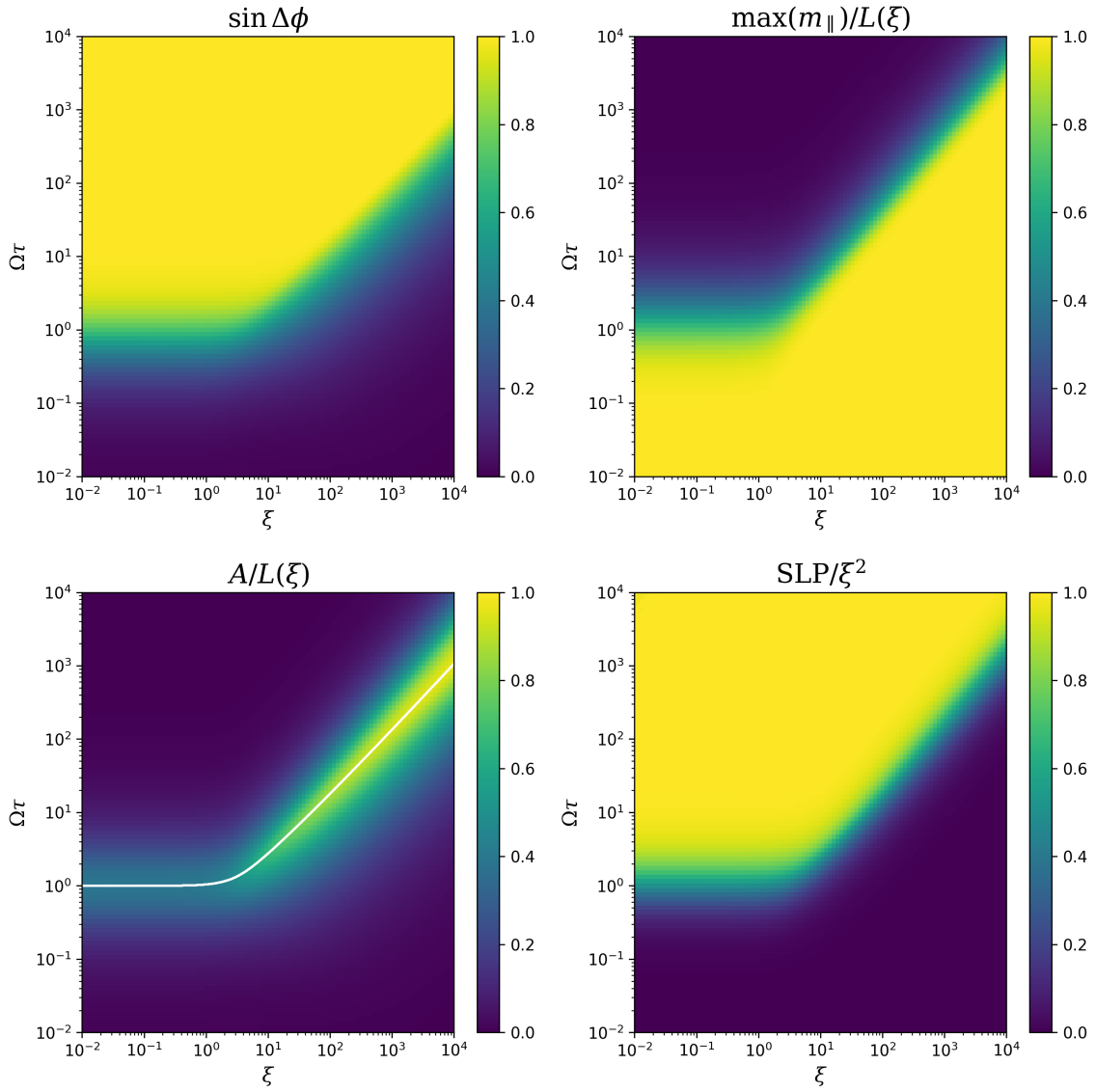

Fig. 13: **Characterization of dipole responses with the effective field method.** The dependence of the induced phase shift (top left) and the maximum magnitude of the dipole (top right) lead to a narrow region where the hysteresis area (bottom left) is maximized, resulting in the characteristic bell curves observed across all parameter ranges. The white line indicates the peak frequency for each field magnitude. To highlight the low-field regions where the amplitude does not exceed the Langevin value, both the amplitude and hysteresis area have been divided by this value. The specific loss power (bottom right) follows a scaling law proportional to ξ^2 and becomes independent of $\Omega\tau$ at high frequencies. All four plots clearly show a transition from the linear to the nonlinear range, where the field magnitude can alter the shape of the dipole trajectory.

7.3 Hybrid Brownian and Néel relaxation

Settled with the situation where the dynamics are entirely of a magnetic or mechanical nature, let us take anisotropy into account. We already derived the governing equations, which are given by

$$\frac{\mathrm{d}\boldsymbol{m}}{\mathrm{d}t^0} = -\boldsymbol{m} \times \frac{\boldsymbol{H}_{\mathrm{eff}}^0}{\alpha} - \boldsymbol{m} \times \left(\boldsymbol{m} \times \boldsymbol{H}_{\mathrm{eff}}^0\right) \tag{7.64}$$

$$\frac{\mathrm{d}\boldsymbol{n}}{\mathrm{d}t^0} = -\frac{\tau_0}{\tau_{\mathrm{B}}}\boldsymbol{n} \times \left(\boldsymbol{m} \times \frac{\boldsymbol{\xi}(t^0)}{2} + \frac{\alpha}{1+\alpha^2}\frac{\mathrm{d}\boldsymbol{m}}{\mathrm{d}t^0} + \frac{\tau_{\mathrm{B}}}{\gamma_{\mathrm{r}}}\boldsymbol{T}_{\mathrm{th}}\right) \tag{7.65}$$

$$\boldsymbol{H}_{\mathrm{eff}}^0 = \frac{\boldsymbol{\xi}(t^0)}{2} + \sigma(\boldsymbol{m}\cdot\boldsymbol{n})\boldsymbol{n} + \frac{\mu_0 M_{\mathrm{s}} V_{\mathrm{m}}}{2k_{\mathrm{B}}T}\boldsymbol{H}_{\mathrm{th}}. \tag{7.66}$$

The complexity of these equations surpasses that of the uncoupled system by far, and finding approximations for the nonlinear region has not been accomplished. However, the linear model for weak fields can be modified, albeit this requires more sophisticated considerations based on perturbation theory.

Perturbation theory states that the response of a dipole to a weak field can be derived from the zero-field properties of the system up to the first order. This can be understood as that there is no difference between the response to an external field and that to random thermal excitation, leading to the Green-Kubo relation [33]

$$\chi(\omega) = -\frac{\mu_0 M_{\mathrm{s}}^2 V_{\mathrm{m}}}{k_{\mathrm{B}}T}\int_0^\infty e^{-i\omega t}\frac{\partial}{\partial t}\left\langle m_\parallel(0)m_\parallel(t)\right\rangle. \tag{7.67}$$

Neglecting high-frequency responses, the susceptibility is of the same form as in the zero and infinite anisotropy case given by

$$\chi(\omega) \propto \frac{1}{1+i\omega\tau}. \tag{7.68}$$

Regarding the characteristic time scale τ, it is evident that neither τ_0 nor τ_{B} are suitable for modeling the hybrid system. This is because both magnetic and Brownian relaxation take place in parallel. Moreover, we need to insert the anisotropy into the equation. The Néel relaxation time

$$\tau_{\mathrm{N}} = \tau_0 \frac{\sqrt{\pi}}{2}\frac{e^\sigma}{\sigma^{3/2}} \quad \text{for} \quad \sigma \geq 2 \tag{7.69}$$

is the characteristic time scale of magnetic relaxation with finite anisotropy. The given definition [50] is an asymptotic expression for the formula derived by Raikher and Stepanov [33], although other authors [26, 51] and Néel himself [52] proposed an alternative value, namely $\tau_{\mathrm{N}} = \tau_{\mathrm{a}} \exp\sigma$, where τ_{a} is the attempt time that denotes the time frame the magnetization should stay stable.

Despite this uncertainty, there is a general consensus regarding the characteristic time scale of the hybrid system, which can be expressed by the effective time scale

$$\tau_{\text{eff}} = \frac{\tau_{\text{N}}\tau_{\text{B}}}{\tau_{\text{N}} + \tau_{\text{B}}}, \tag{7.70}$$

which is always smaller than the smaller of the two values. Hence, it is the faster process that takes the more important role, which for zero anisotropy, is the Néel time τ_0, while for increasing σ approaches τ_{B}. This heuristic expression is in good accordance with the actual relaxation time, despite being in no way an exact result of the underlying Fokker-Planck equation.

Regarding the susceptibility χ, there are several propositions to adapt the susceptibility given by the case of zero and infinite anisotropy. Raikher and Stepanov [33] suggested the expression

$$\chi(\omega') = \frac{\mu_0 M_{\text{s}}^2 V_{\text{m}}}{3k_{\text{B}}T}\left(\frac{B(\sigma)}{1 + i\omega\tau_{\text{eff}}} + 1 - B(\sigma)\right), \tag{7.71}$$

where B is a monotone function that satisfies $B(0) = 1/3$ and approaches 1 as σ goes to infinity. Although this formula is limited to the low-frequency range $\omega\tau_0 < 1$, the authors state that the adiabatic term $1 - B$ emerges as a direct consequence of the inclusion of these.

A more general form is provided by Shliomis [44], in which two distinct relaxation times are derived. The parallel relaxation time remains unaltered and is given by $\tau_{\parallel} = \tau_{\text{eff}}$. This indicates that the time required to overcome the energy barrier increases exponentially with increasing anisotropy. However, in the event that a spin is deflected from the easy axis, the time required to return the spin to its original alignment is expected to decrease with anisotropy. Accordingly, the proposed transverse relaxation time is given by

$$\tau_{\perp} = \frac{\tau_{11}\tau_{\text{B}}}{\tau_{11} + \tau_{\text{B}}} \quad \text{with} \quad \tau_{11} = 2\tau_0 \frac{R(\sigma) - R'(\sigma)}{R(\sigma) + R'(\sigma)}, \tag{7.72}$$

where R is the function defined in the last chapter. These two time scales as well as the parallel and transverse initial susceptibility lead to the approximation

$$\chi = \frac{1}{3}\left(\frac{\chi_{\parallel}}{1 + i\omega\tau_{\parallel}} + \frac{2\chi_{\perp}}{1 + i\omega\tau_{\perp}}\right) \tag{7.73}$$

for the dynamic susceptibility of the system, resulting in the typical phenomena of two appearing peaks in the imaginary part.

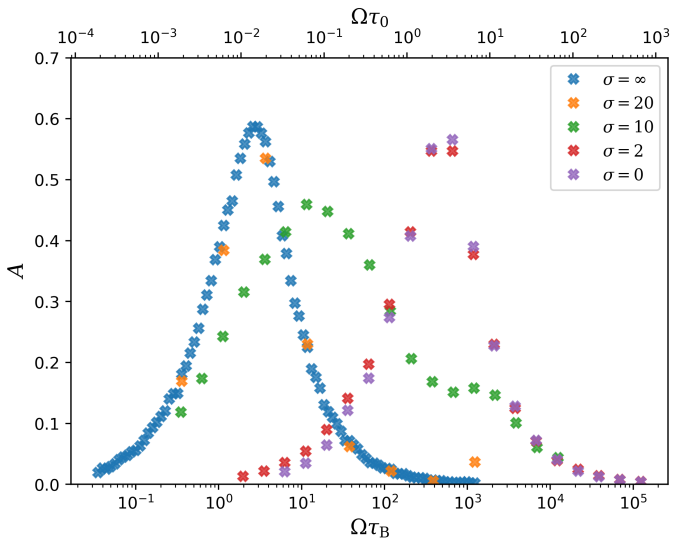

Fig. 14: **Influence of anisotropy on magnetization dynamics.** The simulated ensemble consists of 100 particles. The Gilbert damping is set to $\alpha = 0.08$ and the ratio of time scales $\tau_B/\tau_0 \approx 187$.

As previously discussed, these derivations do not hold for $\xi > 1$, as nonlinear contributions to ξ generate additional frequencies in the response of the dipole. This is illustrated in Fig. 14, where the hysteresis area has been computed from simulations at a field magnitude $\xi = 10$. Despite the emergence of a secondary peak for $\sigma = 10$, attempts to fit it against a function of the form (7.73) have not yielded successful results.

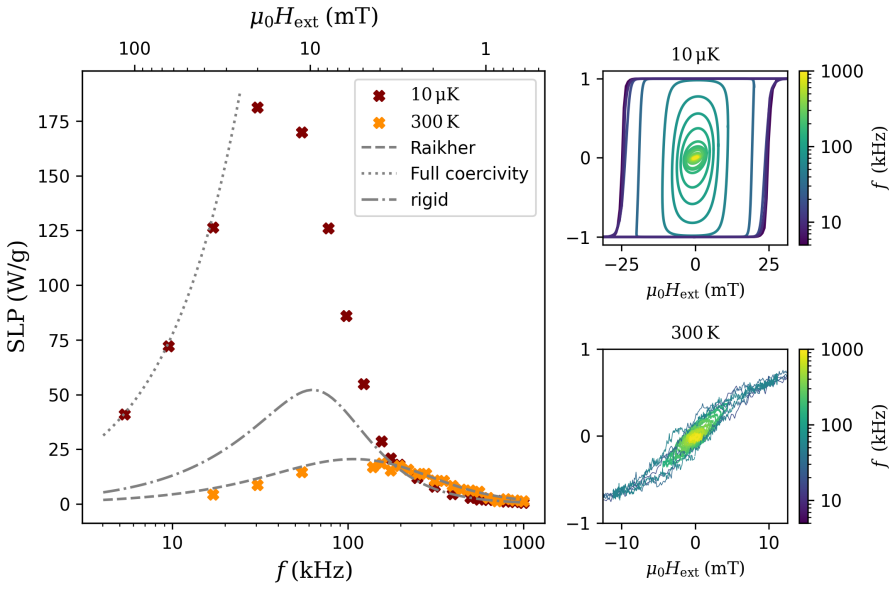

Fig. 15: **Specific loss power for 9 nm magnetite spheres.** To circumvent numerical errors that may arise when the dipole is fully aligned with the field, zero-temperature simulations are performed at 1 microkelvin. For higher fields at zero temperature, the dipole inevitably reverses at half the coercive field (25 mT), thus establishing an upper limit for the hysteresis area (Full coercivity). At room temperature, the loss power is significantly diminished and can be adequately approximated by the expression proposed by Raikher and Rosenzweig.

Fig. 15 demonstrates the field-dependent specific loss power for a magnetite sphere with a radius of $R = 9\,\text{nm}$, whose material parameters are given in Tab. 4. The external field is set to achieve the human discomfort level for hyperthermia treatments as defined by the Brezovich criterion [53] $C = H_{\text{ext}} f = 4.85 \times 10^8\,\text{A}\,\text{m}^{-1}\,\text{Hz}$. It shows that the maximum possible dissipation of $190\,\text{W}\,\text{g}^{-1}$ can be approached at zero temperature. However, thermal effects result in a significant reduction in the heating power, reaching below $20\,\text{W}\,\text{g}^{-1}$ at room temperature.

8 Conclusion

It was demonstrated that variational calculus can be used to derive a self-consistent system of equations of motion for multidomain particles of arbitrary shape suspended in a liquid carrier. Subsequently, the introduction of viscous and magnetic damping, as well as thermal fluctuations, led to the equations of motion for a dissipative system, where cross terms arose from the requirement that the angular momentum may only change due to random collisions with fluid particles or due to the influence of an external excitation. Regarding the Barnett effect, it can be traced back to the proposition that magnetic damping is a direct consequence of interactions between atomic spins and atomic sites within the crystal lattice.

Although expressions for statistical averages for multi-domain particles could not be obtained, a reduction to a few independent parameters allows further investigation of the impact of micromagnetic contributions on the macroscopic behavior of the particle. Moreover, integrating the rotational degree of freedom led to the averaged external field that gives a significant performance improvement in finding equilibrium states of a suspended particle by only using a micromagnetic solver. It provides a meaningful characterization of the particle's response to a static field without the need to specify the angle between the field and the easy axis.

Regardless of the chosen model complexity, understanding the nonlinear responses to larger fields at zero or infinite magnetic anisotropy is crucial. It has been shown that the Landau-Lifshitz-Gilbert equation and the Langevin equation are equivalent if inertia is neglected and the external field oscillates only along a single axis. The application of the well-studied linear range is limited, especially for increasing particle sizes, as the non-dimensionalized field magnitude ξ is proportional to the magnetic volume. The effective field method is an astonishingly reliable approximation for all field parameters, enabling the acquisition of ensemble averages within seconds. However, it is devoid of analytical insights.
These can be provided by the proposed response function R (7.55) based on a zero-temperature ensemble solution. The uncorrected version of the model accurately reflects the response to high fields and frequencies, with the ratio of these parameters serving as the defining characteristic that determines the trajectory. Although the phase shift observed when this ratio is lowered cannot be explained, the introduction of fitting parameters causes the trajectories to coincide. The tunability of R to a majority of the observed hysteresis shapes suggests that its consideration is indeed useful as it accommodates otherwise unrelated higher-order susceptibilities within the Taylor expansion of R.

As the software library ESPResSo is well-established and equipped with many more

features, such as dipolar interactions and hydrodynamic flows, the demonstrated coupling to magnumn.np facilitates including these in hybrid simulations. Furthermore, the effort invested in implementing appropriate reference frame conversions and developing a reliable time integrator paves the way for new inquiries into the dynamical behavior of multi-domain particles.

Bibliography

[1] N. A. Usov and B. Y. Liubimov, "Dynamics of magnetic nanoparticle in a viscous liquid: Application to magnetic nanoparticle hyperthermia", J. Appl. Phys. **112**, 023901 (2012).

[2] A. Jordan, R. Scholz, P. Wust, H. Fähling, and Roland Felix, "Magnetic fluid hyperthermia (MFH): Cancer treatment with AC magnetic field induced excitation of biocompatible superparamagnetic nanoparticles", J. Magn. Magn. Mater. **201**, 413–419 (1999).

[3] A. Chicheł, J. Skowronek, M. Kubaszewska, and M. Kanikowski, "Hyperthermia – description of a method and a review of clinical applications", Rep. Pract. Oncol. Radiother. **12**, 267–275 (2007).

[4] D. B. Reeves and J. B. Weaver, "Combined Néel and Brown rotational Langevin dynamics in magnetic particle imaging, sensing, and therapy", Appl. Phys. Lett. **107**, 223106 (2015).

[5] R. Dhavalikar and C. Rinaldi, "On the effect of finite magnetic relaxation on the magnetic particle imaging performance of magnetic nanoparticles", J. Appl. Phys. **115**, 074308 (2014).

[6] C. Abert, "Micromagnetics and spintronics: models and numerical methods", Eur. Phys. J. B **92**, 120 (2019).

[7] T. Gilbert, "A phenomenological theory of damping in ferromagnetic materials", IEEE Trans. Magn. **40**, 3443–3449 (2004).

[8] K. K. Liang, "Efficient conversion from rotating matrix to rotation axis and angle by extending Rodrigues' formula", arXiv:1810.02999.

[9] R. Pathria and P. D. Beale, *Statistical Mechanics*, 3rd ed. (Academic Press, Boston, 2011).

[10] K. Okada and A. Satoh, "Analysis of a Stokes Flow Past a Cube (Friction and Diffusion Coefficients for Brownian Dynamics Simulations)", in ASME International Mechanical Engineering Congress and Exposition, Vol. 7 (Nov. 2019).

[11] M. Kaiser and S. S. Kantorovich, "The importance of being a cube: Active cubes in a microchannel", Journal of Molecular Liquids **360**, 119318 (2022).

[12] J. D. Sherwood, "Resistance coefficients for Stokes flow around a disk with a Navier slip condition", Phys. Fluids **24**, 093103 (2012).

[13] S. Zhao, "Time Derivative of Rotation Matrices: A Tutorial", arXiv:1609.06088.

[14] R. Marino, "Dynamics and Thermodynamics of Translational and Rotational Diffusion Processes Driven out of Equilibrium", PhD thesis (KTH Royal Institute of Technology, 2019).

[15] N. G. van Kampen, "Itô versus Stratonovich", J. Stat. Phys. **24**, 175–187 (1981).

[16] J. L. García-Palacios and F. J. Lázaro, "Langevin-dynamics study of the dynamical properties of small magnetic particles", Phys. Rev. B **58**, 14937–14958 (1998).

[17] D. V. Berkov and N. L. Gorn, "Thermally activated processes in magnetic systems consisting of rigid dipoles: equivalence of the Ito and Stratonovich stochastic calculus", J. Phys. Condens. Matter **14**, L281 (2002).

[18] P. Ilg and M. Kröger, "Field- and concentration-dependent relaxation of magnetic nanoparticles and optimality conditions for magnetic fluid hyperthermia", Sci. Rep. **13**, 16523 (2023).

[19] H. Löwen, "Inertial effects of self-propelled particles: From active Brownian to active Langevin motion", J. Chem. Phys. **152**, 040901 (2020).

[20] W. A. Steele, "Molecular Reorientation in Liquids. II. Angular Autocorrelation Functions", J. Chem. Phys. **38**, 2411–2418 (1963).

[21] L. D. Landau and E. M. Lifshitz, *Mechanics, Third Edition: Volume 1 (Course of Theoretical Physics)*, 3rd ed. (Butterworth-Heinemann, 1976).

[22] S. Bretzel, G. E. W. Bauer, Y. Tserkovnyak, and A. Brataas, "Barnett effect in thin magnetic films and nanostructures", Appl. Phys. Lett. **95**, 122504 (2009).

[23] H. Keshtgar, S. Streib, A. Kamra, Y. M. Blanter, and G. E. W. Bauer, "Magnetomechanical coupling and ferromagnetic resonance in magnetic nanoparticles", Phys. Rev. B **95**, 134447 (2017).

[24] K. D. Usadel and C. Usadel, "Dynamics of magnetic single domain particles embedded in a viscous liquid", J. Appl. Phys. **118**, 234303 (2015).

[25] S. J. Barnett, "Magnetization by Rotation", Phys. Rev. **6**, 239–270 (1915).

[26] S. Helbig, C. Abert, P. A. Sánchez, S. S. Kantorovich, and D. Suess, "Self-consistent solution of magnetic and friction energy losses of a magnetic nanoparticle", Phys. Rev. B **107**, 054416 (2023).

[27] E. Martinez, L. Lopez-Diaz, L. Torres, and C. Garcia-Cervera, "Micromagnetic simulations with thermal noise: Physical and numerical aspects", J. Magn. Magn. Mater. **316**, Proceedings of the Joint European Magnetic Symposia, 269–272 (2007).

[28] J. A. Osborn, "Demagnetizing Factors of the General Ellipsoid", Phys. Rev. **67**, 351–357 (1945).

[29] M. Sato and Y. Ishii, "Simple and approximate expressions of demagnetizing factors of uniformly magnetized rectangular rod and cylinder", J. Appl. Phys. **66**, 983–985 (1989).

[30] M. Beleggia, M. D. Graef, Y. T. Millev, D. A. Goode, and G. Rowlands, "Demagnetization factors for elliptic cylinders", Journal of Physics D: Applied Physics **38**, 3333 (2005).

[31] K. D. Usadel, "Dynamics of magnetic nanoparticles in a viscous fluid driven by rotating magnetic fields", Phys. Rev. B **95**, 104430 (2017).

[32] F. L. Durhuus, M. Beleggia, and C. Frandsen, "Conservation laws for interacting magnetic nanoparticles at finite temperature", Phys. Rev. B **109**, 054421 (2024).

[33] Y. L. Raikher and V. Stepanov, "Physical aspects of magnetic hyperthermia: Low-frequency ac field absorption in a magnetic colloid", J. Magn. Magn. Mater. **368**, 421–427 (2014).

[34] F. Weik, R. Weeber, K. Szuttor, K. Breitsprecher, J. de Graaf, M. Kuron, J. Landsgesell, H. Menke, D. Sean, and C. Holm, "ESPResSo 4.0 – an extensible software package for simulating soft matter systems", Eur. Phys. J. Spec. Top. **227**, 1789–1816 (2019).

[35] F. Bruckner, S. Koraltan, C. Abert, and D. Suess, "magnum.np: a PyTorch based GPU enhanced finite difference micromagnetic simulation framework for high level development and inverse design", Sci. Rep. **13**, 12054 (2023).

[36] M. Kaiser, "Directing magneto-active particles with applied fields", PhD thesis (University of Vienna, 2022).

[37] R. Sonnenschein, "An improved algorithm for molecular dynamics simulation of rigid molecules", J. Comput. Phys. **59**, 347–350 (1985).

[38] N. S. Martys and R. D. Mountain, "Velocity Verlet algorithm for dissipative-particle-dynamics-based models of suspensions", Phys. Rev. E **59**, 3733–3736 (1999).

[39] W. Brown, *Micromagnetics*, Interscience tracts on physics and astronomy (Interscience Publishers, 1963).

[40] D. Mostarac, P. A. Sánchez, and S. Kantorovich, "Characterisation of the magnetic response of nanoscale magnetic filaments in applied fields", Nanoscale **12**, 13933–13947 (2020).

[41] E. C. Stoner and E. P. Wohlfarth, "A mechanism of magnetic hysteresis in heterogeneous alloys", Philos. Trans. R. Soc. A **240**, 599–642 (1948).

[42] C. Tannous and J. Gieraltowski, "The Stoner–Wohlfarth model of ferromagnetism", Eur. J. Phys. **29**, 475 (2008).

[43] M. A. Chuev and J. Hesse, "Nanomagnetism: extension of the Stoner–Wohlfarth model within Néel's ideas and useful plots", J. Phys. Condens. Matter **19**, 506201 (2007).

[44] M. I. Shliomis and V. I. Stepanov, "Theory of the Dynamic Susceptibility of Magnetic Fluids", in *Advances in Chemical Physics* (John Wiley & Sons, Ltd, 1994), pp. 1–30.

[45] J. Tranchida, P. Thibaudeau, and S. Nicolis, "Hierarchies of Landau-Lifshitz-Bloch equations for nanomagnets: A functional integral framework", Phys. Rev. E **98**, 042101 (2018).

[46] M. A. Martsenyuk, Y. L. Raikher, and M. Shliomis, "On the kinetics of magnetization of suspensions of ferromagnetic particles", Zh. Eksp. Teor. Fiz **65**, 834–841 (1973).

[47] D. B. Reeves and J. B. Weaver, "Comparisons of characteristic timescales and approximate models for Brownian magnetic nanoparticle rotations", en, J. Appl. Phys. **117**, 233905 (2015).

[48] A. A. Kuznetsov and A. F. Pshenichnikov, "Nonlinear response of a dilute ferrofluid to an alternating magnetic field", J. Mol. Liq. **346**, 117449 (2022).

[49] R. Jedynak, "New facts concerning the approximation of the inverse Langevin function", J. Non-Newton. Fluid Mech. **249**, 8–25 (2017).

[50] R. Rosensweig, "Heating magnetic fluid with alternating magnetic field", J. Magn. Magn. Mater. **252**, Proceedings of the 9th International Conference on Magnetic Fluids, 370–374 (2002).

[51] J.-P. Fortin, C. Wilhelm, J. Servais, C. Ménager, J.-C. Bacri, and F. Gazeau, "Size-Sorted Anionic Iron Oxide Nanomagnets as Colloidal Mediators for Magnetic Hyperthermia", J. Am. Chem. Soc. **129**, 2628–2635 (2007).

[52] L. Néel, "Théorie du traînage magnétique des ferromagnétiques en grains fins avec application aux terres cuites", Annales de géophysique **5**, 99–136 (1949).

[53] R. Hergt and S. Dutz, "Magnetic particle hyperthermia—biophysical limitations of a visionary tumour therapy", J. Magn. Magn. Mater. **311**, Proceedings of the Sixth International Conference on the Scientific and Clinical Applications of Magnetic Carriers, 187–192 (2007).

List of Figures

1 Laboratory frame micromagnetics 39

2 Zero-field phase space for spherical particles 48
3 Zero-field ground state of a magnetite sphere with $R = 90\,\mathrm{nm}$. 48
4 Hysteresis of suspended 90 nm magnetite spheres 54
5 Equilbrium values for suspended single-domain particles 56
6 Magnetization curve of an immobilized system at zero temperature 58
7 Angle-dependent susceptibility for external fields of small magnitude . . . 59

8 Parameters to be specified for the models discussed 63
9 SLP and susceptibilty in the linear regime 72
10 The (corrected) deterministic model 76
11 Fitted phase shift and prefactor for $\mathfrak{H}_{\mathrm{fit}}$ 76
12 Comparison of the effective field method and simulated trajectories 77
13 Characterization of dipole responses with the effective field method 79
14 Influence of anisotropy on magnetization dynamics 82
15 Specific loss power for 9 nm magnetite spheres 83